NUREG/CR–4469
PNL–5711
Vol. 9

Nondestructive Examination (NDE) Reliability for Inservice Inspection of Light Water Reactors

Semi-Annual Report
April – September 1988

Prepared by S. R. Doctor, J. D. Deffenbaugh, M. S. Good, E. R. Green
P. G. Heasler, F. A. Simonen, J. C. Spanner, T. T. Taylor

Pacific Northwest Laboratory
Operated by
Battelle Memorial Institute

Prepared for
U.S. Nuclear Regulatory Commission

DISCLAIMER

The following pages are an exact representation of what is in the original document folder.

AVAILABILITY NOTICE

Availability of Reference Materials Cited in NRC Publications

Most documents cited in NRC publications will be available from one of the following sources:

1. The NRC Public Document Room, 2120 L Street, NW, Lower Level, Washington, DC 20555

2. The Superintendent of Documents, U.S. Government Printing Office, P.O. Box 37082, Washington, DC 20013-7082

3. The National Technical Information Service, Springfield, VA 22161

Although the listing that follows represents the majority of documents cited in NRC publications, it is not intended to be exhaustive.

Referenced documents available for inspection and copying for a fee from the NRC Public Document Room include NRC correspondence and internal NRC memoranda; NRC Office of Inspection and Enforcement bulletins, circulars, information notices, inspection and investigation notices; Licensee Event Reports; vendor reports and correspondence; Commission papers; and applicant and licensee documents and correspondence.

The following documents in the NUREG series are available for purchase from the GPO Sales Program: formal NRC staff and contractor reports, NRC-sponsored conference proceedings, and NRC booklets and brochures. Also available are Regulatory Guides, NRC regulations in the *Code of Federal Regulations*, and *Nuclear Regulatory Commission Issuances*.

Documents available from the National Technical Information Service include NUREG series reports and technical reports prepared by other federal agencies and reports prepared by the Atomic Energy Commission, forerunner agency to the Nuclear Regulatory Commission.

Documents available from public and special technical libraries include all open literature items, such as books, journal and periodical articles, and transactions. *Federal Register* notices, federal and state legislation, and congressional reports can usually be obtained from these libraries.

Documents such as theses, dissertations, foreign reports and translations, and non-NRC conference proceedings are available for purchase from the organization sponsoring the publication cited.

Single copies of NRC draft reports are available free, to the extent of supply, upon written request to the Office of Information Resources Management, Distribution Section, U.S. Nuclear Regulatory Commission, Washington, DC 20555.

Copies of industry codes and standards used in a substantive manner in the NRC regulatory process are maintained at the NRC Library, 7920 Norfolk Avenue, Bethesda, Maryland, and are available there for reference use by the public. Codes and standards are usually copyrighted and may be purchased from the originating organization or, if they are American National Standards, from the American National Standards Institute, 1430 Broadway, New York, NY 10018.

DISCLAIMER NOTICE

NUREG/CR--4469-Vol.9
TI90 006254

Nondestructive Examination (NDE) Reliability for Inservice Inspection of Light Water Reactors

Semi-Annual Report
April – September 1988

Manuscript Completed: October 1989
Date Published: November 1989

Prepared by
S. R. Doctor, J. D. Deffenbaugh, M. S. Good, E. R. Green
P. G. Heasler, F. A. Simonen, J. C. Spanner, T. T. Taylor

Pacific Northwest Laboratory
Richland, WA 99352

Prepared for
Division of Engineering
Office of Nuclear Regulatory Research
U.S. Nuclear Regulatory Commission
Washington, DC 20555
NRC FIN B2289

THIS PAGE

WAS INTENTIONALLY

LEFT BLANK

ABSTRACT

Evaluation and Improvement of NDE Reliability for Inservice Inspection of Light Water Reactors (NDE Reliability) Program at the Pacific Northwest Laboratory was established by the Nuclear Regulatory Commission to determine the reliability of current inservice inspection (ISI) techniques and to develop recommendations that will ensure a suitably high inspection reliability. The objectives of this program include determining the reliability of ISI performed on the primary systems of commercial light-water reactors (LWRs); using probabilistic fracture mechanics analysis to determine the impact of NDE unreliability on system safety; and evaluating reliability improvements that can be achieved with improved and advanced technology. A final objective is to formulate recommended revisions to ASME Code and Regulatory requirements, based on material properties, service conditions, and NDE uncertainties. The program scope is limited to ISI of the primary systems including the piping, vessel, and other inspected components. This is a progress report covering the programmatic work from April 1988 through September 1988.

EXECUTIVE SUMMARY[a]

A multi-year program entitled the Evaluation and Improvement of NDE Reliability for Inservice Inspection of Light Water Reactors (NDE Reliability) was established at the Pacific Northwest Laboratory (PNL) to determine the reliability of current inservice inspection (ISI) techniques and to develop recommendations that would ensure a suitably high inspection reliability if fully implemented.

The objectives of this Nondestructive Examination (NDE) Reliability program for the Nuclear Regulatory Commission (NRC) include:

- Determine the reliability of ultrasonic ISI performed on the primary systems of commercial light-water reactors (LWRs).
- Use probabilistic fracture mechanics analysis to determine the impact of NDE unreliability on system safety and determine the level of inspection reliability required to ensure a suitably low failure probability.
- Evaluate the degree of reliability improvement that could be achieved using improved and advanced NDE techniques.
- Based on material properties, service conditions, and NDE uncertainties, formulate recommended revisions to ASME Code, Section XI and Regulatory requirements needed to ensure suitably low failure probabilities.

The scope of the program is limited to the ISI of primary coolant systems, but the results and recommendations are also applicable to Class 2 piping systems.

The program consists of three basic tasks: a Piping task, a Pressure Vessel task, and a New Inspection Criteria task. Because of the problems associated with the reliable detection, correct interpretation, and accurate characterization of defects during ultrasonic testing/inservice inspection (UT/ISI) of piping, the major efforts during this reporting period were concentrated in the Piping task and the New Inspection Criteria task. However, some work was initiated on the Pressure Vessel Task.

The major highlights during this reporting period were:

- ASME Code Activity

  The proposed Appendix VII on Personnel Training and Qualification was formally approved by the Main Committee and submitted for consideration by the Board on Nuclear Codes and Standards (BNCS). The proposed Appendix VIII on UT/ISI Performance Demonstration was approved by the Subgroup on Nondestructive Examination (SGNDE) and the Section XI Subcommittee for submittal to the Main Committee. A proposed revision to Code Case N-409

(a) RSR FIN Budget No. B2289; RSR Contact: J. Muscara

(N-409-1) received final approval from Section XI, the ASME Main Committee, and the BNCS. Code Case N-409-1 specifies a statistically designed performance demonstration to qualify the personnel, equipment, and procedures used for UT/ISI of piping welds in accordance with Section XI requirements.

- Pressure Vessel Inspection

  Analysis of PISC-II Data. The original PISC-II data set was revised according to information received from the Joint Research Centre. These data were checked for correctness by attempting to reproduce results from the PISC-II reports. Problems, both with the data and with our interpretation, were corrected.

  Equipment Interaction Matrix. This work is directed toward evaluating the effects of frequency domain equipment interactions and determining tolerance values for improving ultrasonic inspection reliability. Preliminary analysis using model-predicted, worst-case flaws indicated that the equipment bandwidth tolerance of ±10% in ASME Code Case N-409-1 is sufficient to ensure ±10% measurement repeatability. The ±10% center frequency tolerance in the ASME Code was found to be too broad to ensure ±10% measurement repeatability.

  The model results suggested that the equipment center frequency and bandwidth interactions are due in part to phase cancellation along the receiving transducer face. Therefore, the receiving transducers for dual element and tandem search units should be as small as practical to minimize sensitivity to equipment changes. It was found that even though the flaw model was two-dimensional, the calculated transfer functions were very similar to those that would be calculated by a three-dimensional model. Thus, these sensitivity study results can be extended to three-dimensional systems.

- New Inspection Criteria

  Work continued on assessing the adequacy of existing ASME Code requirements for ISI and on developing technical bases for improving these requirements. Several interrelated activities were directed to the development of probabilistically based inspection requirements. The PNL program interacted with other industry efforts, notably a newly organized ASME Task Group on Risk-Based Guidelines. Contacts have also continued with other organizations such as the Electric Power Research Institute and the Oak Ridge National Laboratory. To review and evaluate various concepts for probabilistic inspection criteria, a "road map" document on improved inspection requirements was prepared. A pilot application of probabilistic risk assessment (PRA) methods to the inspection of piping, vessels, and related components was completed. A ranking of important systems to assess priorities for inservice inspection was performed using an existing PRA for the Oconee-3 reactor. The possible use of actual failure data as a guide for inservice inspection requirements was also addressed. A sample set of data on piping failures

and repairs was obtained by performing a computer search of the Nuclear Power Plant Reliability Data System (NPRDS).

- Program Management and Consultation on Field Problems

  A matrix depicting the inspection practices of other countries with respect to ISI of reactor pressure vessels was developed and provided to the NRC program manager. Cooperative agreements were established with EPRI on the subtasks relating to surface roughness effects, and re-analysis of the PISC-II data base. A letter discussing the value of the NRC endorsing Code Case N-409-1, versus the present BWROG/EPRI/NRC Coordination Plan Agreement, was provided to the NRC project manager. Several hundred viewgraphs describing prior and current work on this program were prepared in conjunction with the NRC program manager's trip to Taiwan.

- Piping Inspection Task

  This task is designed to address the NDT problems associated with piping used in light water reactors. The primary thrust of the work has been on wrought and cast stainless steel since these materials are harder to inspect than carbon steel. However, many of the subtasks' results also pertain to carbon steel. The current subtasks are: mini-round robin report, piping inspection round robin report, qualification document, cast stainless steel inspection, surface roughness, field pipe characterization), and PISC-III activities.

  MRR Report. The Mini-Round Robin (MRR) subtask was conducted to provide an engineering data base for UT/ISI that would help: a) quantify the effect of training and performance demonstration testing required by IEB 83-02, b) quantify the differences in capability between detecting long versus short cracks, and c) quantify the capability of UT/ISI technicians to determine length and depth of intergranular stress corrosion cracks (IGSCC). A NUREG report has been prepared and submitted for NRC review to document the work conducted on this subtask.

  Qualification Criteria for UT/ISI Systems. The objective of this subtask is to improve the reliability of UT/ISI through the development of new criteria and requirements for qualifying UT/ISI systems. Revisions to the qualification document (NUREG/CR-4882) to resolve technical issues and address PNL and NRC comments were completed. This document has received PNL clearance and been submitted to the NRC for final pre-publication review.

  Inspection of CCSS. The objective of this subtask is to evaluate the effectiveness and reliability of ultrasonic inspection of cast materials within the primary pressure boundary of LWRs. Due to the coarse microstructure of this material, many inspection problems exist and are common to structures such as cladded pipe, inner-surface cladding of pressure vessels, statically cast elbows, statically cast pump bowls, centrifugally cast stainless steel (CCSS) piping, dissimilar metal welds, and weld-overlay-repaired pipe joints. Far-side weld inspection is

included in the scope of this work since the ultrasonic beam passes through weld material. Activities conducted during this reporting period included evaluations of weld-overlay-repaired pipe joints and CCSS materials.

Surface Roughness. The objective of this subtask is to establish specifications such that an effective and reliable ultrasonic inspection is not prevented by the condition of the inspection surface. Past efforts included an attempt to quantify the effect produced by irregularities of the inspection surface. The approach was redefined to cooperate with an EPRI-funded program at Ames Laboratory in establishing a mathematical model to be used as an engineering tool for deriving guidelines for surface specifications. Activities conducted during this reporting period included formulation of a coordination plan between EPRI, NRC, the Center for NDE (CNDE) at Ames Laboratory, and PNL; a visit by CNDE personnel to PNL; a CNDE/PNL data exchange; and PNL development of better experimental procedures for obtaining quantitative data to compare model predictions.

Field Pipe Characterization. The objective of this subtask is to provide pipe weld specimens that can be used for studies to evaluate the effectiveness and reliability of UT/ISI performed on BWR piping. Weld specimens were removed from replaced pipe remnants at the Monticello and Vermont Yankee BWR nuclear power plants in FY 1986. These weld specimens have subsequently been decontaminated and characterized by ultrasonic and penetrant examinations. Some specimens were also examined in detail with conventional UT and Synthetic Aperture Focusing Technique (SAFT) methods. A specimen set has been prepared for shipment to Europe for use in PISC-III program studies; however, actual shipment has been deferred until the program activities are finalized in PISC III.

PISC III. This activity involves the participation in the PISC-III program to ensure that the work is of use in addressing NDT reliability problems for materials and practices in U.S. LWR ISI. This includes the support for the co-leader of the Action 4 on Austenitic Steel Tests (AST); providing five safe-ends from the Monticello plant; a sector of the Hope Creek reactor pressure vessel containing two recirculation system inlet nozzles; coordination of the inspections to be conducted by U.S. teams on the various actions; input to the studies on reliability and specimens for use in the parametric, capability, and reliability studies of the AST. The highlight during this reporting period was further planning for carrying out the action plans.

CONTENTS

FIGURES

TABLES

PREVIOUS REPORTS AND SERIES

Doctor, S. R., J. D. Deffenbaugh, M. S. Good, E. R. Green, P. G. Heasler, F. A. Simonen, J. C. Spanner, and T. T. Taylor. 1989. Nondestructive Examination (NDE) Reliability for Inservice Inspection of Light Water Reactors. NUREG/CR-4469, PNL-5711, Vol. 8. Pacific Northwest Laboratory, Richland, Washington.

Doctor, S. R., J. D. Deffenbaugh, M. S. Good, E. R. Green, P. G. Heasler, F. A. Simonen, J. C. Spanner, and T. T. Taylor. 1988. Nondestructive Examination (NDE) Reliability for Inservice Inspection of Light Water Reactors. NUREG/CR-4469, PNL-5711, Vol. 7. Pacific Northwest Laboratory, Richland, Washington.

Doctor, S. R., J. D. Deffenbaugh, M. S. Good, E. R. Green, P. G. Heasler, G. A. Mart, F. A. Simonen, J. C. Spanner, T. T. Taylor, and L. G. Van Fleet. 1987. Nondestructive Examination (NDE) Reliability for Inservice Inspection of Light Water Reactors. NUREG/CR-4469, PNL-5711, Vol. 6. Pacific Northwest Laboratory, Richland, Washington.

Doctor, S. R., D. J. Bates, J. D. Deffenbaugh, M. S. Good, P. G. Heasler, G. A. Mart, F. A. Simonen, J. C. Spanner, T. T. Taylor, and L. G. Van Fleet. 1987. Nondestructive Examination (NDE) Reliability for Inservice Inspection of Light Water Reactors. NUREG/CR-4469, PNL-5711, Vol. 5. Pacific Northwest Laboratory, Richland, Washington.

Doctor, S. R., D. J. Bates, J. D. Deffenbaugh, M. S. Good, P. G. Heasler, G. A. Mart, F. A. Simonen, J. C. Spanner, A. S. Tabatabai, T. T. Taylor, and L. G. Van Fleet. 1987. Nondestructive Examination (NDE) Reliability for Inservice Inspection of Light Water Reactors. NUREG/CR-4469, PNL-5711, Vol. 4. Pacific Northwest Laboratory, Richland, Washington.

Collins, H. D. and R. P. Gribble. 1986. Siamese Imaging Technique for Quasi-Vertical Type (QVT) Defects in Nuclear Reactor Piping. NUREG/CR-4472, PNL-5717. Pacific Northwest Laboratory, Richland, Washington.

Doctor, S. R., D. J. Bates, R. L. Bickford, L. A. Charlot, J. D. Deffenbaugh, M. S. Good, P. G. Heasler, G. A. Mart, F. A. Simonen, J. C. Spanner, A. S. Tabatabai, T. T. Taylor, and L. G. Van Fleet. 1986. Nondestructive Examination (NDE) Reliability for Inservice Inspection of Light Water Reactors. NUREG/CR-4469, PNL-5711, Vol. 3. Pacific Northwest Laboratory, Richland, Washington.

Doctor, S. R., D. J. Bates, L. A. Charlot, M. S. Good, H. R. Hartzog, P. G. Heasler, G. A. Mart, F. A. Simonen, J. C. Spanner, A. S. Tabatabai, and T. T. Taylor. 1986. Evaluation and Improvement of NDE Reliability for Inservice Inspection of Light Water Reactors. NUREG/CR-4469, PNL-5711, Vol. 2. Pacific Northwest Laboratory, Richland, Washington.

Doctor, S. R., D. J. Bates, L. A. Charlot, H. D. Collins, M. S. Good, H. R. Hartzog, P. G. Heasler, G. A. Mart, F. A. Simonen, J. C. Spanner, and T. T. Taylor. 1986. Integration of Nondestructive Examination (NDE) Reliability and Fracture Mechanics, Semi-Annual Report, April 1984 - September 1984. NUREG/CR-4469, PNL-5711, Vol. 1. Pacific Northwest Laboratory, Richland, Washington.

Good, M. S. and L. G. Van Fleet. 1986. Status of Activities for Inspecting Weld Overlaid Pipe Joints. NUREG/CR-4484, PNL-5729. Pacific Northwest Laboratory, Richland, Washington.

Heasler, P. G., D. J. Bates, T. T. Taylor, and S. R. Doctor. 1986. Performance Demonstration Tests for Detection of Intergranular Stress Corrosion Cracking. NUREG/CR-4464, PNL-5705, Pacific Northwest Laboratory, Richland, Washington.

Simonen, F. A. 1984. The Impact of Nondestructive Examination Unreliability on Pressure Vessel Fracture Predictions. NUREG/CR-3743, PNL-5062. Pacific Northwest Laboratory, Richland, Washington.

Simonen, F. A. and H. H. Woo. 1984. Analyses of the Impact of Inservice Inspection Using Piping Reliability Model. NUREG/CR-3753, PNL-5070. Pacific Northwest Laboratory, Richland, Washington.

Taylor, T. T. 1984. An Evaluation of Manual Ultrasonic Inspection of Cast Stainless Steel Piping. NUREG/CR-3753, PNL-5070. Pacific Northwest Laboratory, Richland, Washington.

Bush, S. H. 1983. Reliability of Nondestructive Examination, Volumes I, II, and III. NUREG/CR-3110-1, -2, and -3; PNL-4584. Pacific Northwest Laboratory, Richland, Washington.

Simonen, F. A. and C. W. Goodrich. 1983. Parametric Calculations of Fatigue Crack Growth in Piping. NUREG/CR-3059, PNL-4537. Pacific Northwest Laboratory, Richland, Washington.

Simonen, F. A., M. E. Mayfield, T. P. Forte, and D. Jones. 1983. Crack Growth Evaluation for Small Cracks in Reactor-Coolant Piping. NUREG/CR-3176, PNL-4642. Pacific Northwest Laboratory, Richland, Washington.

Taylor, T. T., S. L. Crawford, S. R. Doctor, and G. J. Posakony. 1983. Detection of Small-Sized Near-Surface Under-Clad Cracks for Reactor Pressure Vessels. NUREG/CR-2878, PNL-4373. Pacific Northwest Laboratory, Richland, Washington.

Busse, L. J., F. L. Becker, R. E. Bowey, S. R. Doctor, R. P. Gribble, and G. J. Posakony. 1982. Characterization Methods for Ultrasonic Test Systems. NUREG/CR-2264, PNL-4215. Pacific Northwest Laboratory, Richland, Washington.

Morris, C. J. and F. L. Becker. 1982. State-of-Practice Review of Ultrasonic In-service Inspection of Class I System Piping in Commercial Nuclear Power Plants. NUREG/CR-2468, PNL-4026. Pacific Northwest Laboratory, Richland, Washington.

Becker, F. L., S. R. Doctor, P. G. Heasler, C. J. Morris, S. G. Pitman, G. P. Selby, and F. A. Simonen. 1981. Integration of NDE Reliability and Fracture Mechanics, Phase I Report. NUREG/CR-1696-1, PNL-3469. Pacific Northwest Laboratory, Richland, Washington.

Taylor, T. T. and G. P. Selby. 1981. Evaluation of ASME Section XI Reference Level Sensitivity for Initiation of Ultrasonic Inspection Examination. NUREG/CR-1957, PNL-3692. Pacific Northwest Laboratory, Richland, Washington.

NONDESTRUCTIVE EXAMINATION (NDE) RELIABILITY FOR INSERVICE INSPECTION OF LIGHT WATER REACTORS

1.0 INTRODUCTION

The Evaluation and Improvement of NDE Reliability for Inservice Inspection of Light Water Reactors (NDE Reliability) Program at Pacific Northwest Laboratory (PNL) was established to determine the reliability of current inservice inspection (ISI) techniques and to develop recommendations that would ensure a suitably high inspection reliability if fully implemented. The objectives of this program for the Nuclear Regulatory Commission (NRC) are:

- Determine the reliability of ultrasonic ISI performed on commercial light-water reactor (LWR) primary systems.
- Use probabilistic fracture mechanics analysis to determine the impact of NDE unreliability on system safety and determine the level of inspection reliability required to insure a suitably low failure probability.
- Evaluate the degree of reliability improvement that could be achieved using improved and advanced NDE techniques.
- Based on material properties, service conditions, and NDE uncertainties, formulate recommended revisions to ASME Code, Section XI, and Regulatory requirements needed to ensure suitably low failure probabilities.

The scope of this program is limited to ISI of primary coolant systems, but the results and recommendations are also applicable to Class 2 piping systems.

The program consists of three basic tasks: a Piping task, a Pressure Vessel task, and a New Inspection Criteria task. Because of the problems associated with the reliable detection and accurate characterization of defects during ultrasonic testing/inservice inspection (UT/ISI) of piping, the major efforts were concentrated in the Piping task and the New Inspection Criteria task. However, some work was initiated on the Pressure Vessel Task.

This report is divided into the following sections.

- ASME Code Related Activities
- Pressure Vessel Inspection
- New Inspection Criteria
- Program Management and Consultation on Field Problems
- Piping Task Activities

2.0 ASME CODE RELATED ACTIVITIES

2.1 SUMMARY

Participation in ASME Section XI activities continued toward achieving Code acceptance of NRC-funded PNL research to improve the reliability of NDE/ISI. The proposed Appendix VII on Personnel Training and Qualification was formally approved by the Main Committee and submitted for consideration by the Board on Nuclear Codes and Standards (BNCS). The proposed Appendix VIII on UT/ISI Performance Demonstration was approved by the Subgroup on Nondestructive Examination and the Section XI Subcommittee for submittal to the Main Committee. A proposed revision to Code Case N-409 (N-409-1) received final approval from Section XI, the Main Committee, and the BNCS. Code Case N-409-1 describes a statistically designed performance demonstration to qualify the personnel, equipment, and procedures used for UT/ISI of piping welds in accordance with Section XI requirements.

2.2 INTRODUCTION

The objective of this task is to develop and/or evaluate new criteria and requirements for qualifying UT/ISI systems. The primary goal is for these criteria and requirements to be incorporated into Section XI of the ASME Boiler and Pressure Vessel Code. If that goal cannot be met or if the requirements adopted by ASME Section XI (SC-XI) are inadequate, PNL also prepared input for a draft Regulatory Guide as a backup approach. A NUREG report (NUREG/CR-4882) was prepared to document the criteria and requirements developed to date, as well as to document the background and rationale associated with these activities.

The "Proposed Appendix VII" developed in 1986 by an ASME Ad Hoc Task Group has been extensively restructured and revised by the SC-XI Subgroup on Nondestructive Examination (SGNDE). This Ad Hoc Task Group document was restructured as two companion Mandatory Appendices for incorporation into Section XI of the ASME Code. For convenience, these two Appendices are identified as a) Appendix VII on Personnel Training and Qualification and b) Appendix VIII on UT System Performance Demonstrations.

2.3 STATUS OF WORK PERFORMED

Proactive participation of PNL personnel in ASME Code activities continued toward achieving Code acceptance of NRC-funded PNL research to improve the reliability of nondestructive examination/inservice inspection (NDE/ISI). Agendas and minutes of SGNDE meetings held in conjunction with Section XI Subcommittee meetings were prepared and distributed by J. C. Spanner who serves as SGNDE Secretary. During this reporting period, Section XI meetings were held April 18-21, 1988, in Atlanta, Georgia, and August 29-September 1, 1988, in Colorado Springs, Colorado. T. T. Taylor chaired a Special Task Group to develop acoustic emission criteria and requirements, and served as a member of the Working Group on Volumetric Examination and Procedure Qualification. J. C. Spanner serves as Secretary of the Subgroup on Nondestructive Examination (SGNDE) and as a member of the Working Group on Surface Examination and

Personnel Qualification. In May, a joint meeting of the ASME Boiler and Pressure Vessel Code Committees and the National Board of Pressure Vessel Inspectors provided an opportunity for J. C. Spanner to attend ASME Section V Subcommittee meetings and serve as technical liaison between Section V and the SC-XI SGNDE. Input was also prepared for an annual program review held in conjunction with the 16th Water Reactor Safety Research Information Meeting.

A proposed revision to Code Case N-409 (N-409-1) received final approval from Section XI, the Main Committee, and the Board on Nuclear Codes and Standards. Code Case N-409-1 consists of an expansion of N-409 that describes a statistically designed performance demonstration to qualify the personnel, equipment, and procedures used for UT/ISI of piping welds in accordance with ASME Section XI requirements.

The proposed Appendix VII on Personnel Training and Qualification was formally approved by the Main Committee (M.C.), although two letter ballot negatives were received during second consideration of this item. A response to these two negatives was prepared, along with a proposed editorial revision, to accommodate concerns expressed by the negators, resulting in withdrawal of one negative. Reaffirmation of the proposed Appendix VII, including the editorial change, was approved by the cognizant Working Group, the SGNDE, and the Section XI Subcommittee. This item was then submitted for consideration by the Board on Nuclear Codes and Standards (BNCS). Four negatives were received from the initial BNCS ballot on Appendix VII, and an extensive response was prepared to address concerns raised in these negative ballots. Two BNCS members were contacted regarding their ballots, and both tentatively agreed to withdraw their negative votes on this item. It is expected that the proposed Appendix VII will be approved by BNCS on a second consideration ballot expected to be issued in early October.

The proposed Appendix VIII on UT/ISI Performance Demonstrations was approved by the SGNDE and Section XI Subcommittee for submittal to the Main Committee. Editorial review of this document by the Special Working Group on Editorial Review (SWGER) was also completed. Hence, it is expected that this document will be submitted for consideration by the M.C. during the December 1988 meeting. Appendix VIII includes essentially all of the provisions of Code Case N-409-1, plus it extends the performance demonstration concept to other Section XI applications such as the clad/base metal interface of pressure vessel shell welds, nozzle inner radius areas, pressure vessel shell welds other than the clad/base metal interface, nozzle-to-shell welds, and bolting and studs. When adopted, this Appendix will represent a significant enhancement in the performance demonstration requirements for all of the key Section XI UT applications, and could provide a basis for extending the concept of performance demonstrations to the other NDT/ISI methods required by ASME Section XI.

A proposed rewrite (restructuring) of IWA-2300 was approved by the SGNDE and SC-XI and was included as an introductory element in the proposed Appendix VII package. PNL staff have also been assigned to a Task Group responsible for re-evaluating the current Section XI visual acuity requirements, and work on this complex task is continuing.

2.4 FUTURE WORK

In preparation for the Section XI meetings to be held October 24-27, 1988, in Albuquerque, New Mexico, all of the SWGER revisions to the proposed Appendix VIII on UT/ISI Performance Demonstrations has been incorporated and finalized copies of this document has been distributed. Upon receipt of the results from the second consideration BNCS ballot on Appendix VII, PNL staff will either prepare appropriate responses or celebrate the successful completion of an important task assignment. It is expected that additional effort will be required as the proposed Appendix VIII on UT/ISI Performance Demonstrations winds its way through the ASME Code approval process.

3.0 PRESSURE VESSEL INSPECTION

3.1 ANALYSIS OF PISC-II DATA

3.1.1 Summary

The original PISC-II data set was revised according to information received from the Joint Research Centre (JRC) in Ispra, Italy. These data were checked for correctness by attempting to reproduce results from the PISC-II reports. Problems, both with the data and with our interpretation, were corrected.

3.1.2 Introduction

PNL received a complete set of the PISC-II round robin data on the four plates from the JRC in June 1986. The initial objectives of this task were to review the data and attempt to duplicate some of the results in the PISC-II reports to be sure that the data are understood and correct. The specific work completed during this reporting period included:

- Assemble complete information on the true state and computerize the data. The original computer data did not contain a complete description of the flaws and blocks. It was necessary to extract the relevant information from PISC reports and conversations with the JRC staff.

- Attempt to duplicate selected defect detection probabilities from PISC-II Report 5. This was an attempt to identify exactly what set of data was used in the PISC-II reports and verify the procedures that Ispra used to calculate defect detection probability.

- Implement a scoring procedure for the PISC data. It was necessary to utilize different scoring methods than those employed by Ispra and also to verify their results.

3.1.3 Status of Work Performed

Assemble Complete Information on the True State and Computerize the Data. A consistent X location relative to the weld centerline has been added to the true-state records. Different values were used for the centerline from different reports, and the most reasonable values have been chosen. The original X-minimum (Xmin) and X-maximum (Xmax) values in the true-state data represented the entire width of the block. However, the X dimension of the area inspected is considered to be the most relevant variable. Therefore, the specified width of material to be inspected according to the ASME Code was determined, and these values were used for Xmin and Xmax. The width of the inspected weld was approximately 300 mm for each block.

The Y dimension for Plate 2 was found to be incorrect, and the inspectors frequently recorded negative values in this dimension. The true Y dimension of the block was found to vary from -30 mm to 1500 mm.

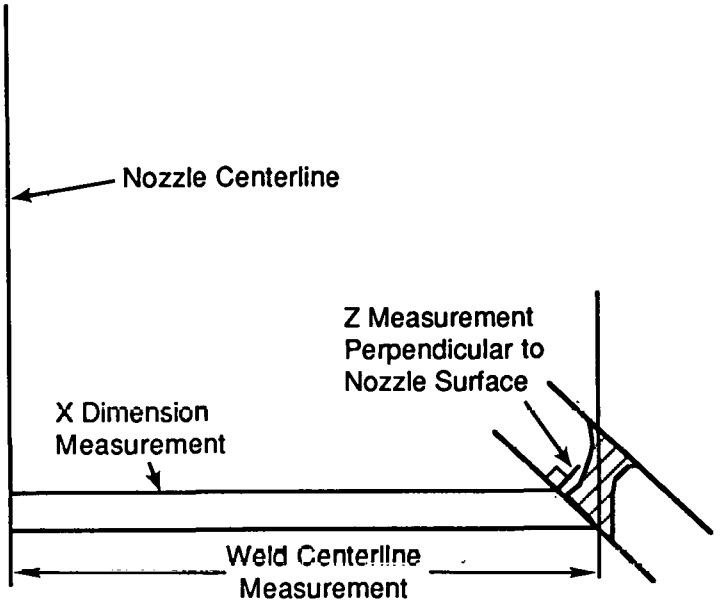

FIGURE 3.1. Coordinate System Used at Bottom of Saddle for Nozzle 3

Nozzle 3 had a complicated non-planar geometry that had to be deciphered. The employed X, Y, Z coordinates are a "deformed" system of polar coordinates (X-radius, Y-angle, Z-thickness). One should note that the Z axis was always perpendicular to the inner surface and consequently "twists" as it proceeds around the weld saddle. The Z axis was, therefore, orthogonal to the X axis at the top of the saddle but pointed away from the nozzle centerline at the bottom of the saddle. The radius value for the weld centerline was measured from the nozzle centerline to the point where the weld centerline intersected with the inner surface. Figure 3.1 summarizes our understanding of the coordinate system.

Attempt to Duplicate Selected Defect Detection Probabilities. After reviewing the data file "CLEAN.PROC" that was received from the JRC, it was determined that the summary tables on pages 23-27 in PISC II Report No. 5 were developed as follows:

The best detection results from each team (selection normally made by computer program that compiled the results of several inspection reports) were compared with intended defects only. A list of intended defects for each specimen may be found in PISC II Report No. 2. Other defects such as unintended weld fabrication defects or implantation defects, etc. were not used in scoring. None of the inner radius cracks (which were intended defects) were used in scoring the data. Also, no false calls were reported in the tables.

Table 3.1 provides a detailed comparison of the data reported in PISC II Report No. 5 and the PNL analysis of the data in "CLEAN.PROC." When reviewing Table 3.1, remember PNL did not score any inspection results -- "CLEAN.PROC" contains scored results (i.e., PISC personnel have associated the intended defects with each team's inspection results). All PNL did was to divide the total number of intended defects that should have been detected into the defects that "CLEAN.PROC" indicates were detected. The following examples will illustrate the content of Table 3.1.

Example 1:

Team EC005499	Plate 1
PISC II Results	DDP = 1.00
PNL Results	DDP = 1.00
Number of Defects	15

Team EC005499 is a computer-compiled selection of the best results of all procedures/techniques used by Team EC. PISC Report No. 2 indicated that PISC Plate 1 had 15 intended defects. Reviewing data in "CLEAN.PROC" indicated that EC005499 did indeed detect all 15 flaws; therefore, its defect detection probability (DDP) is 1.00. In this example, the PNL results agree with the results reported in Report No. 5 for Plate 1.

Example 2:

Team DB005599	Plate 1
PISC II Results	DDP = 0.92
PNL Results	DDP = 0.93
Number of Defects	14

In this example, note that the number of defects is 14 instead of 15 for Plate 1. Fourteen defects were used in this instance because the inspection coverage coordinates in "CLEAN.PROC" indicated that team DB005599 (again a computer selection) did not entirely scan Plate 1 and an area where one defect was located was not scanned; therefore, only 14 defects were used to determine DDP.

Reviewing the detection data in "CLEAN.PROC" indicated that 13 of the 14 defects were detected. The PNL results and the PISC II results are in close agreement ($13 \div 14 = 0.9286$) -- perhaps the PISC-II results were rounded down.

Example 3:

Team ES000799	Plate 1
PISC II Results	DDP = 0.46
PNL Results	DDP = 0.40
Number of Defects	15

TABLE 3.1. Comparison of PISC-II Report No. 5 Defect Detection Probabilities (DDPs) with PNL Calculated DDPs

Block:		Plate 1	Plate 2	Nozzle 3	Nozzle 9
Team					
AN000997	Report No. 5	NA	NA	NA	0.67
	DDP	NA	NA	NA	0.67
	Observations	0	0	0	12
AN001099	Report No. 5	NA	NA	0.52	NA
	DDP	NA	NA	0.52	NA
	Observations	0	0	31	0
AN006499	Report No. 5	0.54	NA	NA	NA
	DDP	0.53	NA	NA	NA
	Observations	15	0	0	0
BA007599	Report No. 5	0.80	0.89	0.50	0.75
	DDP	0.70	0.88	0.42	0.75
	Observations	10	17	31	12
BC020699	Report No. 5	0.23	0.72	0.63	0.67
	DDP	0.27	0.72	0.55	0.67
	Observations	15	18	31	12
BD005599	Report No. 5	NA	NA	0.97	NA
	DDP	NA	NA	0.97	NA
	Observations	0	0	31	0
CB105499	Report No. 5	0.77	1.00	NA	NA
	DDP	0.80	1.00	NA	NA
	Observations	15	18	0	0
DB005599	Report No. 5	0.92	1.00	NA	NA
	DDP	0.93	1.00	NA	NA
	Observations	14	18	0	0
EC005499	Report No. 5	1.00	1.00	1.00	1.00
	DDP	1.00	1.00	1.00	1.00
	Observations	15	18	31	12
EF000299	Report No. 5	NA	0.89	NA	NA
	DDP	0.53	0.89	NA	NA
	Observations	15	18	0	0
EF003699	Report No. 5	NA	NA	0.94	NA
	DDP	NA	NA	0.94	NA
	Observations	0	0	31	0

TABLE 3.1. Cont'd

Block:		Plate 1	Plate 2	Nozzle 3	Nozzle 9
Team					
ES000799	Report No. 5	0.46	0.94	NA	0.83
	DDP	0.40	0.94	NA	0.83
	Observations	15	18	0	12
ES002899	Report No. 5	NA	NA	0.67	NA
	DDP	NA	NA	0.58	NA
	Observations	0	0	31	0
ES002997	Report No. 5	NA	NA	NA	0.83
	DDP	NA	NA	NA	0.83
	Observations	0	0	0	12
EW002699	Report No. 5	NA	1.00	NA	NA
	DDP	NA	1.00	NA	NA
	Observations	0	18	0	0
IC002699	Report No. 5	NA	0.94	NA	NA
	DDP	NA	0.94	NA	NA
	Observations	0	18	0	0
IC004197	Report No. 5	NA	NA	0.61	0.83
	DDP	NA	NA	0.61	0.83
	Observations	0	0	31	12
IS007399	Report No. 5	NA	1.00	0.43	0.75
	DDP	NA	1.00	0.43	0.75
	Observations	0	18	7	12
JS000699	Report No. 5	NA	NA	0.70	0.83
	DDP	NA	NA	0.68	0.83
	Observations	0	0	31	12
JS000799	Report No. 5	0.54	0.94	NA	NA
	DDP	0.53	0.94	NA	NA
	Observations	15	18	0	0
KA005299	Report No. 5	0.62	0.94	NA	NA
	DDP	0.60	0.83	NA	NA
	Observations	15	18	0	0
KR000299	Report No. 5	NA	1.00	NA	NA
	DDP	NA	0.89	NA	NA
	Observations	0	18	0	0

TABLE 3.1. Cont'd

Block: Team		Plate 1	Plate 2	Nozzle 3	Nozzle 9
KRC04199	Report No. 5	NA	NA	NA	NA
	DDP	NA	NA	NA	0.92
	Observations	0	0	0	12
LB004197	Report No. 5	NA	NA	0.84	NA
	DDP	NA	NA	0.84	NA
	Observations	0	0	31	0
LB004199	Report No. 5	NA	NA	NA	0.92
	DDP	NA	NA	NA	0.92
	Observations	0	0	0	12
LBC02699	Report No. 5	NA	1.00	NA	NA
	DDP	NA	1.00	NA	NA
	Observations	0	18	0	0
LC004199	Report No. 5	0.69	NA	0.81	0.83
	DDP	0.67	NA	0.81	0.83
	Observations	15	0	31	12
LC005399	Report No. 5	NA	0.89	NA	NA
	DDP	NA	0.89	NA	NA
	Observations	0	18	0	0
LN009199	Report No. 5	NA	NA	1.00	NA
	DDP	NA	NA	0.90	NA
	Observations	0	0	31	0
LNE1A199	Report No. 5	0.88	NA	NA	NA
	DDP	0.78	NA	NA	NA
	Observations	9	0	0	0
LNE29199	Report No. 5	NA	1.00	NA	NA
	DDP	0.78	1.00	NA	NA
	Observations	9	18	0	0
MT000299	Report No. 5	NA	NA	NA	0.83
	DDP	NA	NA	NA	0.83
	Observations	0	0	0	12
MT000599	Report No. 5	NA	NA	NA	0.83
	DDP	NA	NA	NA	0.83
	Observations	0	0	0	12
MT001099	Report No. 5	0.38	NA	NA	NA
	DDP	0.47	NA	NA	NA
	Observations	15	0	0	0

TABLE 3.1. Cont'd

Block: Team		Plate 1	Plate 2	Nozzle 3	Nozzle 9
MT003699	Report No. 5	NA	0.78	0.74	NA
	DDP	NA	0.78	0.74	NA
	Observations	0	18	31	0
NE003699	Report No. 5	0.69	0.72	0.77	0.92
	DDP	0.67	0.74	0.77	0.92
	Observations	15	18	31	12
NS006599	Report No. 5	0.69	0.83	NA	NA
	DDP	0.71	0.83	NA	NA
	Observations	14	18	0	0
RC000897	Report No. 5	NA	NA	NA	0.75
	DDP	NA	NA	NA	0.75
	Observations	0	0	0	12
RC005399	Report No. 5	NA	0.83	NA	NA
	DDP	NA	0.83	NA	NA
	Observations	0	18	0	0
RK004197	Report No. 5	NA	NA	0.77	1.00
	DDP	NA	NA	0.76	1.00
	Observations	0	0	29	12
SD000797	Report No. 5	NA	NA	NA	0.67
	DDP	NA	NA	NA	0.67
	Observations	0	0	0	12
SD004097	Report No. 5	NA	0.67	NA	NA
	DDP	NA	0.67	NA	NA
	Observations	0	18	0	0
SD004198	Report No. 5	0.77	NA	NA	NA
	DDP	0.67	NA	NA	NA
	Observations	15	0	0	0
SD00P314	Report No. 5	0.50	NA	NA	NA
	DDP	NA	NA	NA	NA
	Observations	NA	NA	NA	NA
SDPT0797	Report No. 5	NA	NA	0.65	NA
	DDP	NA	NA	0.65	NA
	Observations	0	0	31	0

TABLE 3.1. Cont'd

Block: Team		Plate 1	Plate 2	Nozzle 3	Nozzle 9
SE000197	Report No. 5	NA	1.00	NA	NA
	DDP	NA	1.00	NA	NA
	Observations	0	18	0	0
SE003797	Report No. 5	NA	NA	NA	0.75
	DDP	NA	NA	NA	0.75
	Observations	0	0	0	12
SM007297	Report No. 5	NA	0.75	NA	NA
	DDP	NA	0.67	NA	NA
	Observations	0	18	0	0
SM007298	Report No. 5	0.62	NA	NA	NA
	DDP	0.53	NA	NA	NA
	Observations	15	0	0	0
SN002799	Report No. 5	NA	1.00	NA	NA
	DDP	NA	1.00	NA	NA
	Observations	0	18	0	0
SR002499	Report No. 5	NA	1.00	NA	NA
	DDP	NA	1.00	NA	NA
	Observations	0	18	0	0
SR00A299	Report No. 5	NA	NA	0.97	NA
	DDP	NA	NA	0.97	NA
	Observations	0	0	31	0
SVB000699	Report No. 5	NA	NA	0.81	NA
	DDP	NA	NA	0.42	NA
	Observations	0	0	31	0
SV005999	Report No. 5	0.54	0.78	NA	NA
	DDP	0.47	0.78	NA	NA
	Observations	15	18	0	0
TH007061	Report No. 5	0.70	NA	NA	NA
	DDP	0.70	NA	NA	NA
	Observations	10	0	0	0
TH007097	Report No. 5	NA	NA	NA	0.73
	DDP	NA	NA	NA	0.70
	Observations	0	0	0	10

TABLE 3.1. Cont'd

Block:		Plate 1	Plate 2	Nozzle 3	Nozzle 9
Team					
THO07099	Report No. 5	NA	0.94	NA	NA
	DDP	NA	0.83	NA	0.30
	Observations	0	18	0	10
TPO01799	Report No. 5	0.38	0.88	0.55	NA
	DDP	0.33	0.78	0.55	0.75
	Observations	15	18	31	12
VHC05599	Report No. 5	0.77	NA	NA	NA
	DDP	0.73	NA	NA	1.00
	Observations	15	0	0	12
YC008099	Report No. 5	NA	1.00	0.80	1.00
	DDP	NA	NA	0.77	0.83
	Observations	0	0	31	12

Team ES000799 illustrates an example where the PNL results and the PISC II results do not agree and PNL cannot ascribe a logical reason for the disagreement. The data in "CLEAN.PROC" indicated that the entire block was scanned and that six flaws were detected; 6 ÷ 15 = 0.40 DDP, yet the PISC II results indicate a DDP of 0.46.

If one assumes that only 13 flaws should be used, then a DDP of 0.46 is correct; however, using 13 flaws is inconsistent with the inspection coverage data. Perhaps the data in "CLEAN.PROC" is wrong.

Implement a Scoring Procedure for PISC Data. PNL has developed a software algorithm that will score data from the RAW.PROC. data file. The algorithm compares the dimensions of each indication for a specific inspection with flaw dimensions given in true-state data for the test plate that was examined. When all indication dimensions x, y, and z intersect with true-state flaw dimensions, the algorithm associates that specific indication with a specific flaw. Thus, a single flaw may have more than one indication associated with it.

Table 3.2 lists inspection data for the specific Team/Procedure AN006498 and compares PISC II scored results with PNL scored results. The columns in Table 3.2 provide the following information:

Column Title	Description
PISC Flaw Reference Number	Page 148 of the "Evaluation of the PISC II Trials Results" provides a reference number for each of the 15 flaws used in scoring Plate 1; it is this flaw number that is referenced in Column 1.

Raw Data Associated Indication Number	Column 2 lists the indication number from the data in RAW.PROC. that was associated with the reference flaw in Column 1. This column provides the scored associations developed by PISC analysis.
PNL Associated Indication Number	Column 3 provides the results of the PNL algorithm in scoring data from RAW.PROC.

Table 3.3 is a listing of the coordinates describing the defects reported by Team/Procedure AN006498. The columns in Table 3.3 provide the following information:

Indication Number	Column 1 provides the indication number from RAW.PROC.
Indication Dimensions	Columns 2-7 provide the indication dimensions for each of the listed indications in Column 10.

Table 3.4 provides the true-state data for each of the 15 flaws in Plate No. 1.

The following provides guidance on using the data in Tables 3.2, 3.3, and 3.4

Reading across the first row of each column in Table 3.3, note that PISC Flaw No. 1 was associated with Indication 1 by PISC II scoring and that the PNL algorithm associates both Indications 1 and 10 with Flaw 1. The validity of the scoring results can be checked by comparing the indication dimensions in Table 3.3 with the true-state flaw dimensions in Table 3.4.

After reviewing the information in Tables 3.2 through 3.4, PNL feels that it would be helpful to understand several key points in the PISC analysis process.

1) When an indication intersects more than one flaw, what criteria were used to further define associations? For example, both Indications 3 and 6 intersected Flaw 1; why did the PISC II analysis choose Indication 3 over Indication 6 to be associated with Flaw 1?

2) What tolerance was used to make the associations in RAW.PROC?

3) Why was Indication 3 not also associated with Flaw 8?

TABLE 3.2. Comparison of PNL Scored Results with PISC-II Results for Team AN006498 (Example)

Team = AN006498 Block = 1

Inspected Dimension: X = 313, 713; Y = 0, 1045; Z = 0, 246

PISC Flaw Reference Number	Raw Data Associated Indication Number	PNL Associated Indication Number
1	3	3, 6
2	3	3
3	19	0
4	0	0
5	28	3, 28
6	30	0
7	32	32
8	0	3
9	39	0
10	6	3, 6
11	0	0
12	0	0
13	0	0
14	0	0
15	13	0

TABLE 3.3. Indication Dimensions for Team AN006498 (Example)

Indication Number	x1	x2	y1	y2	z1	z2
3	370.4	482.0	75.0	914.5	83.3	147.8
3*	448.0	448.0	75.0	95.0	147.6	147.8
19	488.5	492.0	85.0	105.0	204.3	214.3
28	370.4	475.4	254.5	364.5	93.1	144.5
30	463.4	528.9	325.5	405.5	13.0	44.4
32	432.7	495.0	462.8	545.0	189.7	225.5
39	463.0	463.2	565.0	565.2	64.5	79.5
6	370.9	482.0	643.5	914.5	83.3	145.0
13	463.4	528.9	-67.0	405.5	1.6	44.4

*Indications have same number in raw data.

TABLE 3.4. True State Dimensions for Team AN006498 (Example)

Flaw Reference Number	X1	X2	Y1	Y2	Z1	Z2
1	470	478	3	1000	117	132
2	418	430	86	135	122	132
3	484	488	70	130	216	221
4	434	450	105	171	38	47
5	409	434	235	433	122	142
6	438	446	275	343	8	16
7	461	489	452	545	211	225
8	417	422	469	472	127	130
9	432	443	486	570	36	51
10	418	442	655	763	121	138
11	433	442	682	778	37	42
12	438	448	682	778	8	15
13	452	455	682	790	1	5
14	463	464	465	610	16	18
15	458	461	0	475	8	11

3.1.4 Future Work

The next step will be an analysis of the PISC-II data using the methods proposed in the work plan reported in Volume 8 of this series. This will include the creation of grading units within the test blocks and generation of the corresponding test statistics. Planned analyses include the generation of POD curves, an ROC analysis, and a sizing analysis that employs some suggestions made by Mr. Davies from the United Kingdom.

3.2 EQUIPMENT INTERACTION MATRIX

3.2.1 Summary

This work is directed towards evaluation of the effects of frequency domain equipment interactions and determination of tolerance values for improving ultrasonic inspection reliability. An analysis is being performed to evaluate frequency domain effects using a computer model to calculate the flaw transfer function.

Preliminary analysis using model-predicted, worst-case flaws indicated that the equipment bandwidth tolerance of ±10% in ASME Code Case N-409-1 is sufficient to ensure a ±10% measurement repeatability. The ±10% center frequency tolerance in the ASME Code was found to be too broad to ensure ±10% measurement repeatability.

The model results suggested that the equipment center frequency and bandwidth interactions are due in part to phase cancellation along the receiving transducer face. Therefore, the receiving transducers for dual element and tandem search units should be as small as practical to minimize sensitivity to equipment changes.

It was found that even though the flaw model was two-dimensional, the calculated transfer functions were very similar to those that would be calculated by a three-dimensional model. Thus, these sensitivity study results can be extended to three-dimensional systems.

3.2.2 Introduction

The goal of this work is to define operating tolerance requirements for UT/ISI equipment that minimize the effects of frequency domain interactions, thus, improving ISI reliability. This is to be accomplished in the following steps:

1. Developing and validating a flaw model
2. Integrating the flaw model into the previously developed UT/ISI equipment models
3. Performing a sensitivity study on equipment parameters using the equipment and flaw models
4. Recommending equipment tolerance requirements for UT/ISI

3.2.3 Status of Work Performed

Introduction. In previous reports, a model to calculate the transfer functions (frequency responses) of various flaws in a steel sample was described (Doctor, et al. 1989), and comparisons between model predictions and single frequency (tone-burst signal) experiments were used to establish the validity of the model for beam pattern prediction (Doctor, et al. 1988). Since that time, the following work has been completed:

1. The model predictions were compared with results from several multi-frequency experiments and good agreement was found. This provided evidence for the validity of the model for predicting the transfer functions of worst-case flaws.
2. The transfer functions for seven different worst-case flaws were calculated for use in an equipment parameter sensitivity study for thin sections (piping).

3. Equipment bandwidth and center frequency sensitivity studies were performed for thin sections (piping) using worst-case flaw transfer functions.

4. A paper was presented at the 1988 Review of Progress in QNDE conference and submitted for publication in the conference proceedings (Green and Mart, 1988).

5. A method of reducing frequency domain equipment interactions through the use of a phase-insensitive receiving probe was identified.

6. A simple calculation was performed to examine the differences in flaw transfer functions calculated by the two-dimensional model used in the interaction matrix study and more complex three-dimensional models.

Model Validation. Pulse-echo measurements were made on a set of available aluminum blocks with the ends cut at various angles between 40° and 49° as shown in Figure 3.2. A very broad-band ultrasonic system was used in conjunction with the computer-based ultrasonic spectroscopy system described in Doctor, et al. (1988) to determine transfer functions for the blocks. The block measurements represent specular reflections from large (100% through-wall), smooth flaws at various angles. Corresponding model calculations were made for comparison with the response from the block ends.

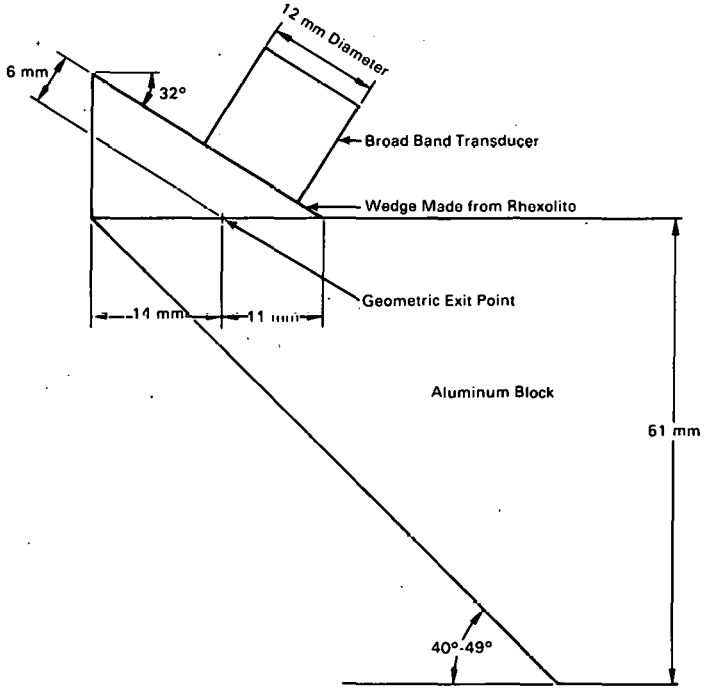

FIGURE 3.2. Configuration Used to Measure the Transfer Functions Associated with Specular Reflection from Large, Smooth Flaws at Various Angles

Preliminary measurements revealed the difficulty of making accurate and repeatable frequency-domain, ultrasonic measurements, so several special experiment controls were used as follows:

1. A wedge made of low-acoustic-attenuation Rhexolite plastic was constructed with an exit angle of 45° in aluminum.

2. Extra care was taken in producing a reliable ultrasonic coupling (petroleum jelly couplant) between the transducer and the wedge.

3. A mixture of 50% Ultragel and 50% tap water was used as couplant between the wedge and the aluminum block. This mixture was found to produce more repeatable results than either water, pure Ultragel, or petroleum jelly.

4. A fixture was used to carefully align the probe with the end of the block. Even very small amounts of probe misalignment (skew) were found to have a significant effect on the frequency domain especially at high frequencies. The effect of skew on the high frequency portion of the frequency spectrum was much greater than the corresponding change in the appearance of the time domain signal.

5. Many settings on the PNL-designed square wave pulser were tried in order to extend the range of the frequency measurements. Eventually a setting was found that provided a range of validity of approximately 700 kHz to 6 MHz.

Model versus experimental results are shown in Figures 3.3 through 3.11. The range of validity for the experimental measurements was 700 kHz to 6 MHz, and the range was similar for the model results. In each case, the results were normalized with respect to the spectrum of the 45° block reflection. In general, the comparisons between experimental data and model predictions were good, but there were some differences.

Figure 3.3 shows the normalized transfer functions for the 49° block. Below 3 MHz, the measured transfer function is significantly greater in amplitude than the predicted result. This trend was also evident for the 48°, 47°, 42°, and 41° blocks; and it grew worse with greater deviation from 45°. This apparent amplification at low frequencies is currently unexplained.

The model did well in predicting the location of the first minimum in the flaw frequency response. Comparisons are made in Table 3.5. The ability to predict the minimum is of primary importance, since this feature distinguishes some flaws as worst case. The response of a flaw having a minimum at the inspection system's center frequency will be sensitive to bandwidth and center frequency changes, and is, thus, considered a worst-case flaw. The 41° and 40° blocks were predicted by the model to be worst-case flaws for a typical 2-MHz inspection system, and the measurements confirmed this prediction. In general, the model was completely successful in its ability to predict worst-case flaws.

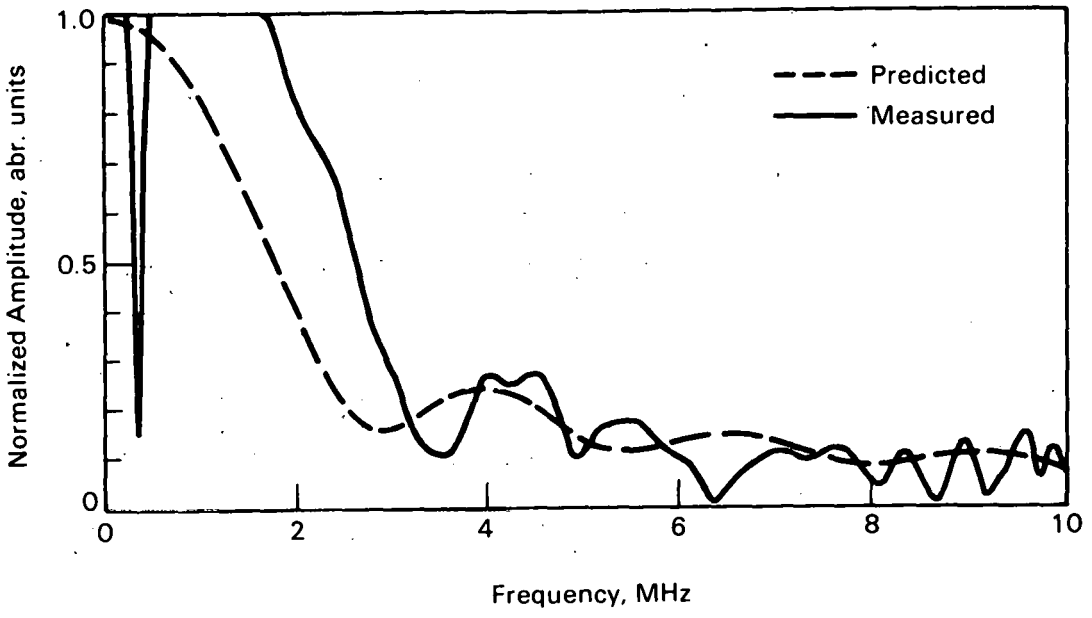

FIGURE 3.3. Measured Versus Predicted Transfer Functions for 49° Flaw Normalized with respect to 45° Flaw

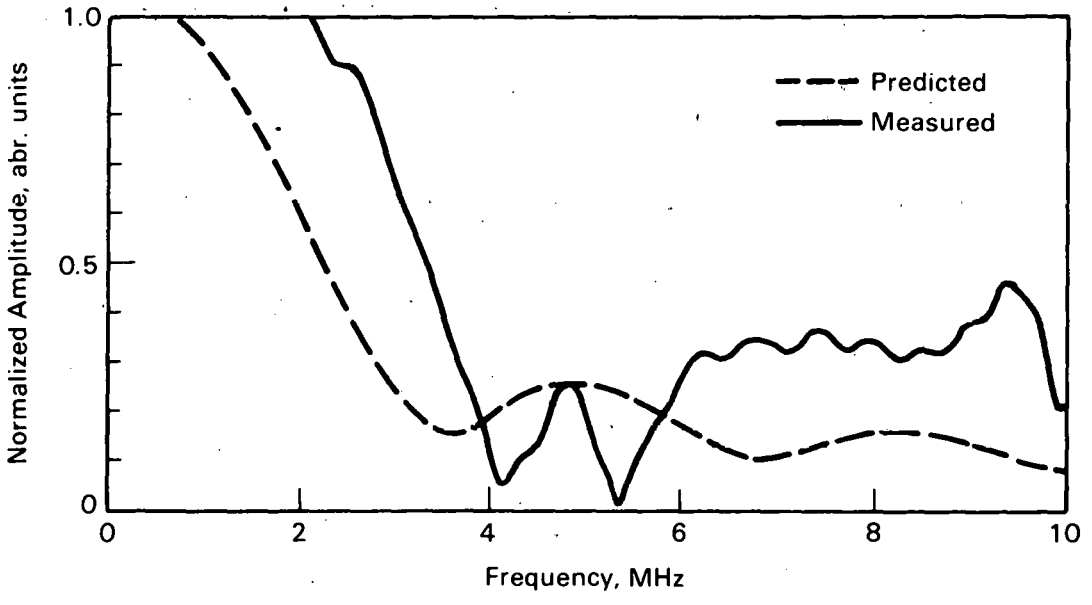

FIGURE 3.4. Measured Versus Predicted Transfer Functions for 48° Flaw Normalized with respect to 45° Flaw

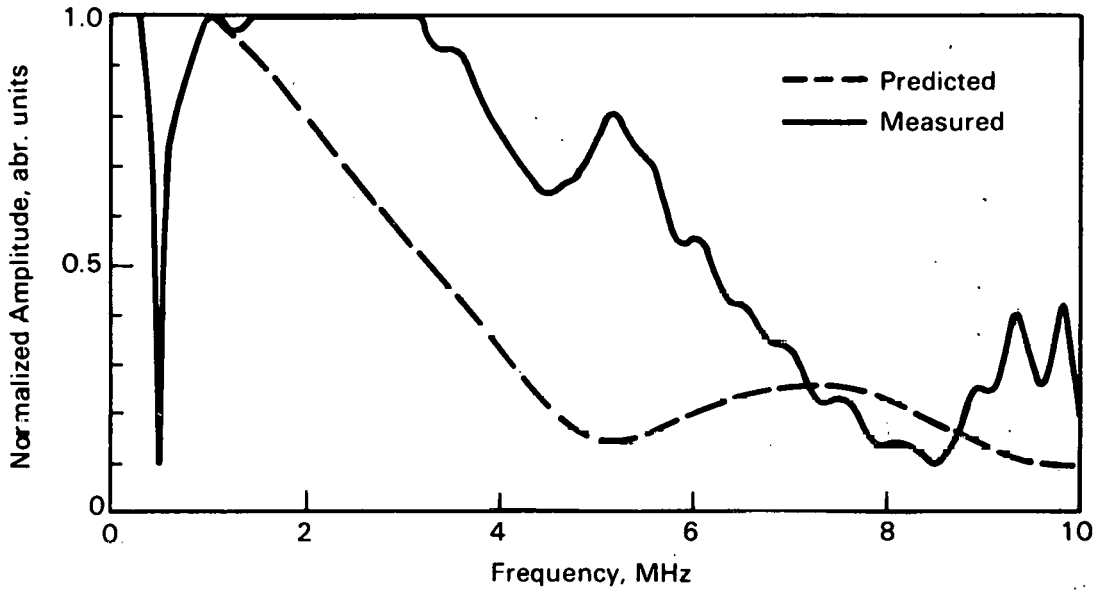

FIGURE 3.5. Measured Versus Predicted Transfer Functions for 47° Flaw Normalized with respect to 45° Flaw

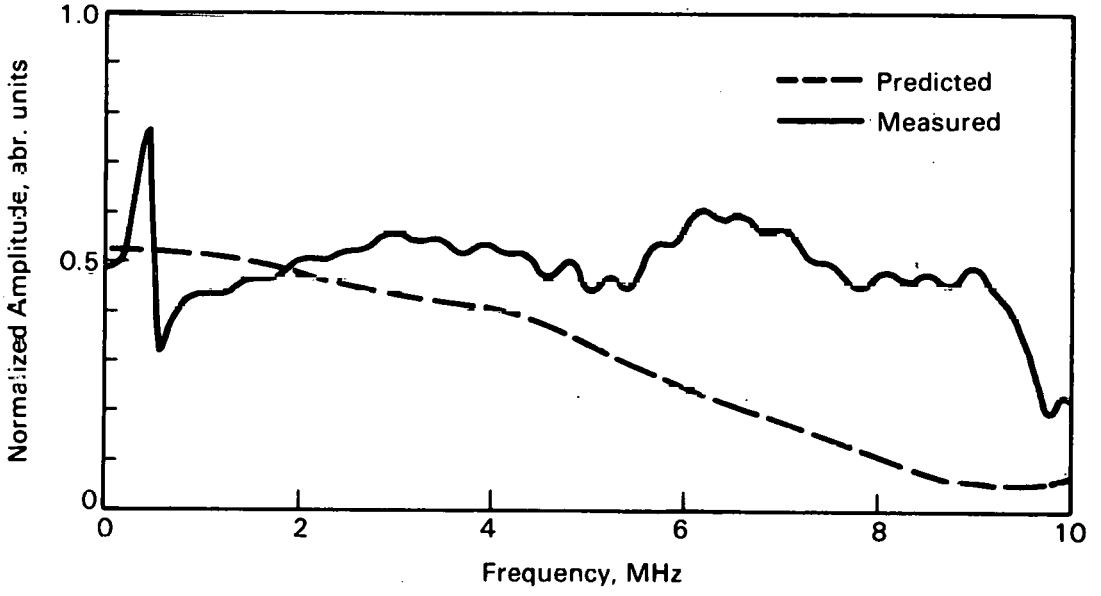

FIGURE 3.6. Measured Versus Predicted Transfer Functions for 46° Flaw Normalized with respect to 45° Flaw

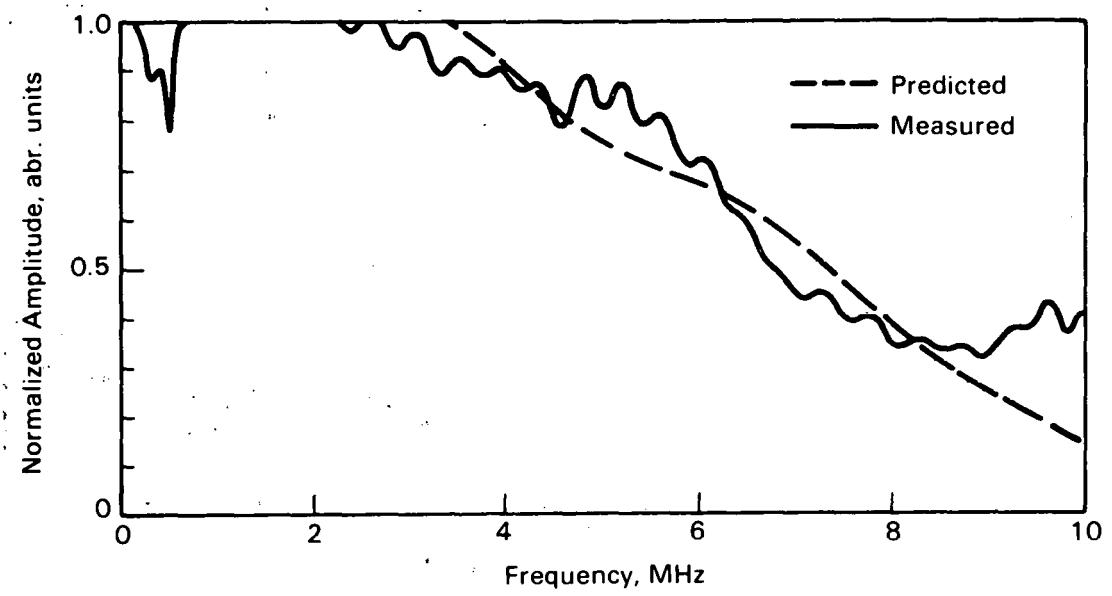

FIGURE 3.7. Measured Versus Predicted Transfer Functions for 44° Flaw Normalized with respect to 45° Flaw

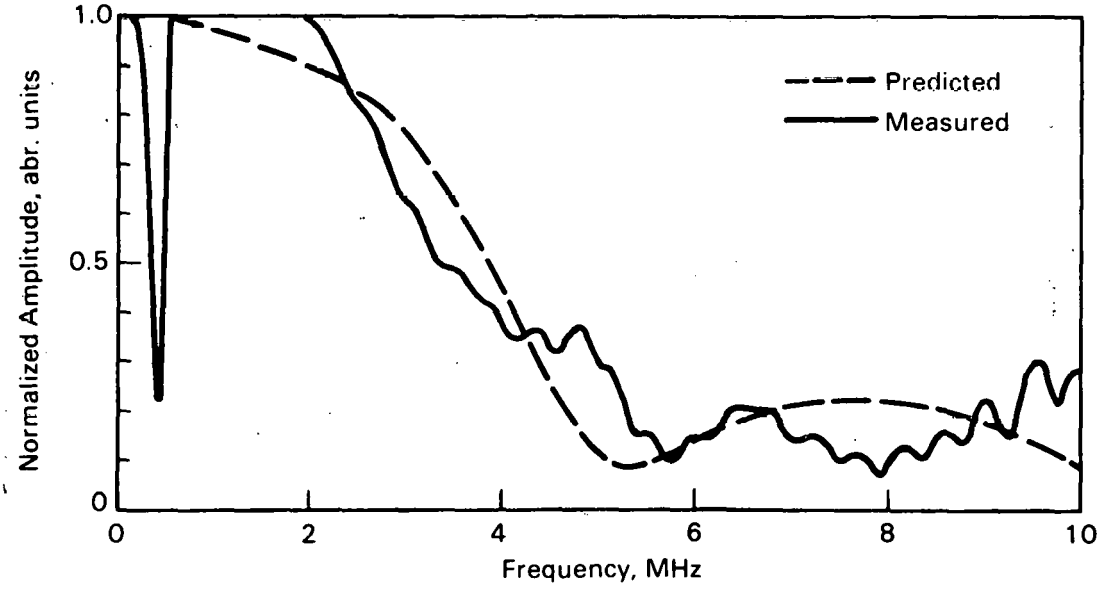

FIGURE 3.8. Measured Versus Predicted Transfer Functions for 43° Flaw Normalized with respect to 45° Flaw

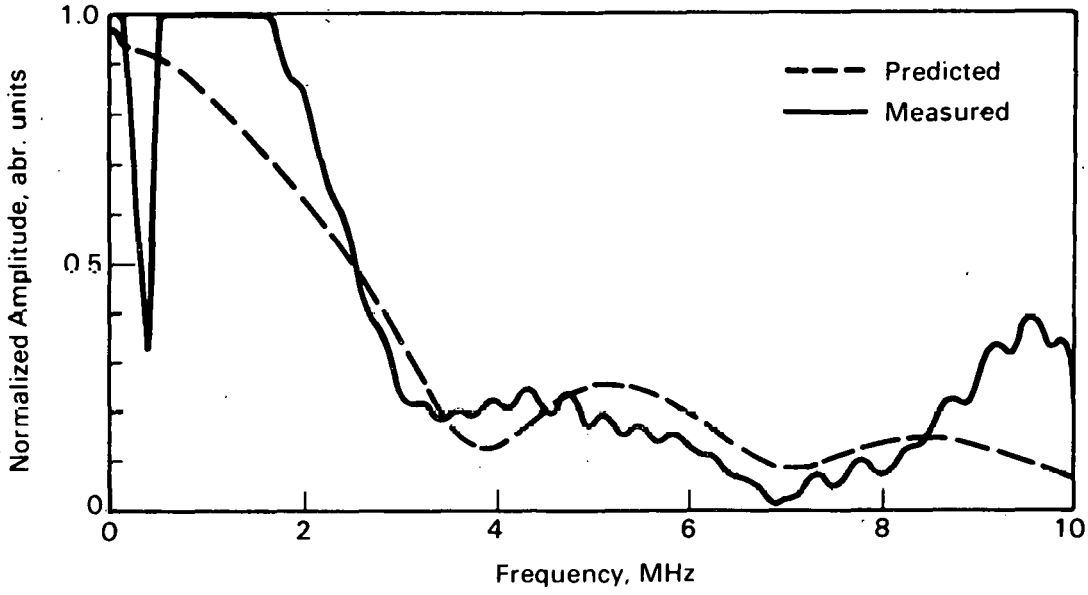

FIGURE 3.9. Measured Versus Predicted Transfer Functions for 42° Flaw Normalized with respect to 45° Flaw

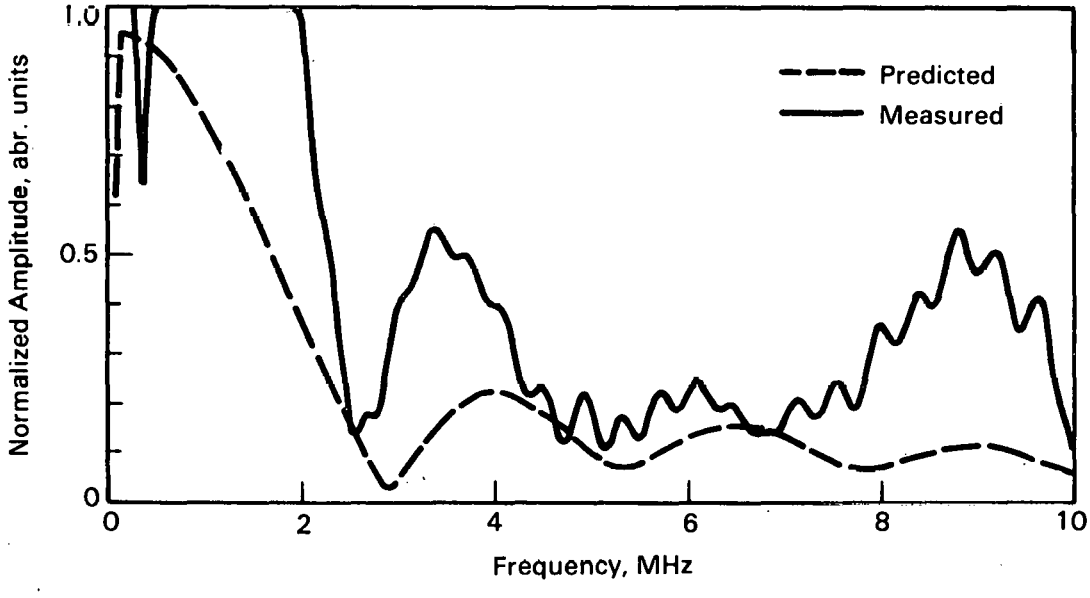

FIGURE 3.10. Measured Versus Predicted Transfer Functions for 41° Flaw Normalized with respect to 45° Flaw

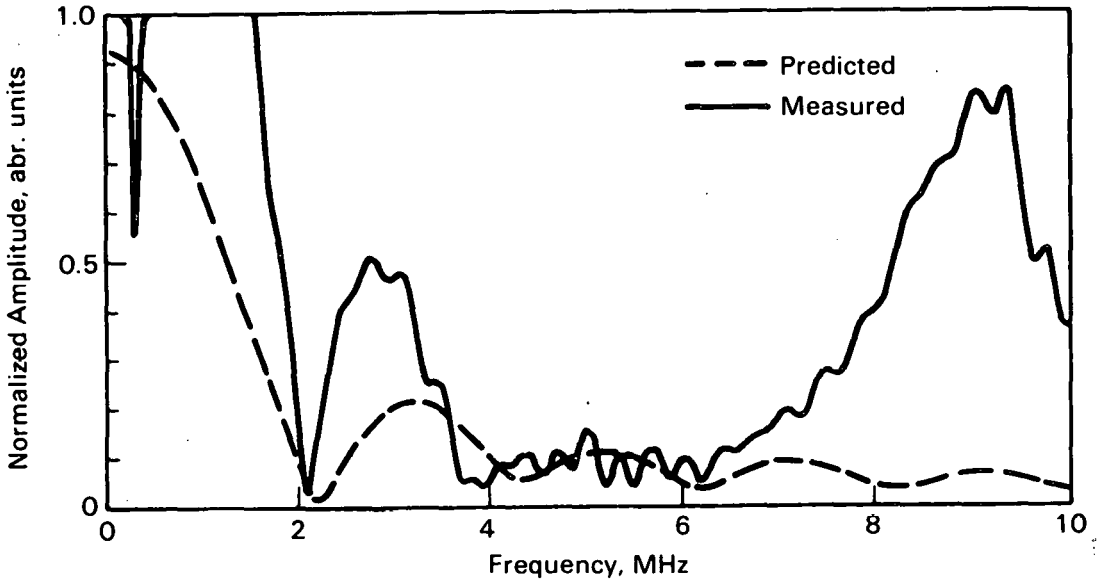

FIGURE 3.11. Measured Versus Predicted Transfer Functions for 40° Flaw Normalized with respect to 45° Flaw

TABLE 3.5. Comparison Between Predicted and Measured First Minimum in the Flaw Transfer Function

Angle Degrees	Measured MHz	Predicted MHz
49	3.5	2.75
48	4.0	3.5
47	4.5	5.0
46	None	None
44	None	None
43	5.75	5.5
42	3.5	4.0
41	2.5	3.0

One last effect to notice is how much the transfer functions changed for a change of block angle of 1°. Part of this effect was due to measurement irrepeatability, but much of it seems to have been real. This suggests that slight flaw shape irregularities may have an impact on detection reliability.

To summarize, comparisons between measured data and model predictions confirmed the model's ability to predict worst-case flaws. Differences between measured data and model results were not large compared to changes associated with slight angle deviations and repeatability errors.

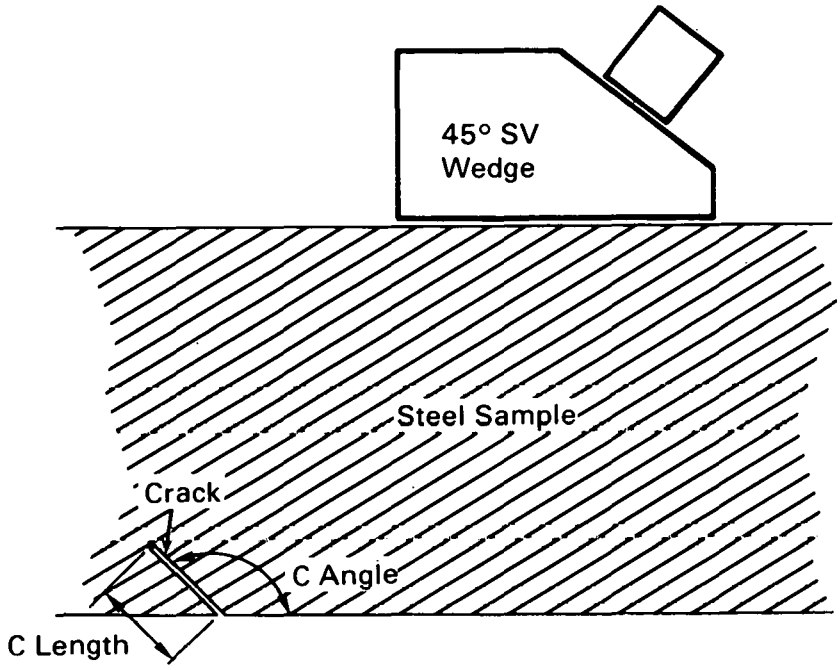

FIGURE 3.12. Configuration of Pulse-Echo Ultrasonic Test System

Worst-Case Flaw Calculations. Seven worst-case flaws were identified for the common pulse-echo inspection configuration shown in Figure 3.12. The seven cases were made up of various combinations of probe size, flaw angle, and pipe section thickness as shown in Table 3.6. In each case, the flaw was smooth, flat, semi-infinite, back surface connected, and 90% through-wall.

TABLE 3.6. Worst-Case Flaw Configurations

Flaw	Pipe Wall Thickness, mm	Transducer Diameter, mm	Flaw Angle, Degrees
B	19	6	33
C	19	13	96.5
D	19	13	42
E	76	13	96.5
F	76	13	41
G	76	25	93.5
H	76	25	44.5

The seven cases were determined by taking common combinations of probe size and pipe wall thickness and adjusting the flaw angle until a transfer function minimum occurred at 2.25 MHz. Transfer functions with minima at 2.25 MHz were chosen as worst case because, when convolved with the typical bell shaped

frequency spectrums of inspection equipment, the resulting responses were sensitive to frequency domain equipment changes such as changes in center frequency and bandwidth. An equipment center frequency of 2.25 MHz was chosen, since this is the most commonly used test frequency. The transfer functions for the seven worst-case flaws as calculated by the model are shown in Figure 3.13. The relative amplitude of the transfer functions in Figure 3.13 should not be directly compared, because no normalizing calibration factors were used in the calculations.

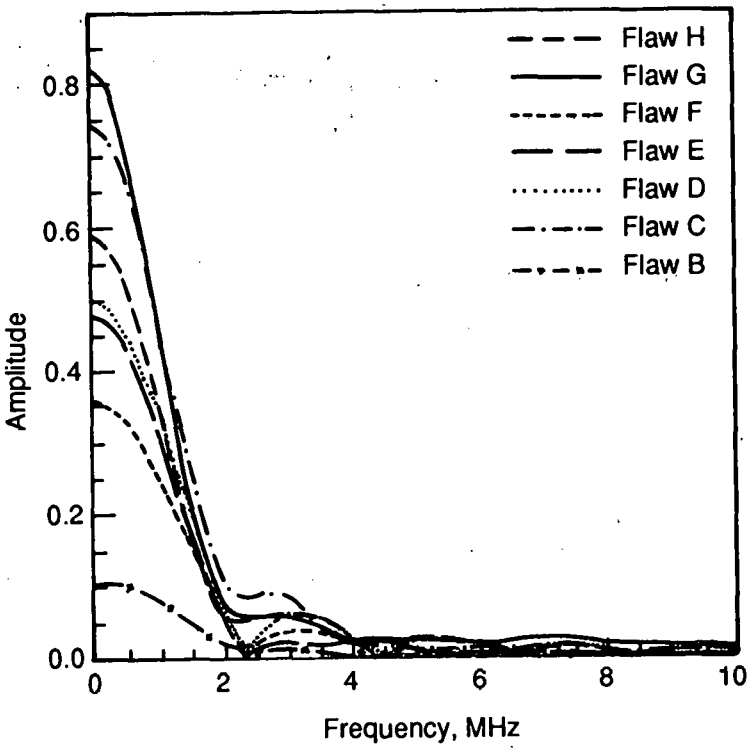

FIGURE 3.13. Worst-Case Flaw Transfer Functions

Equipment Bandwidth Sensitivity Study. An equipment bandwidth sensitivity study was conducted by convolving the worst-case flaw transfer functions with frequency spectra representative of ultrasonic inspection systems (pulser, probes, receiver, and video combined) with bandwidths ranging from 273 kHz (narrow-band) to 3.48 MHz (broad-band). In each case, the equipment center frequency remained at 2.25 MHz. Convolution of the flaw transfer function and equipment spectrum was transformed to the time domain by the inverse Fourier transform and the maximum absolute value of the time domain signal was noted. This result was divided by a calibration factor that was determined by convolving the same equipment spectrum with the transfer function of a 10% through-wall notch and taking the maximum absolute value of the inverse Fourier transform. One curve of calibrated amplitude versus bandwidth was plotted for each worst-case flaw, and the resulting sensitivity curves for all seven worst-case flaws are shown in Figure 3.14.

Assume that it is desired that the calibrated signal response of a flaw change no more than 10% after an equipment change. For the seven worst-case flaws, would the bandwidth tolerance of 10% as given in ASME Code Case N-409-1 be sufficient to satisfy this desire? In Figure 3.15, 10% tolerance curves were superimposed over the sensitivity curves. When the sensitivity curve was steeper than the local 10% tolerance curve, the 10% tolerance would fail to ensure repeatability of 10% after an equipment change. There were only two or three areas where the sensitivity curves were only slightly steeper than the 10% tolerance curves. Assuming that the sensitivity analysis presented here can be considered conservative because it uses only worst-case flaws, the 10% bandwidth tolerance in ASME Code Case N-409-1 is sufficient to ensure 10% calibrated signal response repeatability after an equipment change.

In Figure 3.16, 5% tolerance curves are superimposed over the sensitivity curves. The sensitivity curves are flatter everywhere than the tolerance curves, so a 5% equipment bandwidth tolerance would be sufficient to ensure 10% repeatability even for worst-case flaws.

Figure 3.17 shows 20% tolerance curves superimposed over the sensitivity curves. The sensitivity curves are steeper than the local tolerance curves about half the time and, thus, would not assure a 10% limit in system response to these flaws.

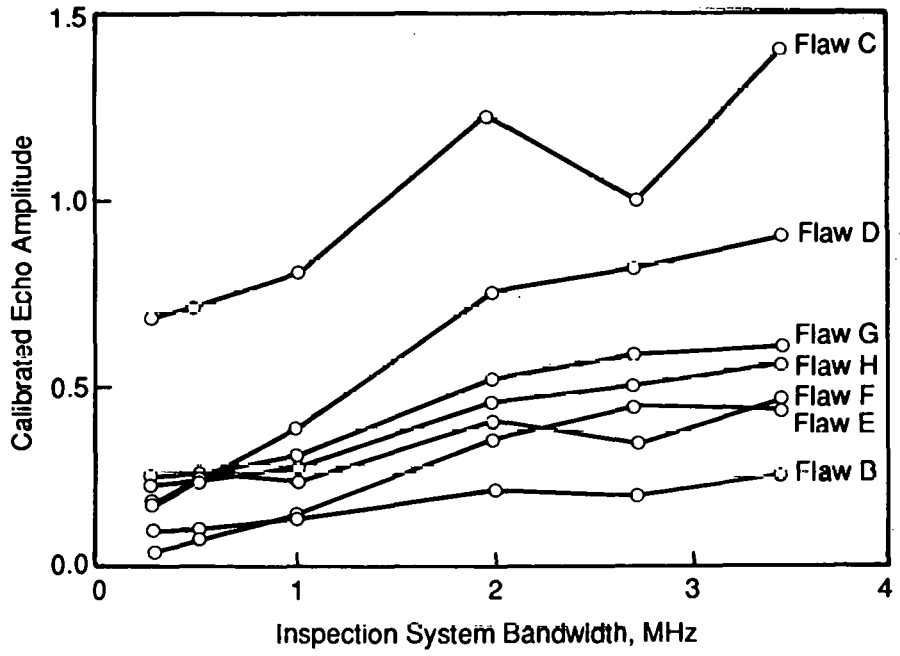

FIGURE 3.14. Bandwidth Sensitivity Study Results

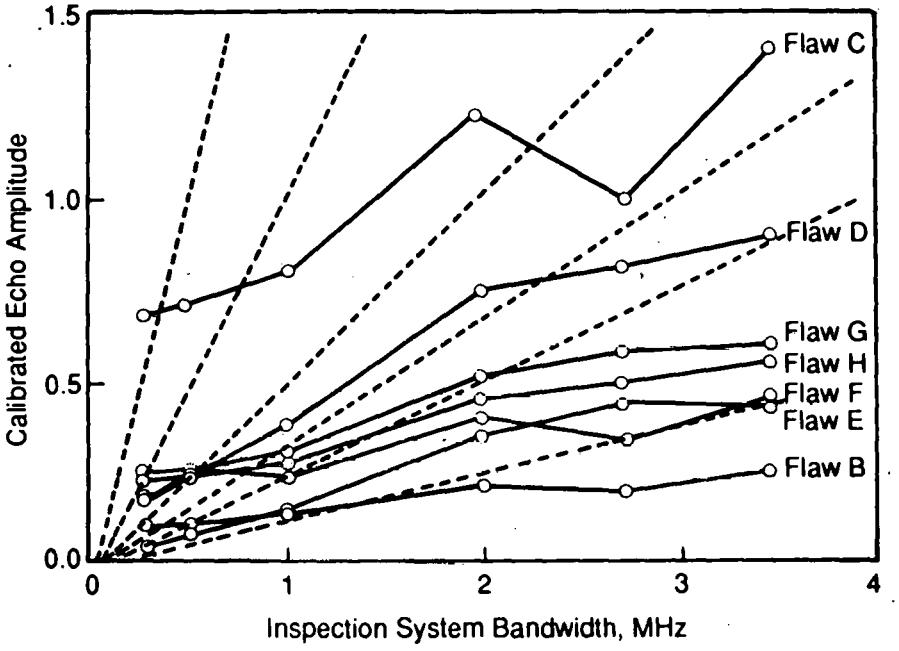

FIGURE 3.15. Bandwidth Sensitivity Study Results with 10% Tolerance Lines Superimposed

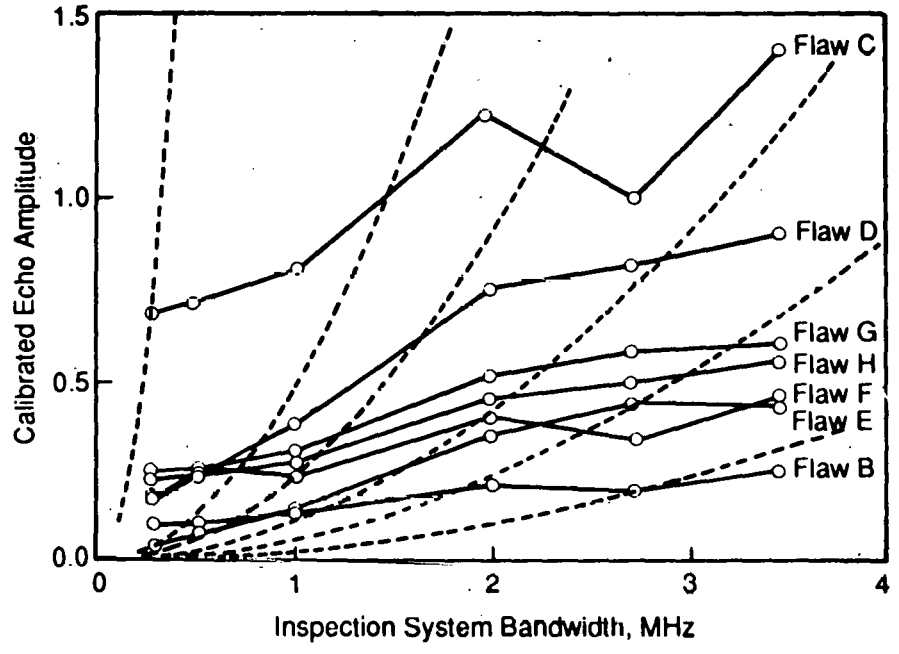

FIGURE 3.16. Bandwidth Sensitivity Study Results with 5% Tolerance Lines Superimposed

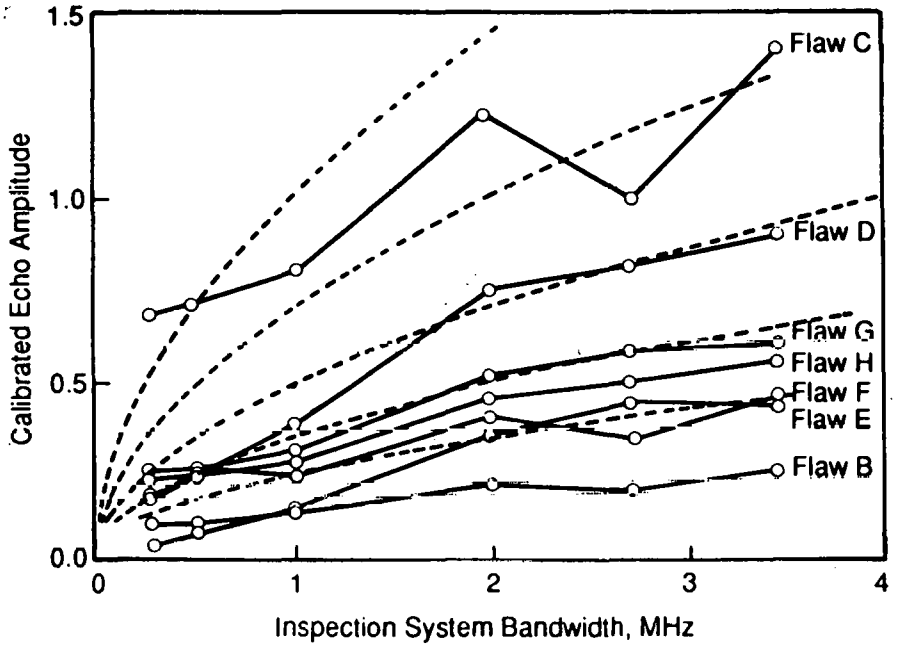

FIGURE 3.17. Bandwidth Sensitivity Study Results with 20% Tolerance Lines Superimposed

Center Frequency Sensitivity Study. The center frequency sensitivity study was similar to the bandwidth study except that center frequency was added to the comparison matrix. In other words, the effect of equipment center frequency changes about a nominal value of 2.25 MHz was determined for various flaw and equipment bandwidth combinations. Center frequency sensitivity calculation results for flaws B, C, D, E, F, G, and H are plotted in Figures 3.18 through 3.24, respectively.

For the seven worst-case flaws, would the center frequency equipment tolerance of 10% as given in ASME Code Case N-409-1 be sufficient to ensure 10% signal amplitude repeatability after an equipment change? In Figures 3.25 through 3.31, 10% tolerance curves are shown superimposed on the sensitivity curves as was done in the bandwidth sensitivity study above. These figures indicate that 10% repeatability was achieved only for equipment with a bandwidth of 3.5 MHz or greater given the 10% center frequency tolerance. This suggests that the response was much more sensitive to equipment center frequency changes than bandwidth changes, and that current ASME Code center frequency standards may not be adequate to ensure repeatable inspection when equipment changes are made.

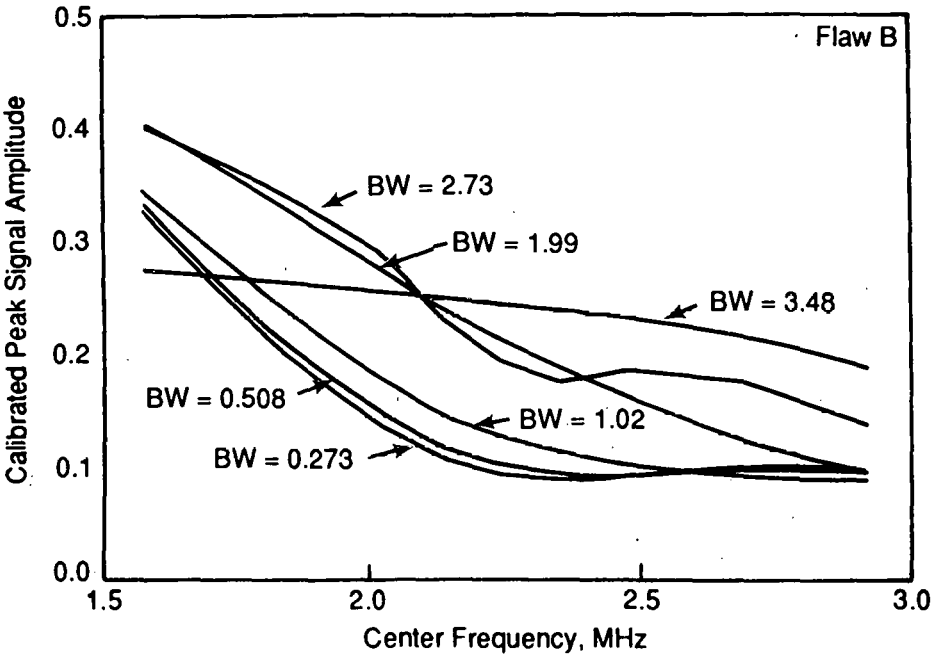

FIGURE 3.18. Center Frequency Sensitivity Study Results for Flaw B

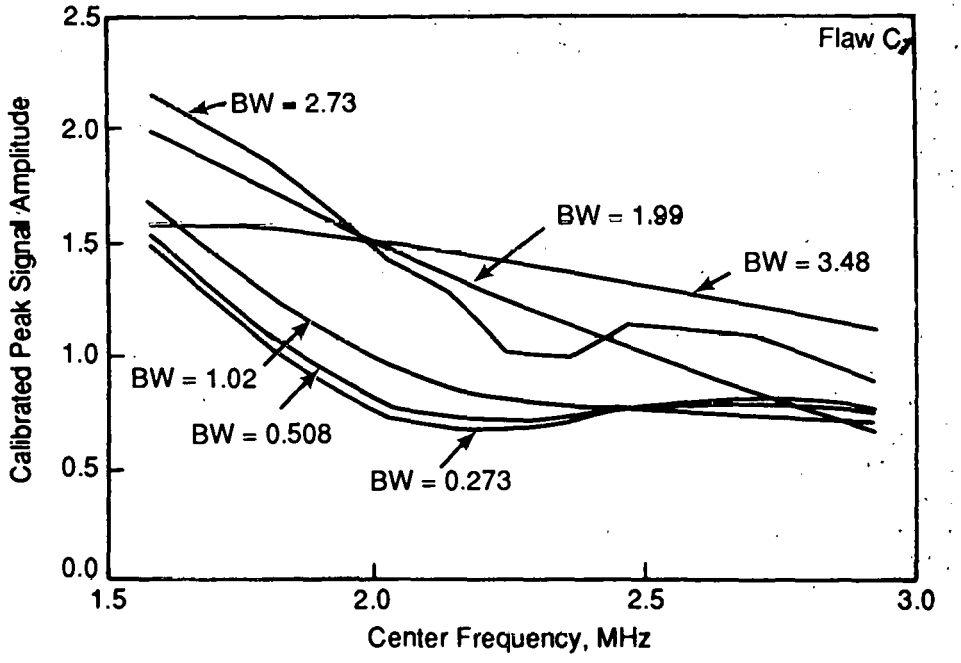

FIGURE 3.19. Center Frequency Sensitivity Study Results for Flaw C

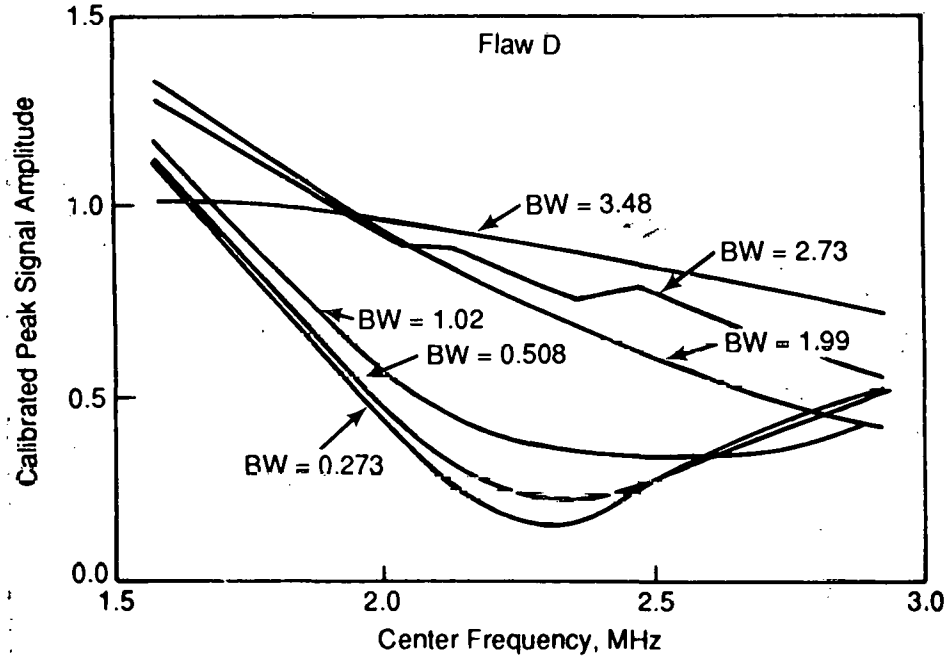

FIGURE 3.20. Center Frequency Sensitivity Study Results for Flaw D

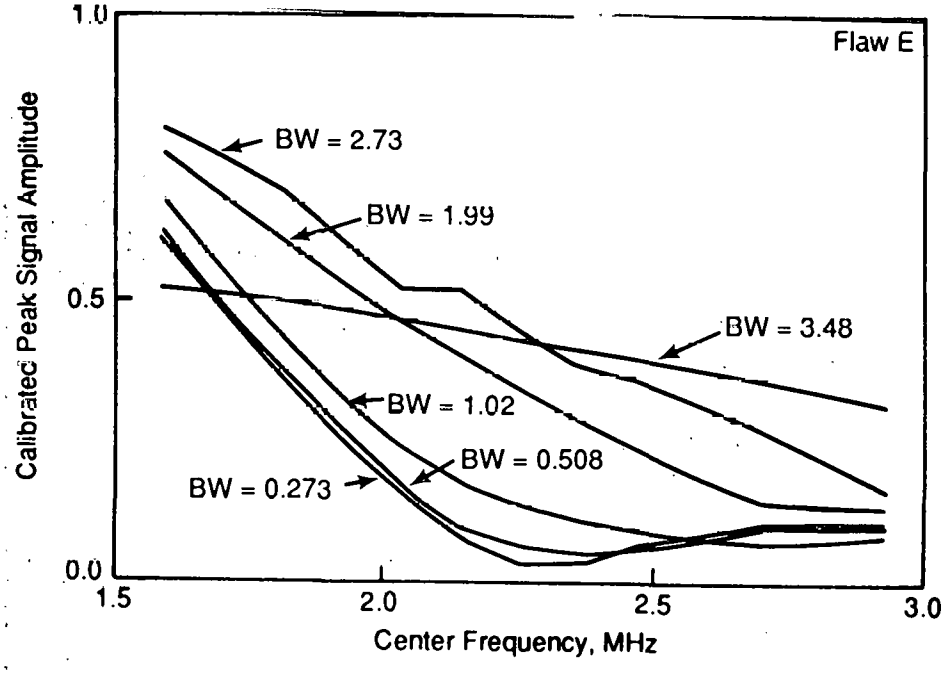

FIGURE 3.21. Center Frequency Sensitivity Study Results for Flaw E

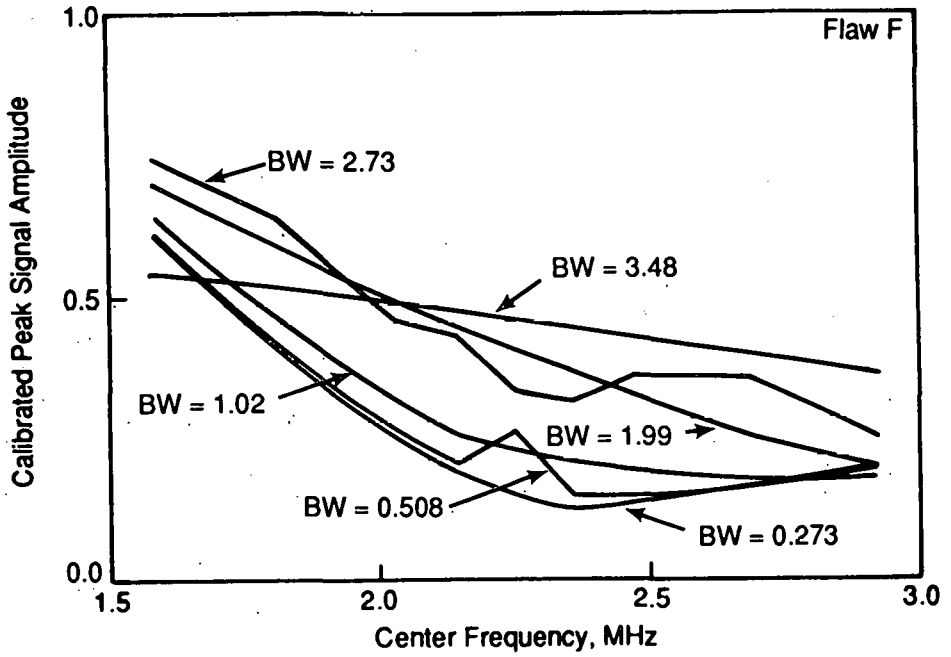

FIGURE 3.22. Center Frequency Sensitivity Study Results for Flaw F

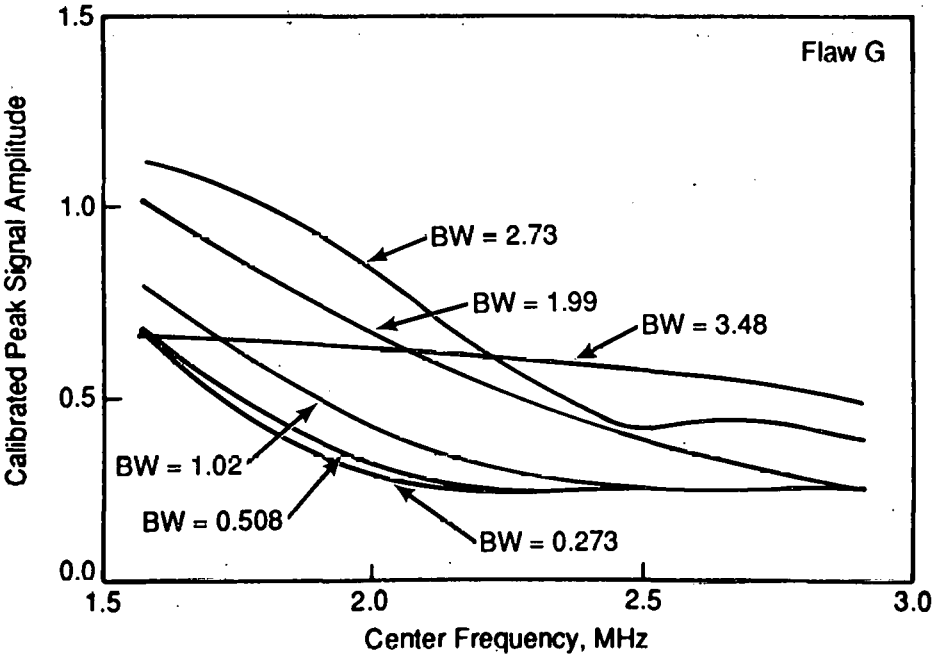

FIGURE 3.23. Center Frequency Sensitivity Study Results for Flaw G

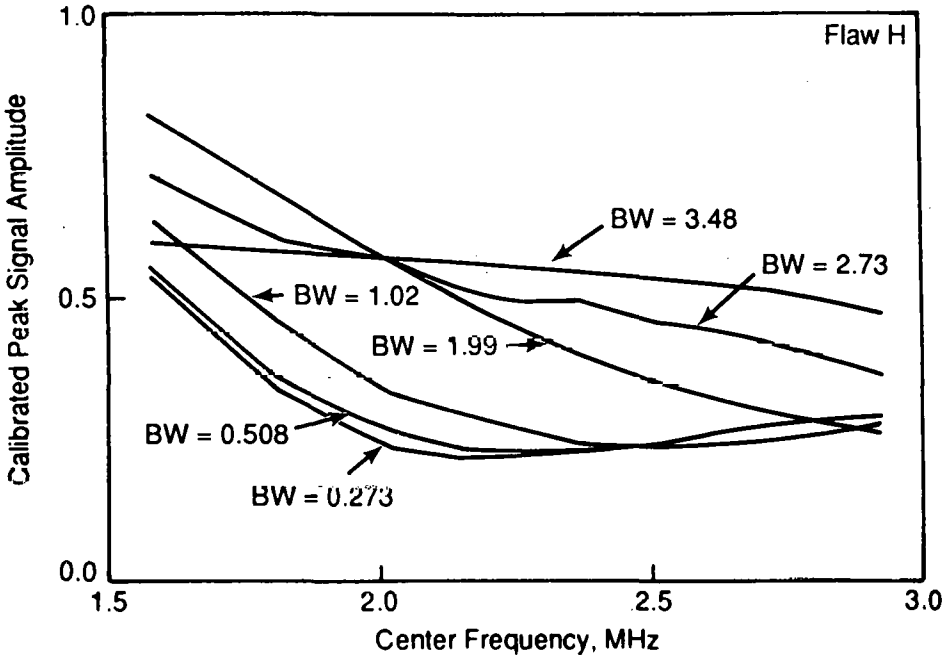

FIGURE 3.24. Center Frequency Sensitivity Study Results for Flaw H

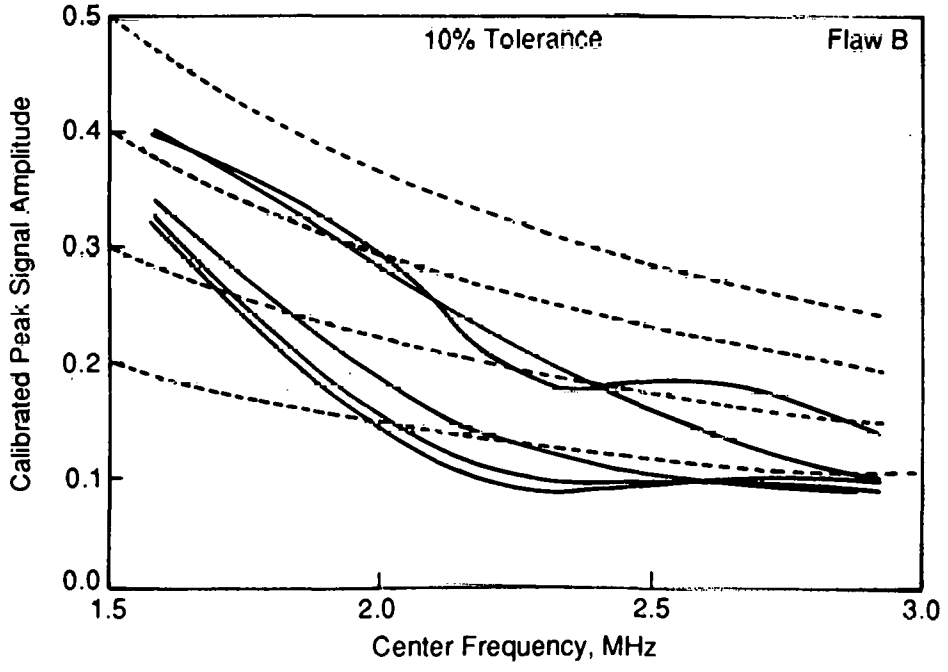

FIGURE 3.25. Center Frequency Sensitivity Study Results for Flaw B with 10% Tolerance Lines Superimposed

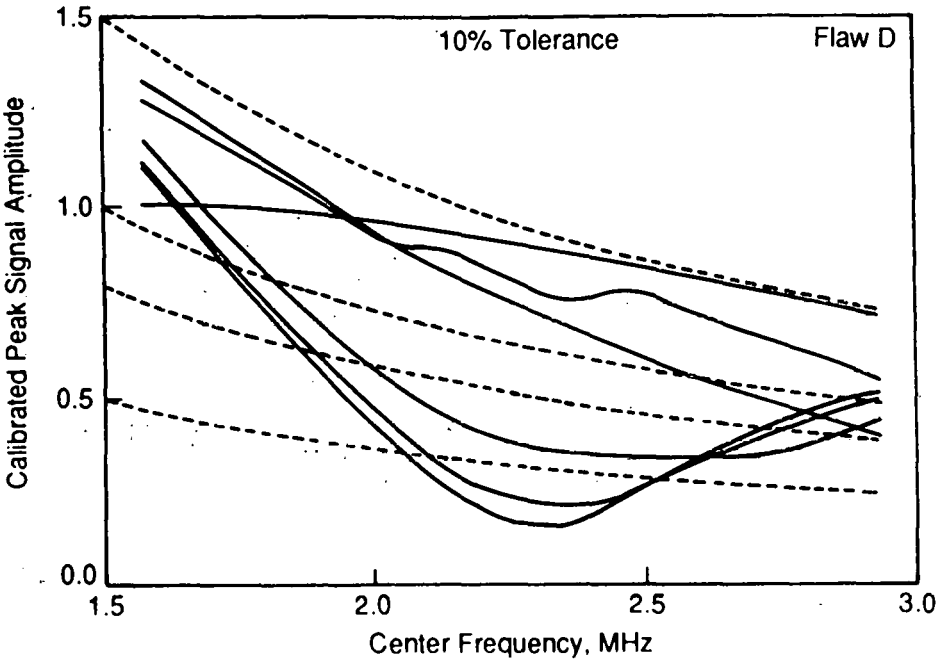

FIGURE 3.26. Center Frequency Sensitivity Study Results for Flaw C with 10% Tolerance Lines Superimposed

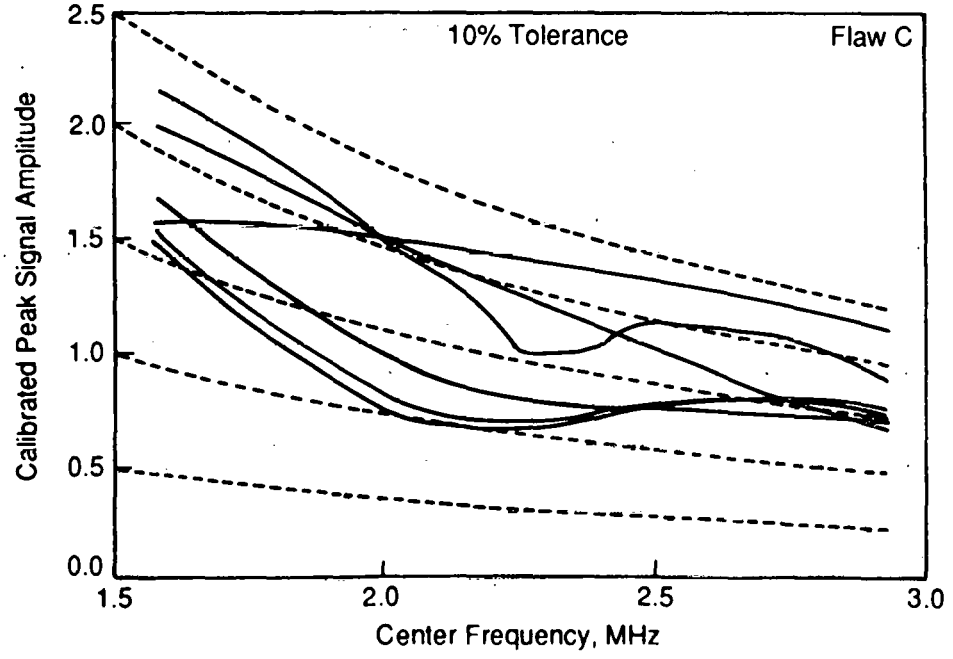

FIGURE 3.27. Center Frequency Sensitivity Study Results for Flaw D with 10% Tolerance Lines Superimposed

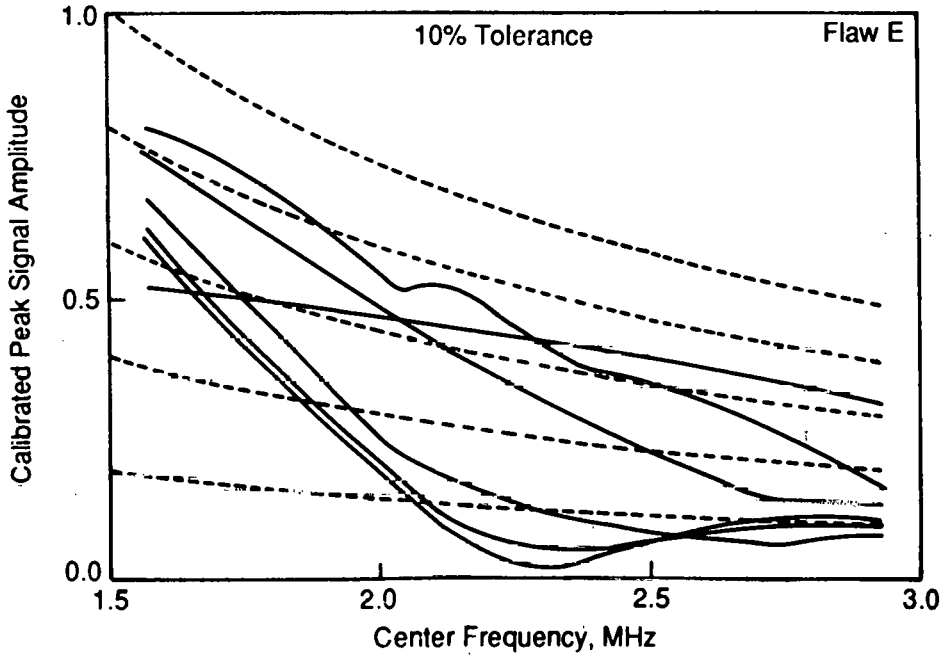

FIGURE 3.28. Center Frequency Sensitivity Study Results for Flaw E with 10% Tolerance Lines Superimposed

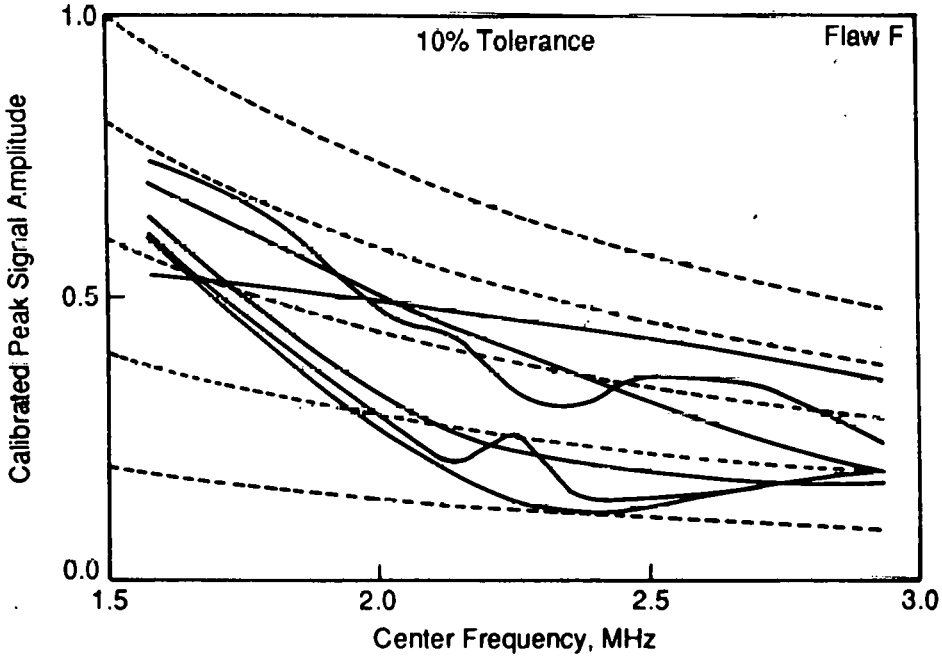

FIGURE 3.29. Center Frequency Sensitivity Study Results for Flaw F with 10% Tolerance Lines Superimposed

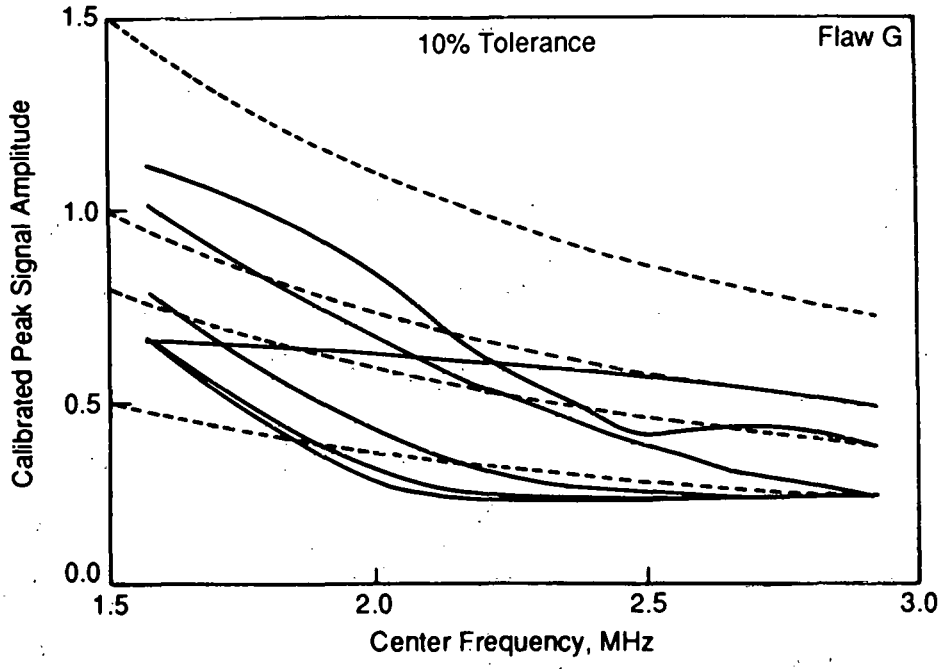

FIGURE 3.30. Center Frequency Sensitivity Study Results for Flaw G with 10% Tolerance Lines Superimposed

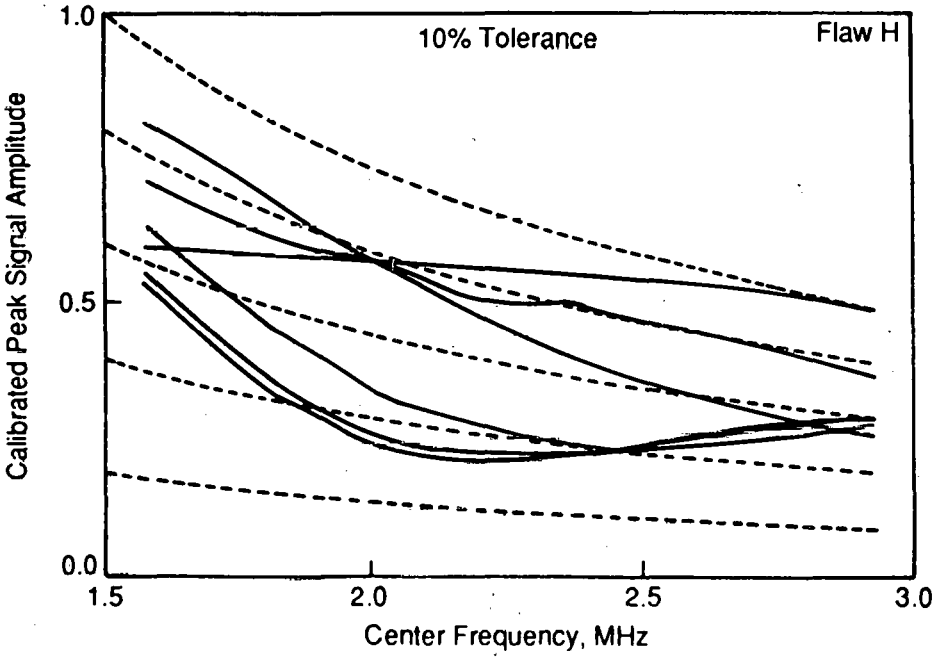

FIGURE 3.31. Center Frequency Sensitivity Study Results for Flaw H with 10% Tolerance Lines Superimposed

In Figures 3.32 through 3.45, 5% and 2.5% tolerance curves are shown superimposed on the sensitivity curves. The 5% tolerance was sufficient for 1.99 MHz and 2.73 MHz bandwidth equipment except in just a few cases. Even tightening the center frequency tolerance to 2.5% did not allow the 0.273 MHz, 0.508 MHz, and 1.02 MHz bandwidth equipment to consistently maintain 10% repeat ability for worst-case flaws.

In summary, specifying an allowable equipment center frequency tolerance for narrow band equipment will be a problem.

Phase Insensitive Receiver. As mentioned above, it is the sharp minima in the flaw transfer functions that produce sensitivity to frequency domain equipment changes. Therefore, eliminating the transfer function minima would greatly decrease frequency domain equipment interactions.

In order to determine why the flaw transfer function minima occur, the amplitude and phase of the sound field were examined along the face of the receiving transducer. Calculations were made for the case of specular reflection from the end of an aluminum block as shown in Figure 3.2. The calculated transfer function as shown in Figure 3.3 has minima at approximately 2 MHz and 4 MHz.

The amplitude of the sound field (as calculated by the model) along the receiving transducer face (i.e., between the transducer and the wedge) is plotted in Figure 3.46 for frequencies of 200 kHz, 500 kHz, 1 MHz, 2 MHz, 5 MHz, and 10 MHz. At each frequency, the receiving transducer was fully insonified, and the peak amplitude was near the center of the transducer. The amplitude decreased gradually as frequency increased. Thus, the amplitude of the sound field does not indicate why the transfer function minima occur at 2 MHz and 4 MHz.

The relative phase of the sound field (as if the sound field were frozen for a moment in time) along the transducer face is shown in Figure 3.47. At 200 kHz and 500 kHz, the phase was nearly constant over the face of the transducer, and at 1 MHz the phase changed a little more than 90°. At 2 MHz, the phase made a full 180° change -- half of the transducer was in tension while the other half was in compression producing a net transducer response near zero. The conclusion is that the transfer function minima were caused by phase cancellation along the receiving transducer face. The change in phase along the transducer face occurred because the wavefront and the transducer face were not parallel.

In summary, the flaw transfer function calculated by the model was made up of two contributions. The first contribution was a gradual decline of the transfer function with increasing frequency due to received wave amplitude, and the second was a series of sharp minima produced by phase cancellation as a result of the wavefront and the transducer face not being parallel. It is interesting to note that the "flaw" transfer functions as they are called in this report were actually strongly dependent upon transducer orientation in addition to flaw size and orientation. The term flaw transfer function is, therefore, somewhat misleading. Names such as geometry dependent transfer function and acoustical system transfer function are probably more accurate,

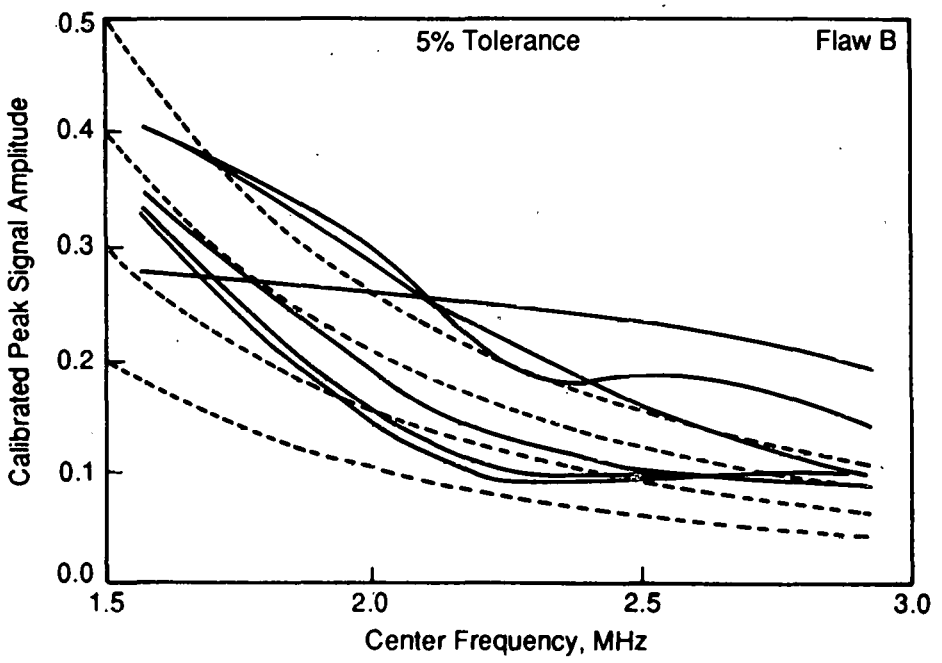

FIGURE 3.32. Center Frequency Sensitivity Study Results for Flaw B with 5% Tolerance Lines Superimposed

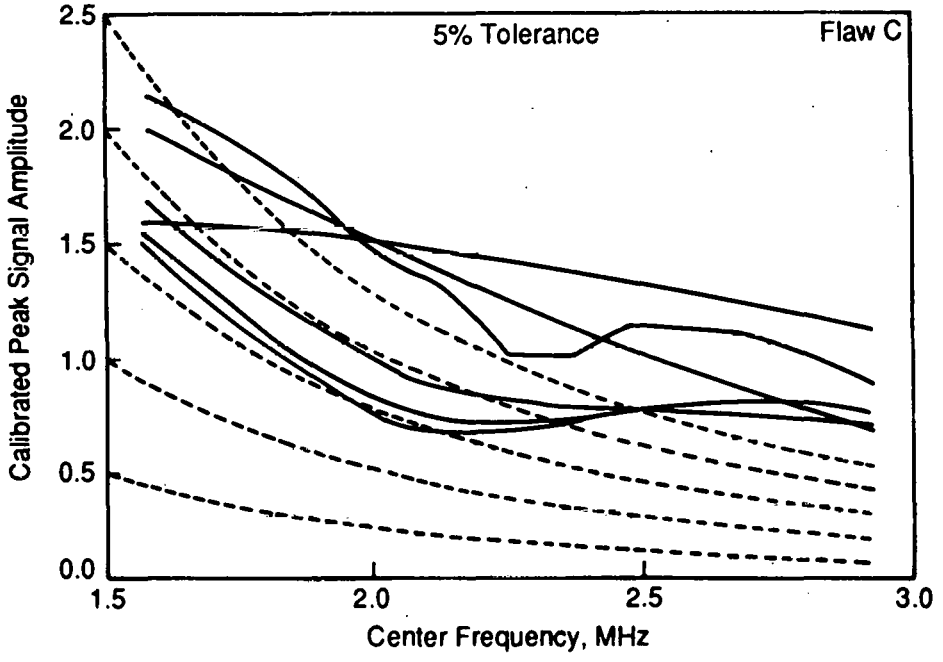

FIGURE 3.33. Center Frequency Sensitivity Study Results for Flaw C with 5% Tolerance Lines Superimposed

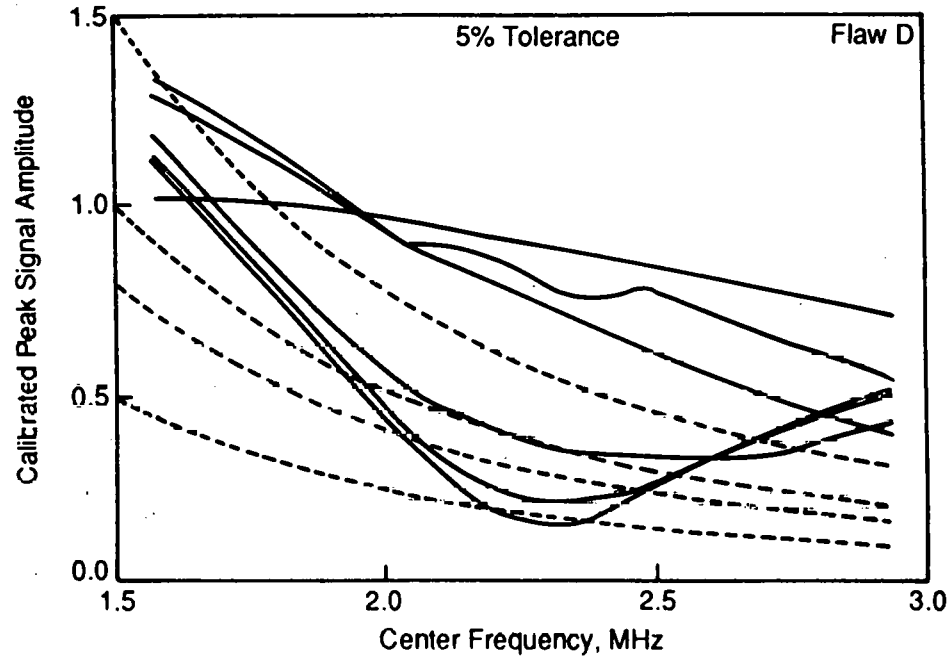

FIGURE 3.34. Center Frequency Sensitivity Study Results for Flaw D with 5% Tolerance Lines Superimposed

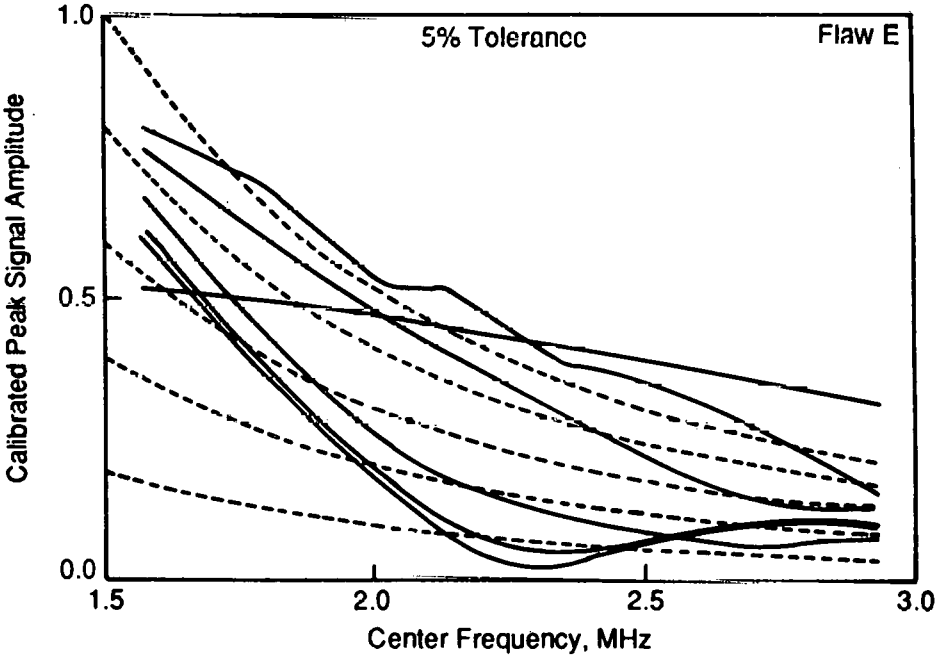

FIGURE 3.35. Center Frequency Sensitivity Study Results for Flaw E with 5% Tolerance Lines Superimposed

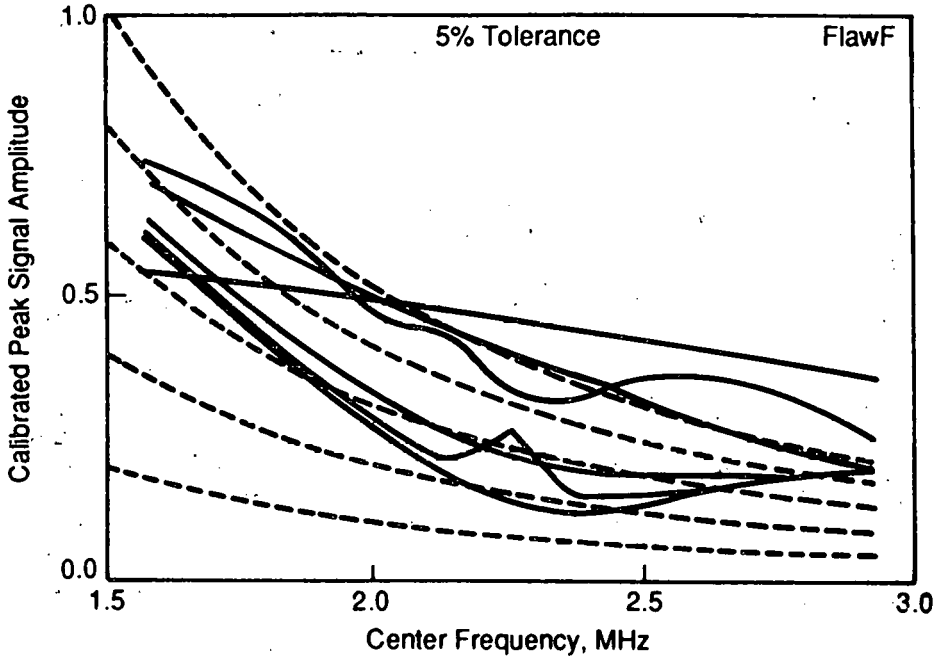

FIGURE 3.36. Center Frequency Sensitivity Study Results for Flaw F with 5% Tolerance Lines Superimposed

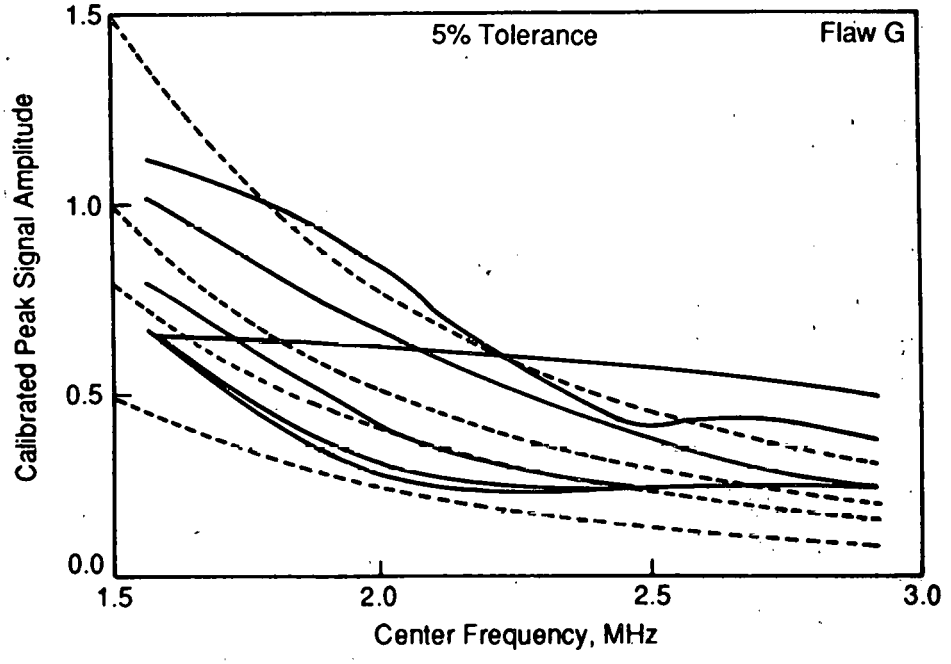

FIGURE 3.37. Center Frequency Sensitivity Study Results for Flaw G with 5% Tolerance Lines Superimposed

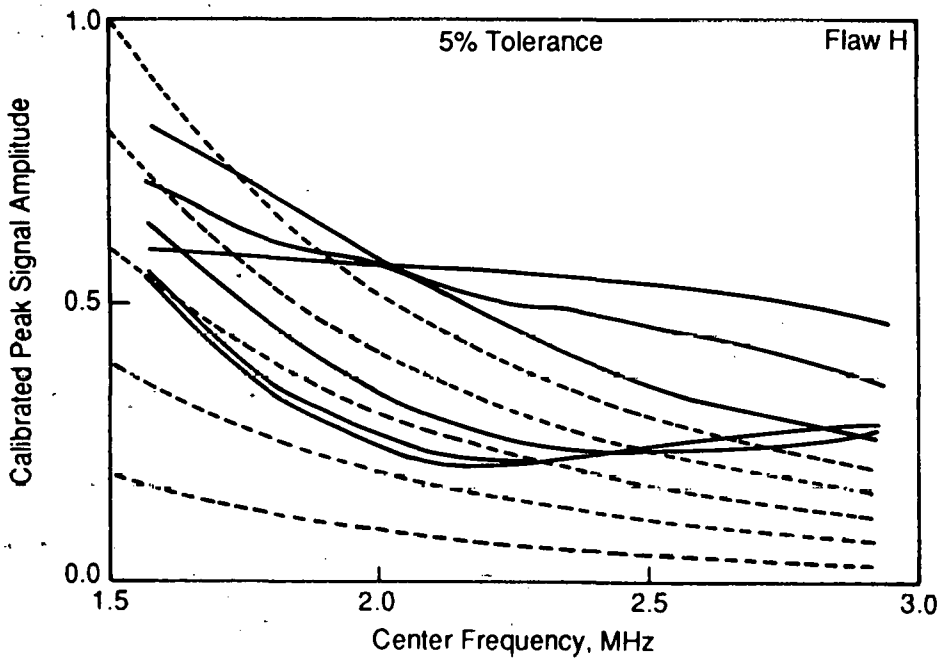

FIGURE 3.38. Center Frequency Sensitivity Study Results for Flaw H with 5% Tolerance Lines Superimposed

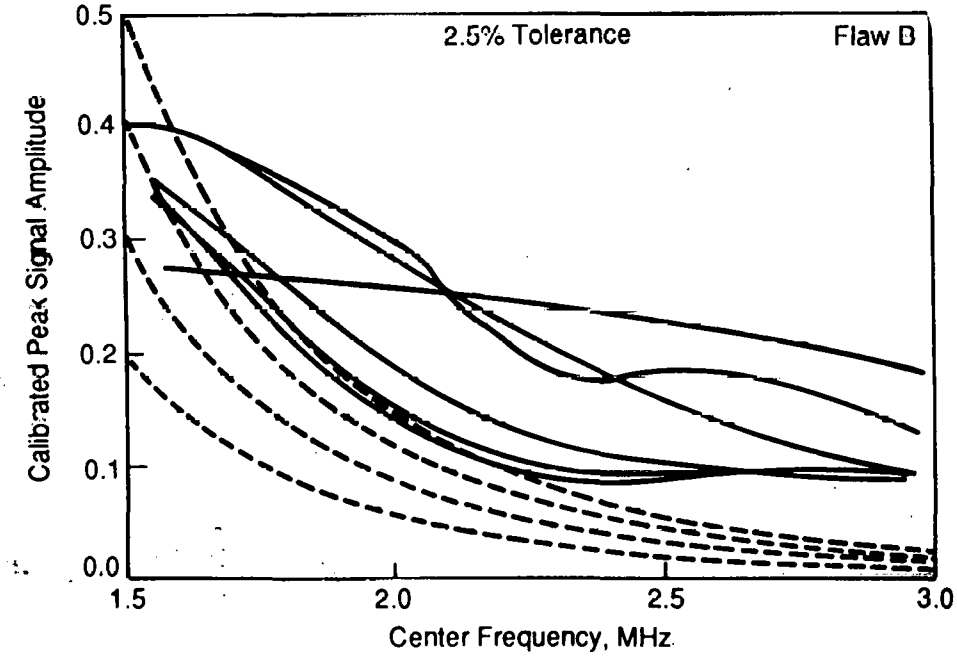

FIGURE 3.39. Center Frequency Sensitivity Study Results for Flaw B with 2.5% Tolerance Lines Superimposed

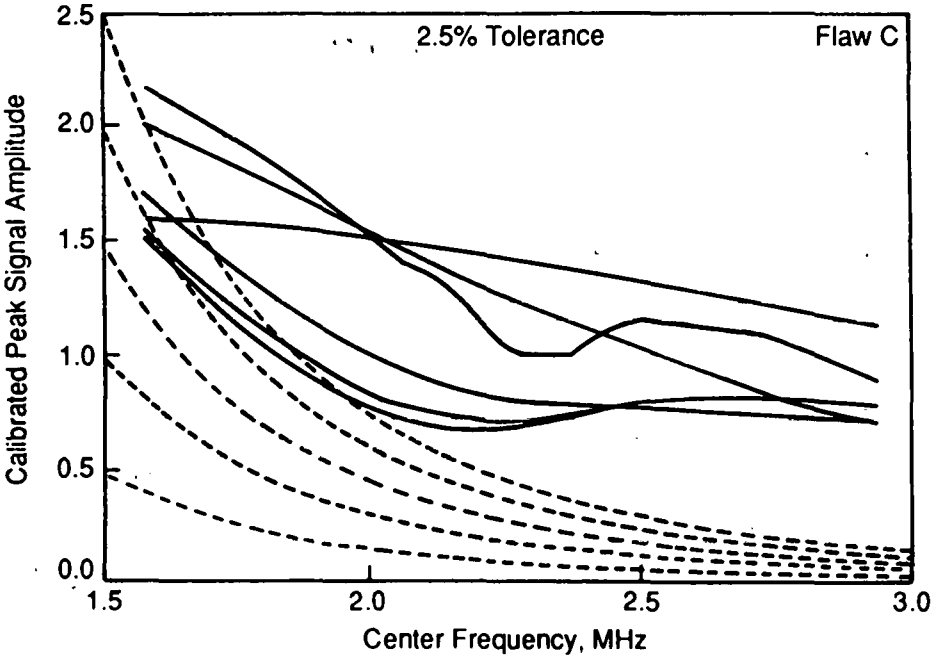

FIGURE 3.40. Center Frequency Sensitivity Study Results for Flaw C with 2.5% Tolerance Lines Superimposed

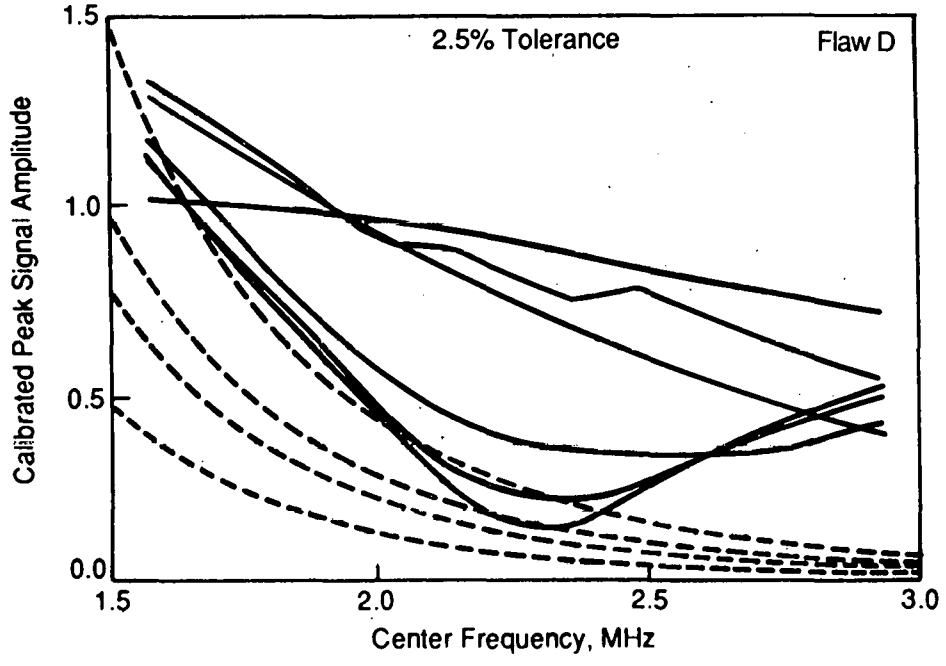

FIGURE 3.41. Center Frequency Sensitivity Study Results for Flaw D with 2.5% Tolerance Lines Superimposed

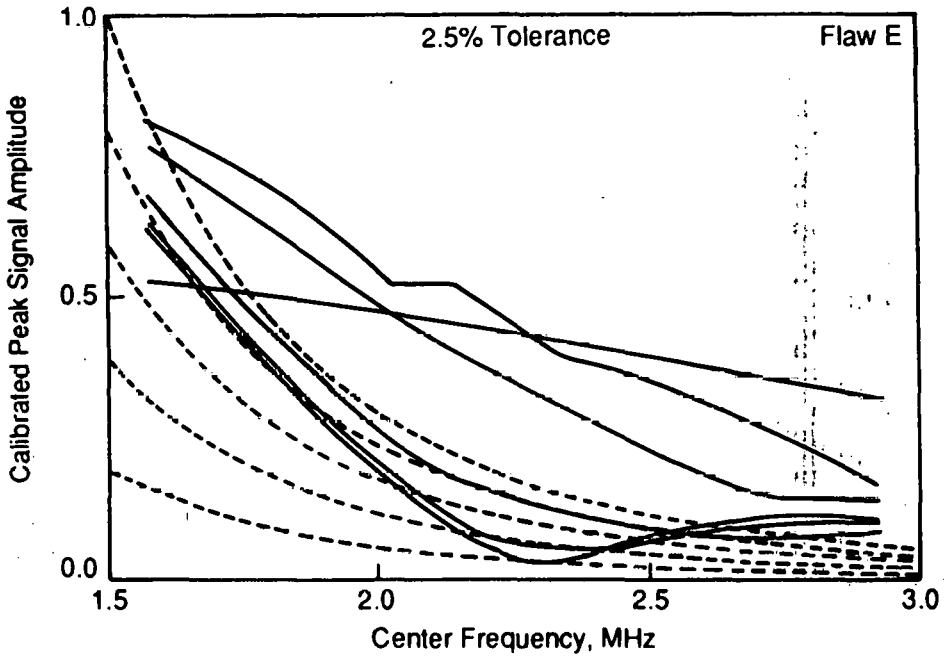

FIGURE 3.42. Center Frequency Sensitivity Study Results for Flaw E with 2.5% Tolerance Lines Superimposed

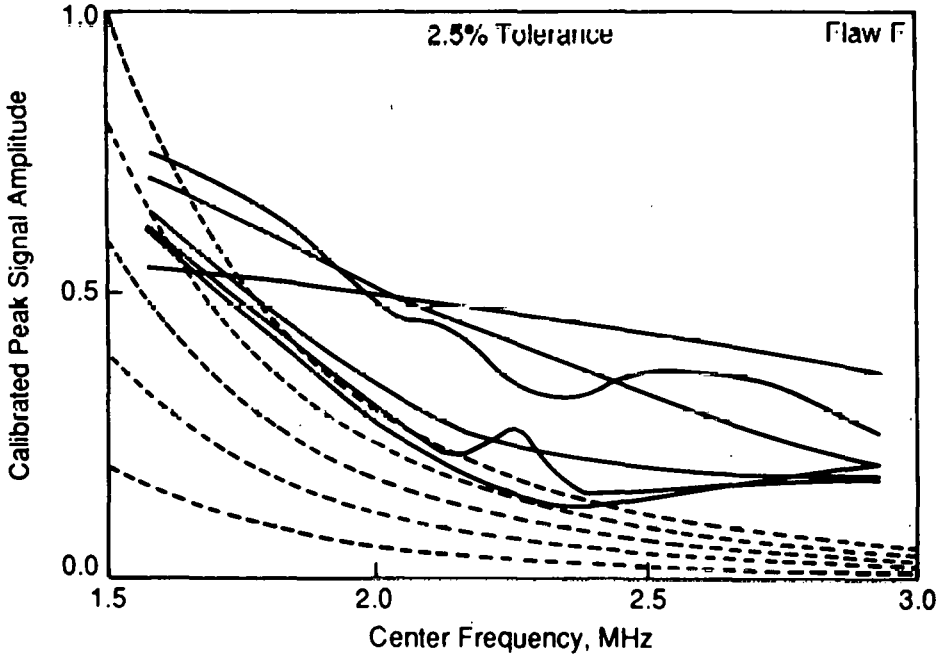

FIGURE 3.43. Center Frequency Sensitivity Study Results for Flaw F with 2.5% Tolerance Lines Superimposed

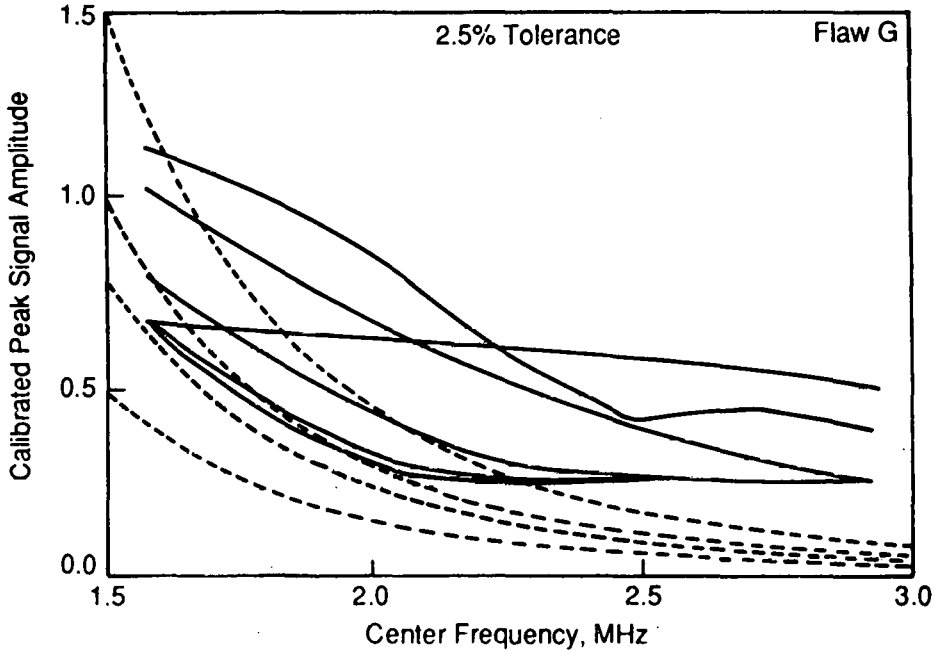

FIGURE 3.44. Center Frequency Sensitivity Study Results for Flaw G with 2.5% Tolerance Lines Superimposed

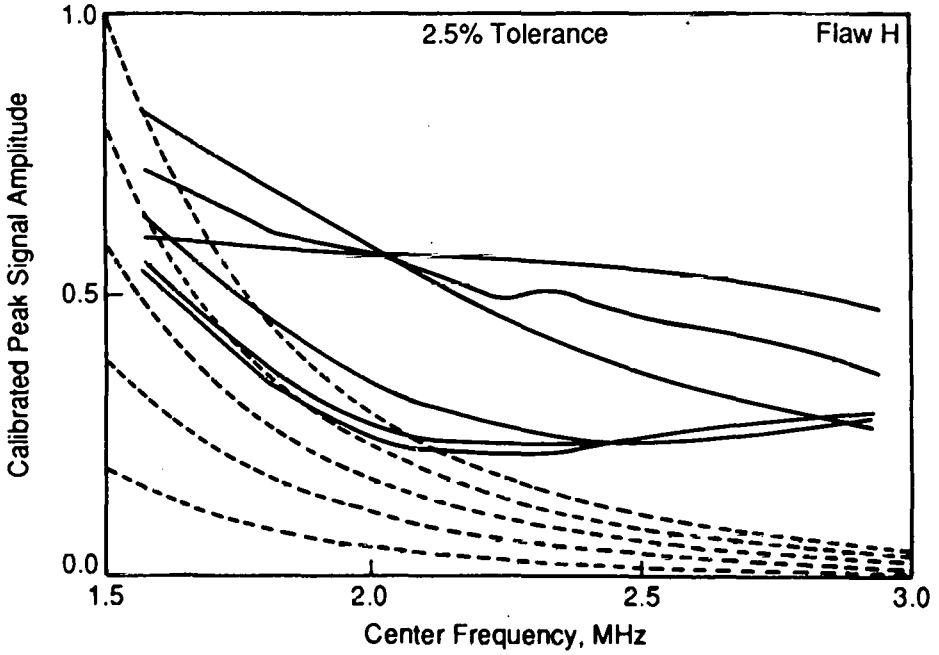

FIGURE 3.45. Center Frequency Sensitivity Study Results for Flaw H with 2.5% Tolerance Lines Superimposed

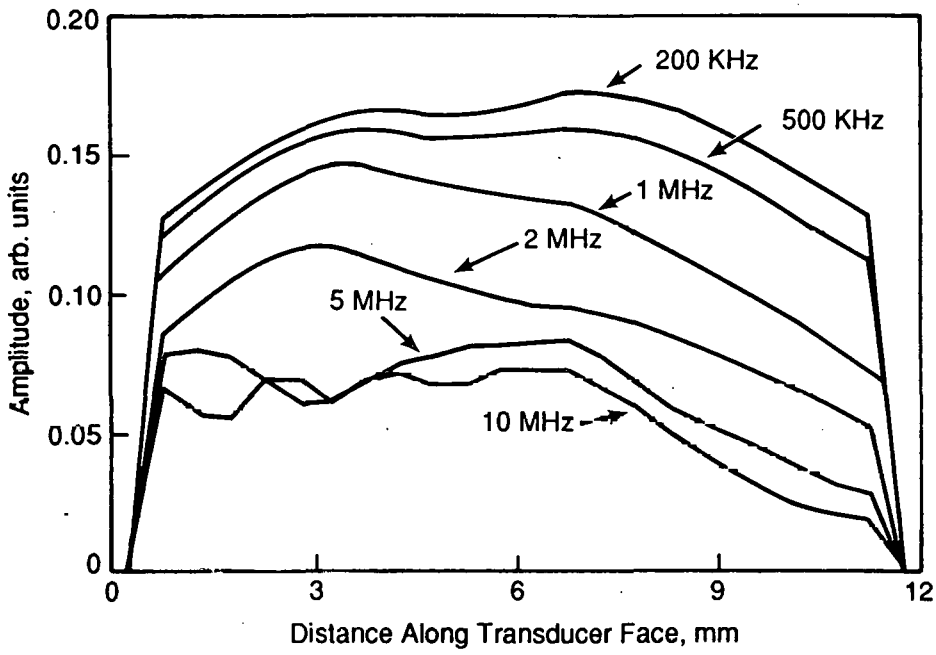

FIGURE 3.46. Sound Field Amplitudes Along the Receiving Transducer Face for 40° Block

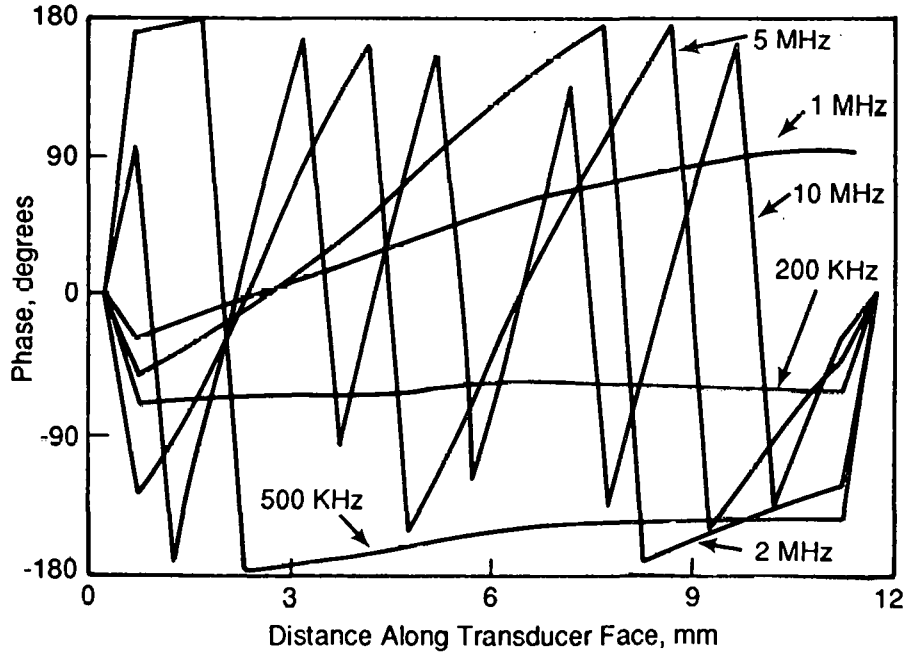

FIGURE 3.47. Sound Field Phase Along the Receiving Transducer Face for 40° Block

though somewhat wordy. The author apologizes for any confusion that the term flaw transfer function might cause, as the term is a result of the author's earlier naivety.

To eliminate the transfer function minima and, thus, decrease the sensitivity to frequency domain equipment parameters, the ideal solution is to use a phase-insensitive receiving piezoelectric element such as a miniature hydrophone receiver, zinc oxide, or cadmium sulphide devices. Such devices unfortunately are not, in general, commercially available. The practical solution for most users at this time is to use dual element and tandem configuration search units with a receiving transducer that is as small as practical given the necessary cable lengths and receiver input impedance.

The argument given above for using a small receiving transducer does not carry over to the sending transducer. Factors such as the length of the near field and the desired volume of insonification should dictate the size of the sending transducer.

Two-Dimensional Versus Three-Dimensional Flaw Transfer Function Calculations. Calculations were made to determine the frequency response differences between a semi-infinite transducer (as assumed in the model) and a transducer with a circular face (typical real-world design). A simplified transfer function calculation was made for both transducer types by making the following assumptions:

1. The sound field incident on the transducer was assumed to be a plane wave of constant amplitude. As shown in Figure 3.46, this was a reasonable assumption.

2. The transducer was assumed to be locally reactive.

3. The transfer function was assumed to be due to phase cancellation at the transducer face caused by the wavefront and the face not being parallel as was seen in the previous section.

Under these conditions the transfer function for the semi-infinite transducer is given by the sinc function:

$$TF(f) \alpha \text{ sinc } (Cf) = \sin (Cf)/Cf,$$

where f is the frequency and C is a constant whose value depends on the system geometry.

The transfer function for the circular transducer is given by the integral:

$$TF(f) \alpha \int \sqrt{2xr - x^2} \cos (Cfx) dx,$$

where r is the transducer radius, and the integral is evaluated from x=0 to x=2r.

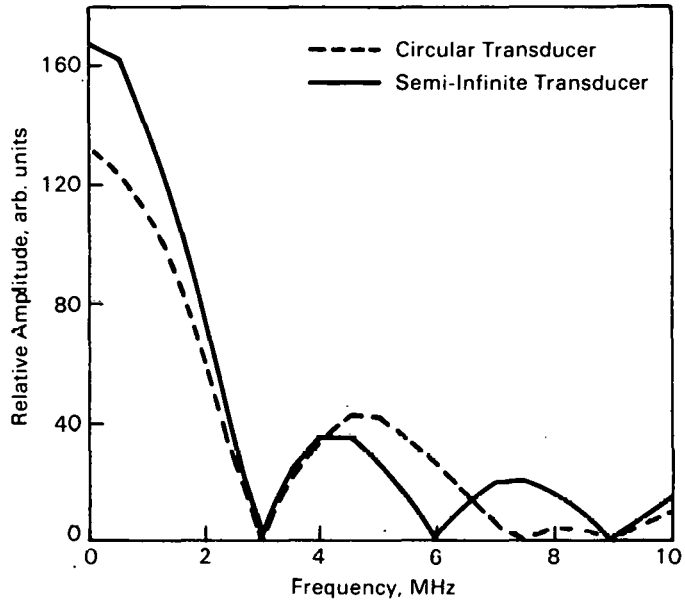

FIGURE 3.48. Comparison of Transfer Functions for Semi-Infinite and Circular Transducers

Transfer functions for the two transducer shapes were calculated for an otherwise identical situation and the results are shown in Figure 3.48. There is a difference between the two cases, but both would have very similar performance as a worst-case flaw in the equipment tolerance sensitivity studies unless the inspection system had an unusually wide bandwidth. The conclusion is that even though the model is two-dimensional, the calculated transfer functions are very similar to those that would be calculated by a three-dimensional model, so the sensitivity study results can be extended with confidence to actual, three-dimensional physical systems.

Summary of Results

- Model predictions were compared with data from multi-frequency experiments, and the validity of the model for predicting and calculating transfer functions for specular reflection from worst-case flaws was established.

- The model was used to calculate worst-case transfer functions for seven different combinations of transducer size, pipe wall thickness, and flaw angle. The transfer functions were identified as worst case, because they displayed distinct minima at the equipment center frequency, and this feature is known to produce sensitivity to changing frequency domain equipment parameters.

- An equipment bandwidth sensitivity study was performed for thin sections (piping) using the worst-case transfer functions. It was found that the ASME Code Case N-409-1 bandwidth equipment tolerance of 10% was sufficient to ensure 10% signal amplitude repeatability except in a few marginal cases. The study was made for equipment with a center frequency of 2.25 MHz; and the results may not be applicable for other center frequencies, geometries, thicknesses, or transducer sizes.

- An equipment center frequency sensitivity study was conducted for thin sections using several combinations of worst-case flaws and equipment bandwidth. It was found that the ASME Code center frequency tolerance of 10% was sufficient to ensure 10% signal amplitude repeatability only for equipment with a bandwidth of 3.5 MHz or greater. Tightening the tolerance to 5% was sufficient for 1.99 MHz and 2.73 MHz bandwidth equipment except in a few marginal cases. Tightening the tolerance to 2.5% still did not allow the 2.73 kHz, 508 kHz, and 1.02 MHz bandwidth equipment to consistently maintain 10% repeatability for worst-case flaws. Specifying allowable equipment center frequency tolerances for narrow-band inspection equipment will be a problem.

- Calculations revealed that much of the frequency domain equipment parameter sensitivity was due to phase cancellation along the receiving transducer face. It is suggested that the receiving transducer for dual element search units and tandem configuration search units be made as small as possible to reduce sensitivity to equipment changes.

- A simple calculation was performed to examine the differences in flaw transfer functions calculated by the two-dimensional model used in the interaction matrix study and more complex three-dimensional models. It was found that even though the model is two-dimensional, the calculated transfer functions are very similar to those that would be calculated by a three-dimensional model, so the sensitivity study results can be extended with confidence to certain three-dimensional physical systems.

- A paper was presented at the 1988 Review of Progress in QNDE conference and submitted for publication in the conference proceedings (Green and Marl 1988).

3.2.4 Future Work

The following work remains to be completed:

- Upgrade flaw model to handle curved sections (nozzles) and perform equipment parameter sensitivity studies for thick sections (reactor pressure vessels) using worst-case flaws.

- Develop input for a RIL or Code recommendations, as appropriate, for equipment parameter tolerances for piping and pressure vessel inspection.

- Write a NUREG/CR report on pipe and pressure vessel section results.

- Publish interaction matrix study work in peer-reviewed journals.

4.0 NEW INSPECTION CRITERIA

4.1 SUMMARY

Several interrelated activities on this task have been directed to the development of probabilistically-based inspection requirements. The PNL program has been interacting with other industry efforts, notably through a newly organized ASME Task Group on Risk-Based Guidelines. Contacts have also continued with other organizations such as the Electric Power Research Institute and Oak Ridge National Laboratory. To review and evaluate various concepts for probabilistic inspection criteria, PNL has prepared a "road map" document on improved inspection requirements. This document ("Probabilistic Approach to the Development of Improved Inservice Inspection Requirements") was in the process of final review at the end of this reporting period and will be published as a NUREG/CR report.

During FY 1988, a pilot application of PRA methods to the inspection of piping, vessels, and related components was completed. In this study, based on an existing PRA for the Oconee-3 reactor, a ranking of important systems which suggested priorities for inservice inspections was performed. In another activity, the possible use of actual failure data as a guide for inservice inspection requirements was addressed. A sample set of data on piping failures and repairs was obtained by performing a computer search of the Nuclear Power Plant Reliability Data System (NPRDS). These data were found to be quite useful, and an evaluation of the full set of data will be performed during the next reporting period.

4.2 INTRODUCTION

Work continued assessing the adequacy of existing ASME Code requirements for ISI and on developing technical bases for improving these requirements to ensure safe nuclear power plant operation. Efforts during this reporting period emphasized the application of probabilistic risk assessment (PRA) and probabilistic fracture mechanics to determine the level of inspection required to assure a suitably low failure probability for reactor systems and components or release of radiation.

4.3 STATUS OF WORK PERFORMED

4.3.1 Development of Probabilistic Approaches

During FY 1988, PNL continued with the development and assessment of alternative approaches for probabilistically-based inspection requirements. This activity has emphasized interaction with NRC staff, other laboratories, ASME groups, and industry efforts as performed by EPRI. PNL was active in the startup of an ASME Task Group on Risk-Based Inspection Guidelines, which is to be funded by ASME as a society research activity. Participation in this group is expected to further the goals of the NDE Reliability Program, and to lead eventually to specific recommendations for the introduction of probabilistic methods as a basis for ASME Section XI requirements. While the initial focus will be on nuclear power applications, the group will also seek

insights from applications in other industries such as aircraft, petrochemical and civil engineering structures. Although the task group held its first meeting on February 18, 1988 at Washington D.C., further activities have been delayed as funding to support the group is being sought.

A "road map" document was written that outlines a comprehensive probabilistic approach for the development of improved inspection requirements. This document provides a flow chart (Figure 4.1) that relates inspection requirements to quantitative goals for improvements in systems safety. The conceptual framework of the proposed approach has been expressed in terms of a three probabilistic parameters as follows:

$$(1 - P_{ISI}) * P_{failure} < P_{acceptable}$$

where

$P_{acceptable}$ = Acceptable failure probability for the weld based directly or indirectly on safety related goals such as core melt frequency, public risk, and occupational exposure.

$P_{failure}$ = Baseline failure probability for the weld given that no inservice inspection is performed.

P_{ISI} = Probability of detecting degradation in the weld before failure occurs. Given that detection is successful, it is then implied that the repair or mitigation of this degradation is 100% effective.

The document reviews the computational methods and data that are now available or will be needed to put this concept into practice. Also, the assumptions and limitations of current probabilistic methods are addressed.

The following statements summarize the preliminary conclusions expressed in the draft "road map" document:

- Current requirements for inservice inspection are based on qualitative consideration of both the consequences and probabilities of failure, but they are not based on systematic application of recent advances in probabilistic risk assessment (PRA) and probabilistic fracture mechanics (PFM).

- There is a real need to re-examine existing ISI requirements to determine their appropriateness in the light of increased knowledge gained through application of risk-based methods.

- Existing probabilistic methods can be used in a qualitative manner to develop more effective inspection requirements, whereby ISI priorities would be directed to those systems and components with the highest consequences and probabilities of failure.

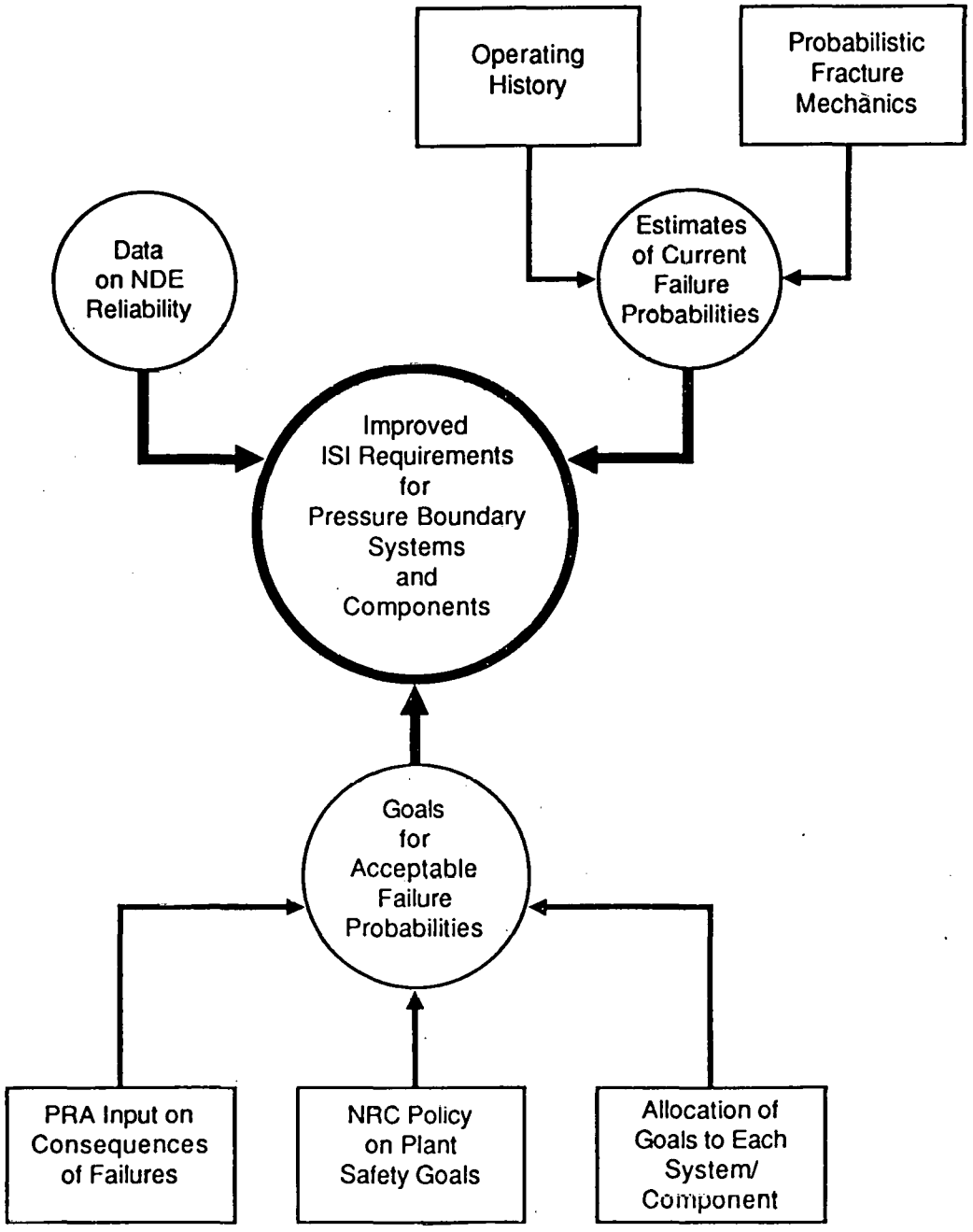

FIGURE 4.1. Probabilistic Approach to Improved ISI Requirements

- Actual revisions to code and regulatory requirements should not be developed and proposed until extensive pilot applications of probabilistic methods have been completed. Such applications will permit these methods to be tested and refined, and the numerical results will indicate opportunities to replace detailed probabilistic evaluations with much more simplified generic requirements.

- The use of PRA and PFM to develop ISI requirements that meet precise quantitative criteria for reliability and/or risk may now be unfeasible because of the limited scope and accuracy of existing calculational methods. Alternative criteria of a less quantitative nature should be considered, based on goals such as the defense in depth concept or attaining a desired factor of reduction of risk.

- Substantial research efforts are recommended to enhance PRA and PFM methods, for the specific purpose of tailoring these methods to develop improved inspection requirements.

- The successful implementation of quantitative criteria will require a consensus on goals for acceptable levels of structural reliability and/or risk. In the light of past difficulties in agreeing on "safety goals", similar goals for structural integrity and acceptable inspection criteria may involve a long and difficult process.

4.3.2 Data Base on Plant Operating Histories

This effort responds to a recommendation made during a March 1987 PNL/NRC workshop. The recommendation was to search data bases and industry records for information on piping system failures and repairs, and also to review the findings of piping inspections. During FY 1988, we established where such information can be found, estimated the effort needed to retrieve and interpret the resulting data, and determined the potential usefulness of the data as a basis to set priorities for future inspection requirements.

Contacts with utilities have indicated that suitable records are maintained at plant sites, and that these records could provide much useful information. However, the costs of on-site visits to locate and compile the desired data would be beyond the scope of the NDE Reliability Program.

Discussions with NRC staff have revealed two potentially useful computerized data bases, namely, Licensing Event Reports (LER) and an industry maintained data base available through the Nuclear Power Plant Reliability System (NPRDS). Being orientated to components, PNL was advised by NRC staff that the NPRDS data base would report more of the types of information of interest to ASME Section XI inspections. Accordingly, a trial search of the NPRDS data was performed. Through a request to the NRC staff, data were provided to PNL in the form of computer diskettes. The discussion below summarizes the relevant aspects of the data, and identifies some interesting trends regarding the effectiveness of inservice inspections.

The following data categories were searched:

Category 1 — Piping failures and repairs in the recirculating piping of a BWR plant with a known record of poor service experience

The objective was to reproduce the expected results for a well known case history of pipe cracking. As expected, the data base provided two significant "hits" corresponding to the years 1982 and 1984. Each of these two hits reported several cracks at several locations.

Category 2 — Piping failures and repairs in the recirculating piping of a BWR plant with a known record of good service experience

The objective was to reproduce the expected results for a newer plant for which there was no history of pipe cracking. As expected, the data base provided no "hits" indicating that there have been no failures or repairs.

Category 3 — Piping failures and repairs for the residual heat removal systems of all BWR plants

The objectives were to determine if data were available in sufficient detail and in a usable format, and also to seek any significant trends from the data. The data base provided 16 hits covering the years 1980 through 1986. These dates confirmed the belief that the NPRDS data base has only limited information on service experience prior to 1980.

No pipe ruptures were reported, with all failures being in the form of leaks or part-through flaws. Some 56% of the hits were cracks in welds, which is the type of degradation addressed by ASME Section XI inspections. Of these weld failures, only 11% of the flaws were detected by ultrasonic examination. Of the remaining weld flaws, 56% were detected by liquid penetrant examination during scheduled inspections, and 33% were found through leakage.

The remaining 44% of the hits consisted of vibrational fatigue cracks in small branch piping (19%), O-ring failures (13%), and a welding defect in a small penetration attachment (13%). All of these failures were detected through leakage, and not covered by ASME Section XI type inspections.

Category 4 — Piping failures and repairs for the primary coolant piping systems of all PWR plants

The objectives were again to determine if the data were available in sufficient detail and in a usable format, and also to seek any significant trends from the data. The data base provided 13 hits covering the years 1982 through 1986. This time period reconfirmed a prior understanding that the NPRDS data base has only limited information on service experience prior to 1980.

There were no pipe ruptures nor were there any part-through flaws reported. This confirmed prior knowledge regarding the excellent service performance of PWR primary piping systems.

Some 38% of the hits were gasket leaks. Thermal sleeve failures at one plant (detected as loose parts) made up another 31% of the reported failures. Except for the thermal sleeves, all the failures were detected by leakage. Another class of failure can be described as small attachment piping welds (23%) that failed from vibrational fatigue or mechanical abuse. There was also one case of surface corrosion due to boric acid leakage. None of the failures for the primary coolant system piping corresponded to the types of degradation addressed by ASME Section XI ultrasonic inspections.

Category 5 All piping failures and repairs in the NPRDS data base

In addition to the above four categories, an interrogation was made to see how many piping failures were reported in the NPRDS data base. This provided a total of 400 hits. While the detailed information on these hits was not extracted, the number of hits was a useful piece of information in itself for estimating the effort needed for a more complete study of the data base.

The trial search indicated that most of the information related to "failures" of minor consequence (gasket leaks, cracks in small diameter fittings, etc.) and that these "failures" were typically found visually through evidence of leakage. Nevertheless, inservice inspection has in many cases been effective in detecting weld cracks. The NPRDS data were determined to be relatively accessible, and easy to interpret. Therefore a complete evaluation of all the piping related failures (400 hits) will be performed during the next reporting period.

It must be recognized that the NPRDS data base is not a complete record of all nuclear power plant operating experience, and in particular is quite incomplete regarding data for years before 1980. Nevertheless, the trends from the incomplete sample of failures covered by the data base should provide useful information in guiding the development of improved inspection requirements.

Data are provided to NPRDS by utilities on a voluntary basis. Discussions with knowledgeable individuals at PNL and NRC gave estimates of the fraction of the total operating experience that is actually being entered into the data base that ranged from 10% to 50%. The 10% estimate came from one comparison of the complete records from one particular utility on valve maintenance with the corresponding NPRDS information for that same plant. The more optimistic 50% estimate may better apply to other utilities with more systematic reporting practices. Being a voluntary effort, the reporting of data is often preempted by more pressing demands on the time of the plant maintenance organizations at utilities. Even though the data base is known to be incomplete, there nevertheless appears to be general agreement that the data do provide a representative sample of operating experience.

4.3.3 Oconee-3 Pilot Study

The objective of this study was to determine the feasibility of using data from existing Probabilistic Risk Assessments (PRA) to establish inspection priorities for pressure boundary systems and components. A pilot application of PRA methods to the Oconee-3 plant was completed during the past year. The

study was based on PRA data from an EPRI study by Sugnet, Boyd, and Lewis (1984) (NSAC-60) and on data for failure probabilities from an NRC funded evaluation of actual observed failure data given in Wright, Stevenson, and Zuroff (NUREG/CR-4407). Based on the results of the pilot study, the proposed use of PRA methods has been demonstrated to be a useful tool for prioritizing those systems and piping sections or welds that need to be inspected.

Table 4.1 lists a number of Oconee-3 systems and the calculated rankings that provide insight into which systems should be given the highest priority for inservice inspection. Two alternative ranking parameters were employed. The Birnbaum parameter addresses the consequences of failure, given that a failure does occur. This parameter focuses inspection towards the most safety critical systems (based on their importance to preventing core melt), even if the structural reliability of such systems have been very high in the past. In contrast, the Weld Inspection Importance parameter makes use of estimates of system reliability to focus added attention to systems that are seen as more likely to experience service failures. Table 4.2 lists the pipe break probabilities that were estimated for Oconee-3 piping systems by using the information from NUREG-4407. In general, the two ranking parameters of Table 4.1 give similar priorities. However, there are notable exceptions such as the steam generator, which moves up in priority when the relatively poor service performance of steam generator tubes is taken into consideration.

A further step in the pilot study involved a much more detailed assessment for one particular system (emergency feedwater system). Failure Modes and Effects Analysis (FMEA) was applied to identify and prioritize the most risk-important piping sections within this system. The conditional probabilities of core melt given a break were first calculated for each piping section of the EFW system. Failure probabilities were estimated using observed failure rate data (NUREG-4407). These average failure rates were adjusted upwards or downwards for individual welds in accordance with the stress level in each piping section.

Table 4.3 gives the calculated importances for the Oconee-3 EFW piping sections. On the basis of core melt probability, the piping sections between containment and the steam generators are the most risk-important. As a point of interest, these piping sections are governed by the Class 1 requirements of ASME Section XI, and in this respect the results of the probabilistic calculations are consistent with current inspection requirements.

On the other hand, the supply lines from the upper surge tank ranks first, when the ranking disregards the estimated failure probability for this low stress line and considers only consequences of failure. In this context, the supply lines fall outside the scope of the inspection requirements of ASME Section XI, and an upgrade of inspection requirements can be justified by this risk-based evaluation approach.

TABLE 4.1. Rankings of Systems and Components for Inspection Priority as Based on Risk Considerations for Oconee-3

System[a]	Importance		Birnbaum Importance	
	Rank	Value	Rank	Value
Low pressure injection[b]	1	(5.9E-06)	2	(1.5E-02)
High pressure injection	2	(5.1E-06)	5	(5.4E-03)
Reactor pressure vessel	3	(5.0E-06)	1	(1.0)
Steam generators	4	(1.5E-06)	9	(1.5E-04)
Emergency feedwater	5	(7.2E-07)	3	(1.5E-02)
Service water	6	(3.6E-07)	4	(7.7E-03)
Reactor coolant	7	(1.7E-07)	6	(3.6E-03)
Power conversion[c]	8	(8.0E-08)	8	(2.1E-04)
Standby shutdown facility	9	(3.0E-08)	7	(6.9E-04)
Instrument air	10	(7.0E-10)	10	(1.5E-05)

(a) Only systems of interest to Code-Type-ISI are listed.

(b) Under normal conditions, the most frequently used function of the LPI system is decay-heat removal (DHR) after a shutdown.

(c) The PCS system consists of the following: main feedwater, main steam, condensate, condenser circulating water, and vacuum systems.

TABLE 4.2. Pipe Break Probabilities for Oconee-3 Piping Systems[a]

System	Pipe Break Probability[b]
Low Pressure Injection (LPI)[c]	3.8E-04
High Pressure Injection (HPI)	9.5E-04
Reactor Pressure Vessel (RPV)	5.0E-06
Steam Generators (SGs)	1.0E-02
Emergency Feedwater (EFW)	4.7E-05
Service Water (SWS)	4.7E-05
Reactor Coolant (RCS)	4.7E-05
Power Conversion (PCS)[d]	3.8E-04
Standby Shutdown Facility (SSF)	4.7E-05
Instrument Air (IA)	4.7E-05

(a) Only systems of interest to Code-Type-ISI are listed.

(b) For all welds.

(c) Under normal conditions, the most frequently used function is DHR after a shutdown.

(d) Includes the following systems: main feedwater, main steam, condensate, condenser circulating water, and vacuum systems. Pipe break probability is primarily due to main feedwater system.

TABLE 4.3. Oconee-3 EFW System Piping Section Importances

Piping Section	Annual Core Melt Probability	Rank[(a)]	Core Melt Probability Given the Break	Rank[(b)]
Containment (inside to steam generators)	1.1E-07	1	3.2E-03	3
EFW turbine-driven pump discharge lines	2.4E-08	2	7.1E-04	5
Common EFW pump discharge lines to containment isolation valve (outside)	1.3E-08	3	3.5E-04	6
Supply lines from upper surge tank	7.8E-09	4	1.5E-02	1
EFW motor-driven pump discharge lines	7.9E-10	5	3.1E-05	7
EFW turbine driven pump suction lines	1.2E-10	6	8.0E-04	4

(a) Rank based on annual core melt probability using observed weld break.

(b) Rank based on conditional probability of core melt given a break.

4.4 FUTURE WORK

In future work, the PRA pilot study will be expanded to address a representative sample of other plants. The objective will be to better establish and refine the methodology, and to look for generic trends that can be used as a guide for improved inspection requirements. Also, improved fracture mechanics probability analyses, detailed plant systems analyses, state-of-the-art PRA, and other analytical methods will be used to analyze the major systems in the selected plants. The end objective will be to assess current inspection requirements, and ultimately, to develop recommendations for revisions to ASME Code and Regulatory requirements for LWRs.

5.0 PROGRAM MANAGEMENT AND CONSULTATION ON FIELD PROBLEMS

In response to an NRC request, a matrix depicting the inspection practices of other countries with respect to ISI of reactor pressure vessels was assembled and provided to the NRC program manager. Cooperative agreements were established with EPRI on the Surface Roughness work and Re-Analysis of the PISC-II Round Robin Data Base. A letter was prepared and sent to the NRC Program Manager which discussed the value of the NRC endorsing Code Case N-401-1 versus the present BWROG/EPRI/NRC Coordination Plan Agreement.

Several hundred viewgraphs describing prior and current work on this program were prepared and provided to the NRC Program Manager in preparation of his trip to Taiwan. Program reviews were conducted with cognizant NRC personnel in June and September 1988.

6.0 PIPING TASK ACTIVITIES

This task is designed to address the NDT problems associated with piping used in light water reactors. The primary thrust of the work has been on wrought and cast stainless steel since these materials are harder to inspect than carbon steel. However, many of the subtasks' results also pertain to carbon steel. The current subtasks are: mini-round robin report, piping inspection round robin report, qualification document, cast stainless steel inspection, surface roughness, field pipe characterization), and PISC-III activities.

The work accomplished during this reporting period is summarized in the following paragraphs:

- MRR Report - The Mini-Round Robin (MRR) subtask was conducted to provide an engineering data base for UT/ISI that would help: a) quantify the effect of training and performance demonstration testing that resulted from IEB 83-02, b) quantify the differences in capability between detecting long versus short cracks, and c) quantify the capability of UT/ISI technicians to determine length and depth of intergranular stress corrosion cracks (IGSCC). A NUREG/CR report has been prepared and submitted for NRC review to document the work conducted on this subtask, and a paper was submitted for publication in Materials Evaluation.

- Qualification Criteria for UT/ISI Systems - The objective of this subtask is to improve the reliability of UT/ISI through the development of new criteria and requirements for qualifying UT/ISI systems. Revisions to the Qualification Document (NUREG/CR-4882) to resolve technical issues and address PNL and NRC comments were completed. This document has now received PNL clearance and was submitted to the NRC for final pre-publication review.

- Cast Stainless Steel Inspection - The objective of this task is to evaluate the effectiveness and reliability of ultrasonic inspection of cast materials within the primary pressure boundary of LWRs. Due to the coarse microstructure of this material, many inspection problems exist and are common to structures such as cladded pipe, inner-surface cladding of pressure vessels, statically cast elbows, statically cast pump bowls, centrifugally cast stainless steel (CCSS) piping, dissimilar metal welds, and weld-overlay-repaired pipe joints. Far-side weld inspection is included in the scope of this work since the ultrasonic field passes through weld material. Activities conducted during this reporting period included evaluations of weld-overlay-repaired pipe joints and CCSS materials.

- Surface Roughness Conditions - The objective for this work was to establish specifications such that an effective and reliable ultrasonic inspection is not prevented by the condition of the surface from which the inspection is conducted. Past efforts included an attempt to quantify the effect produced by irregularities of the inspection surface. This approach was then redefined to cooperate with EPRI in establishing a mathematical model to be used as an engineering tool for deriving

guidelines for surface specifications. Activities conducted during this reporting period included formulation of a coordination plan between EPRI, NRC, the Center for NDE (CNDE) at Ames Laboratory, and PNL; a visit by CNDE personnel to PNL; a CNDE/PNL data exchange; and PNL development of better experimental procedures for obtaining quantitative data to compare model predictions.

- Field Pipe Characterization - The objective of this subtask is to provide pipe weld specimens that can be used for studies to evaluate the effectiveness and reliability of ultrasonic inservice inspection (UT/ISI) performed on BWR piping. Weld specimens were removed from replaced pipe remnants at the Monticello and Vermont Yankee BWR nuclear power plants in FY 1986. These weld specimens have subsequently been decontaminated and characterized by ultrasonic and penetrant examinations. Some specimens were also examined in detail with conventional UT and Synthetic Aperture Focusing Technique (SAFT) methods. A specimen set has been prepared for shipment to Europe for use in PISC-III program studies; however, actual shipment has been deferred pending receipt of shipping instructions from Ispra.

- PISC-III Activities

  This activity involves the participation in the PISC-III program to ensure that the work is of use in addressing NDT reliability problems for materials and practices in U.S. LWR ISI. This includes the support for the co-leader of the Action 4 on Austenitic Steel Tests (AST); providing five safe-ends from the Monticello plant; a sector of the Hope Creek reactor pressure vessel containing two recirculation system inlet nozzles; coordination of the inspections to be conducted by U.S. teams on the various actions; input to the studies on reliability and specimens for use in the parametric, capability, and reliability studies of the AST. The highlight during this reporting period was further planning for carrying out the action plans.

6.1 MINI-ROUND ROBIN REPORT

6.1.1 Introduction

The Mini-Round Robin (MRR) subtask was conducted to provide an engineering data base for UT/ISI that would help:

- quantify the effect of training and performance demonstration testing that resulted from IEB 83-02,

- quantify the differences in capability between detecting long (greater than 3-in.) cracks versus short (less than 2-in.) cracks, and

- quantify the capability of UT/ISI technicians to determine length and depth of intergranular stress corrosion cracks (IGSCC).

6.1.2 Status of Work Performed

A NUREG/CR report has been prepared and submitted for NRC review to document the work conducted under this subtask. Final review comments from the NRC review were not received by the end of this reporting period. All review comments that were received to date have been incorporated in the final report. A paper entitled "An Evaluation of Ultrasonic Inspection for Intergranular Stress Corrosion Cracks Through Round Robin Testing" was prepared and submitted for publication in Materials Evaluation, the official journal of the American Society for Nondestructive Testing.

6.1.3 Future Work

After all final review comments are received and incorporated, the NUREG/CR report will be submitted for NRC publication.

6.2 QUALIFICATION CRITERIA FOR UT/ISI SYSTEMS

6.2.1 Introduction

The objective of this subtask is to improve the reliability of ultrasonic testing/inservice inspection (UT/ISI) through the development of new criteria and requirements for qualifying UT/ISI systems. Revisions to the Qualification Document (NUREG/CR-4882) to resolve technical issues and address PNL and NRC comments were completed. This document has now received PNL clearance and has been submitted to the NRC for final pre-publication review.

6.2.2 Status of Work Performed

Development of criteria and requirements for qualifying UT/ISI systems continued with final editing of the Qualification Document as a formal report. Technical issues addressed during an internal (PNL) review were identified and the document was revised to accommodate these issues plus other NRC and PNL comments. This document has now received PNL clearance and was submitted to the NRC for final pre-publication review.

6.2.3 Future Work

Comments were received from the NRC review at the end of this reporting period, and the appropriate changes are scheduled to be made in early November. Upon receipt of NRC concurrence, NUREG/CR-4882 entitled "Qualification Process for Ultrasonic Testing on Nuclear Inservice Inspection Applications" will be submitted for publication by the NRC. When published, this document will describe recommended qualification processes for all nondestructive examination/inservice inspection (NDE/ISI) systems, although the document is primarily directed toward criteria and qualification processes for UT/ISI systems.

6.3 CAST STAINLESS STEEL INSPECTION

6.3.1 Introduction

The objective of this task is to evaluate the effectiveness and reliability of ultrasonic inspection of cast materials used within the primary pressure boundary of LWRs. Due to the coarse microstructure of this material, many inspection problems exist and are common to structures such as cladded pipe, inner-surface cladding of pressure vessels, statically cast elbows, statically cast pump bowls, centrifugally cast stainless steel (CCSS) piping, dissimilar metal welds, and weld-overlay-repaired pipe joints. Far-side weld inspection is included in the scope of this work since the ultrasonic field passes through weld material. Activities conducted during this reporting period included evaluations of weld-overlay-repaired pipe joints and CCSS material.

6.3.2 Status of Work Performed

6.3.2.1 Weld Overlay

Weld-overlay repair is being used as a temporary repair mechanism for BWR piping weakened by IGSCC and is being sought as a longer-term repair process. NUREG/CR-4484, Status of Activities for Inspecting Weld Overlaid Pipe Joints, was published in 1986. Activities thereafter were monitored and a status update provided in the form of draft input for a Research Information Letter (RIL). The primary conclusion of the redrafted RIL (April 27, 1988) was that much work has been performed to demonstrate the effective ultrasonic inspection of weld-overlay-repaired pipe joints; however, insufficient data exists to classify this inspection as effective and reliable. The NRC program manager requested that the draft include a recommended evaluation test for providing sufficient data in determining if a technique is effective and reliable. The redraft is now being reviewed by the NRC program manager to determine if it should left in the form of a RIL or rewritten as a NUREG/CR report.

6.3.2.2 Centrifugally Cast Stainless Steel

CCSS piping is used in the primary reactor coolant loop piping of 27 pressurized water reactors (PWRs) manufactured by the Westinghouse Electric Corporation. However, CCSS inspection procedures continue to perform unsatisfactorily due to the coarse microstructure that characterizes this material. The major microstructural classifications are a columnar, equiaxed, and a mixed columnar-equiaxed microstructure of which the majority of installed piping material is believed to be the latter.

Activities during this reporting period included acquiring three additional pipe sections believed to be CCSS, acquiring a second scan matrix of ultrasonic field maps with the upgraded data collection system, and submission of an article to the annual Review of Progress in Quantitative Nondestructive Evaluation (Good and Green, 1988a). A discussion on the newly acquired pipe material is presented and is followed by the a review of the analysis performed on the field maps acquired while performing the scan matrix.

Three CCSS pipe sections were on loan to PNL from Southwest Research Institute (SwRI) and reported in the previous two semi-annual reports. These pipe sections were reserved for use as ultrasonic calibration blocks. With the aid of Mr. Bob Edwards of SwRI, PNL was able to retain a portion of this material (removal of approximately 30 cm, circumferentially, from the end of each open sector) for PNL use (Figure 6.1). The remaining material was returned to SwRI.

The distortion incurred by an ultrasonic field when propagating through coarse-microstructured materials was evaluated. To perform an effective and reliable ultrasonic inspection, the ultrasonic field should be both spatially coherent (i.e., the field is not partitioned into multiple wave fronts traveling to different locations) and stable (i.e., field parameters such as effective refracted angle and field position do not vary sufficiently to make an inspection unreliable). Previous work indicated that the sound field emitted by a 1-MHz, 45°, longitudinal-wave probe with a 38-mm diameter transducer maintained spatial coherency while propagating through the pure microstructural forms of CCSS (Good and Van Fleet 1987a and 1987b). This analysis was extended to the mixed microstructural modes of CCSS. Furthermore, the variation of field distortion incurred by propagating through a selected microstructure was investigated by generating field maps from different material volumes of the same microstructural classification. To accurately map the ultrasonic field, an improved technique was used so that receiver directivity maintained a ±1 dB sensitivity over a broad angular range centered about 45°. Discussions include the samples used, the process of mapping ultrasonic fields utilizing a 45° facet, and an analysis of multiple field maps acquired from selected CCSS microstructures.

Four centrifugally cast stainless steel (CCSS) samples were used to generate ultrasonic field maps: an equiaxed microstructure, a columnar microstructure, and two samples having mixed equiaxed-columnar microstructures. In order to acquire reference field maps from a homogeneous-isotropic material, four carbon steel pipe sections that had an equivalent diameter and wall thickness were used. All samples were field pipe sections and had a 70-cm inner diameter and a 6-cm wall thickness, except the layered columnar-equiaxed microstructured block which had an 80-cm inner diameter and an 8-cm wall thickness.

Four spatial points were established on each block where an ultrasonic field map was to be acquired (Figure 6.2). These points were used later as references for scanner alignment, microprobe placement, and aperture placement relative to the scanned material volume. The self-aligning fixture contained two guide holes separated by 5 cm along the length of the fixture. The two sets of paired spatial points enabled the pipe axial and circumferential axes to be defined as well as points which only differed in radial position and/or axial displacement.

Block #1: ≈90° Sector

22-inch arc length on OD surface
- 6-inch axial length
- 3.25-inch wall thickness
- 29-inch outer diameter, approx.

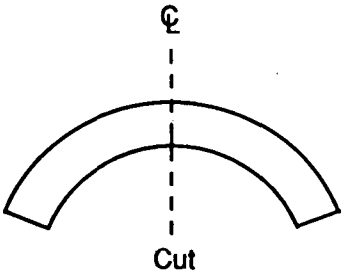

Block #2 ≈270° Sector

- 78-inch arc length on OD surface
- 6-inch axial length
- 3.25-inch wall thickness
- 38-inch outer diameter

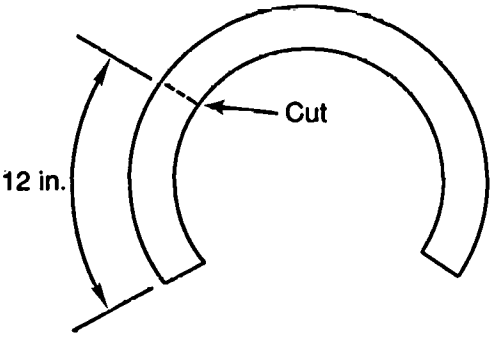

Block #3: ≈270° Sector

- 68 inch arc length on OD surface
- 12-inch axial length
- 2.5-inch wall thickness
- 29-inch outer diameter

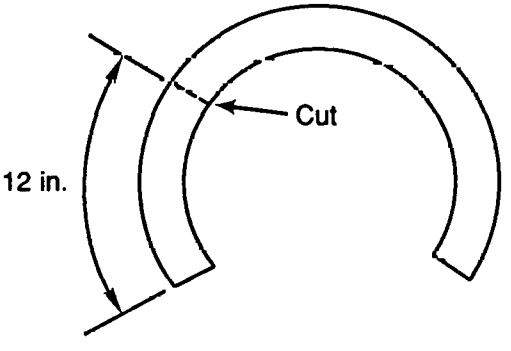

FIGURE 6.1. Southwest Research Institute's CCSS Material that was Loaned to PNL

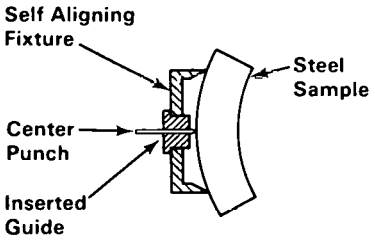

a) Reference Point on Outer Diameter

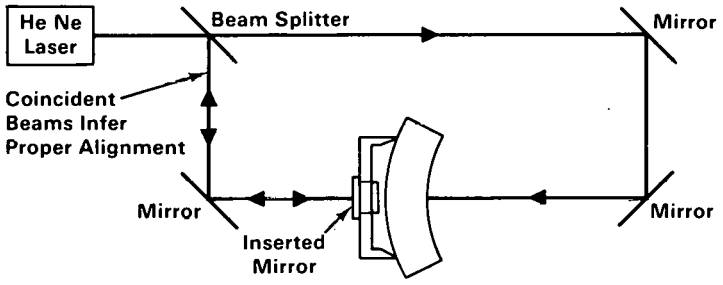

b) Alignment of Steel Sample to Optics

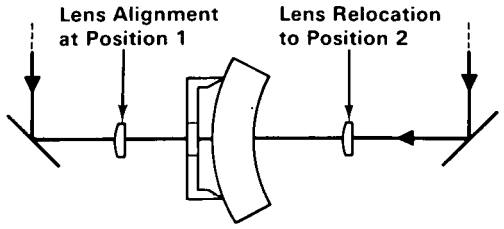

c) Reference Point on Inner Diameter

FIGURE 6.2. Spatial Points for Referencing Coordinates on Steel Samples

The ultrasonic field mapping system provided a two-dimensional map of the ultrasonic field (Figure 6.3). Longitudinal-wave-field maps were obtained using a longitudinal-wave probe as a transmitter(a) and a longitudinal-wave microprobe as a receiver. A scan was accomplished by applying the microprobe(b) to a 45° facet and scanning in a raster format with the transmitting probe. RF data were stored and field maps determined by maximum absolute values in a 3.0 microsecond gate.

(a) The scrubbing surface of the acrylic wedge was contoured to match an outer pipe radius of 41 cm.

(b) The longitudinal-wave microprobe consisted of a 0.3-mm-diameter piezoelectric crystal at the end of a hollow metal needle.

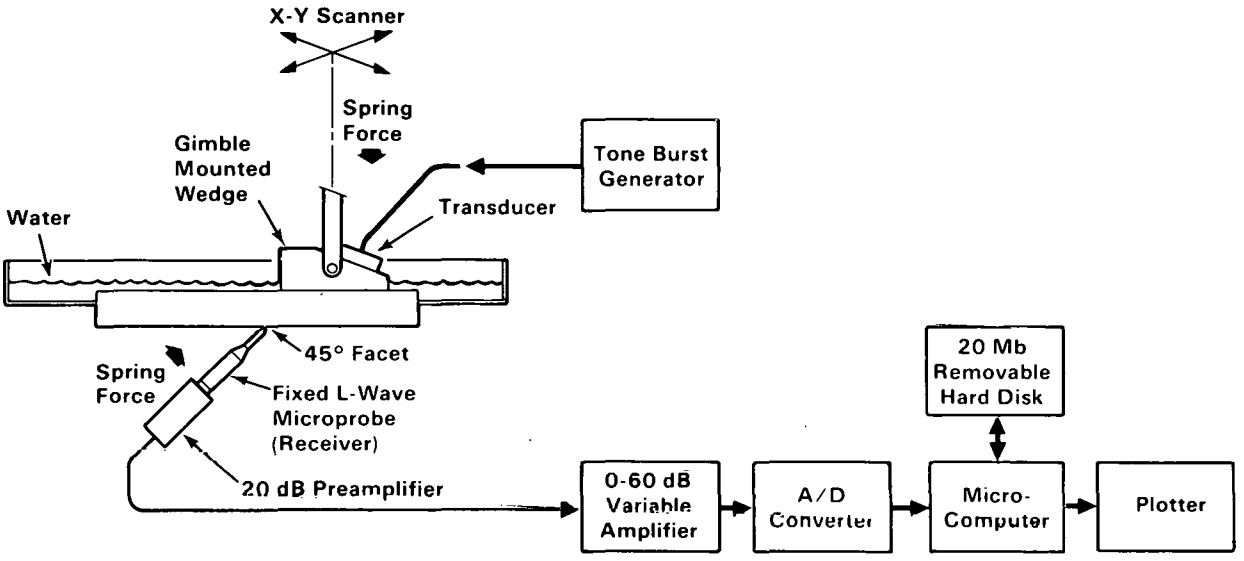

FIGURE 6.3. Ultrasonic Field Mapping System for Examining CCSS

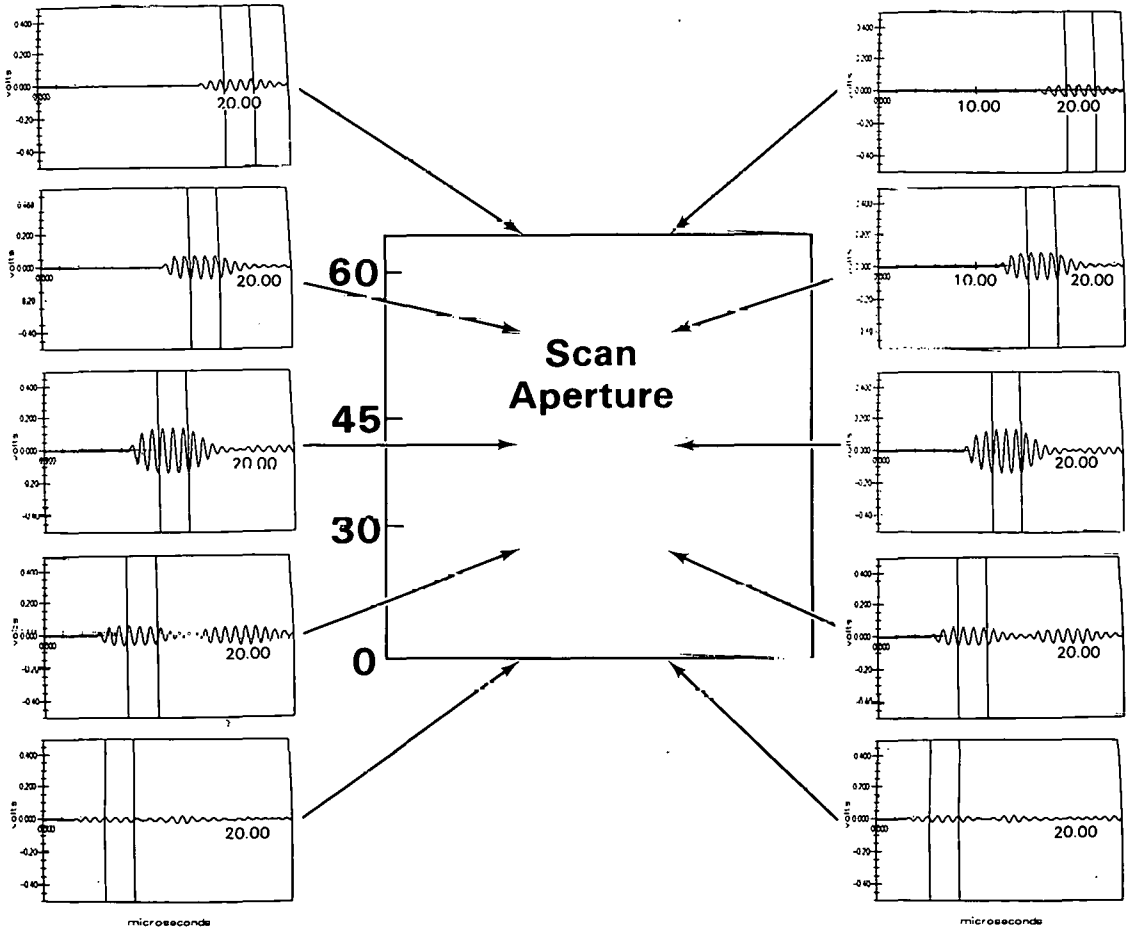

FIGURE 6.4. Monitoring of Gating Process with Windowed Displays

The post-gating process consisted of selecting six points dispersed throughout the scan aperture, centering the gate about the selected signal feature at each point, and checking the gate positions obtained by means of a second-ordered polynomial fit. The check was performed by observing multiple sequences of images displaying the RF signal with the superimposed gate (Figure 6.4). The gating process resulted in mapping the quasi-steady-state response since the transmitter was excited by a five-cycle tone burst.

Placement of the longitudinal-wave microprobe on a 45° facet was found to improve the technique. Previous placement of the microprobe normal to the sample surface biased image features toward smaller refracted angles because of receiver directivity (Good and Van Fleet 1988a). Directivity of the microprobe when applied to a 45° facet resulted in a ± 1 dB change in reception sensitivity over the angular range of 45° ± 20° for a facet machined into a plane and 45° ± 35° for a 45° facet machined into a right angled corner (Figure 6.5). (Application of the microprobe to the corner was performed only for the sample having a layered microstructure due to the logistics of receiving a 45° refracted wave in a block having a thickness-to-axial-length ratio of 0.5.)

Ultrasonic field maps were formed by post-gating the digitized RF signals, determining the absolute peak response in the gated window, and determining dB values relative to the maximum gated amplitude value. The two-dimensional plot was made according to the coordinate system of the scanner and assigning color codes according to a preselected dB scale. Although one field map for each of the microstructural classifications was displayed (Figure 6.6), four maps were taken, each in unique material volumes.

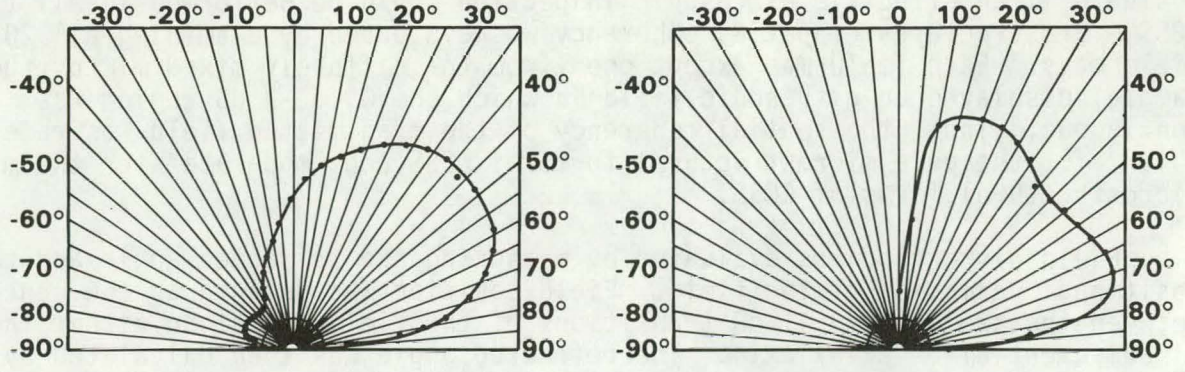

a) Hemi-cylinder block: 1 MHz, longitudinal wave directivity pattern

b) Quarter-cylinder block: 1 MHz, longitudinal wave directivity pattern

FIGURE 6.5. Directivity of Longitudinal-Wave Microprobe when Applied to a 45° Facet Cut

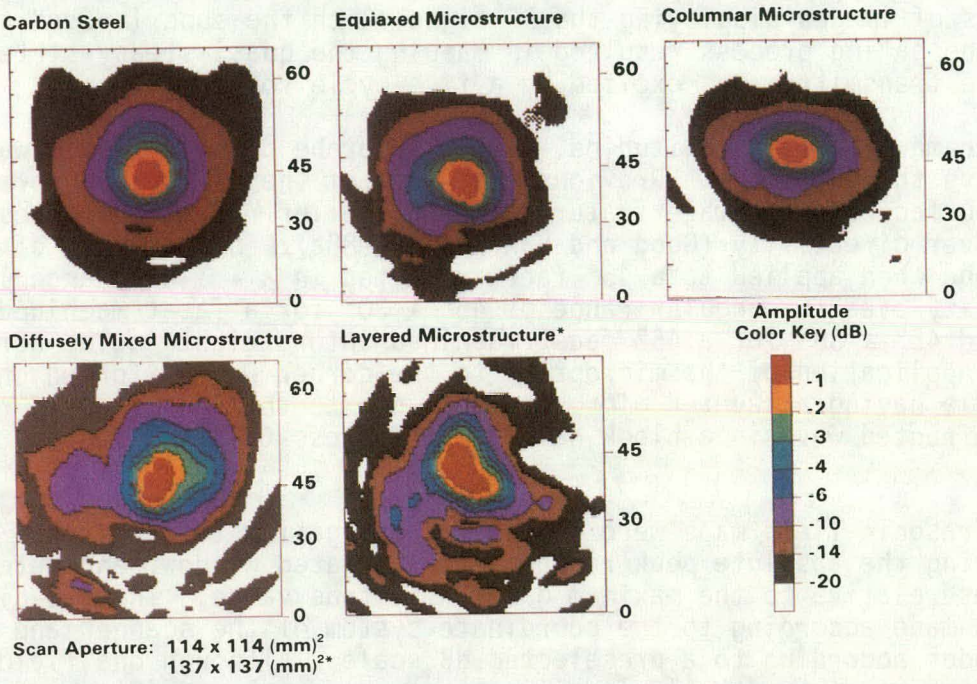

FIGURE 6.6. Ultrasonic Field Maps of 1-MHz, 45°, Longitudinal-Wave Fields

The objectives of this work were to determine if a 1-MHz, 45°, longitudinal field maintained spatial coherence in all the microstructural forms of CCSS, to quantify the degree of distortion incurred by the ultrasonic field, and to evaluate if an effective ultrasonic inspection could be performed in all the CCSS microstructures. Spatial coherency was evaluated by examining all 20 field maps. Each field map except one (from the diffusely mixed microstructural sample) displayed an ultrasonic field in which the 0 to -3 dB region was contiguous. Thus, the spatial coherency of the transmitted field was rated "high" for the pure microstructural forms of CCSS and "moderate" for the mixed microstructural forms of CCSS.

Field distortion was evaluated by measuring the refracted angle and the positional variation of the field. Field position was defined as the center between the two extreme -1 dB transitions of the field map along either the circumferential or axial axis. The refracted angle was then calculated by a trigonometric relation between axial field position and pipe-wall thickness (Figure 6.7).

Data from the equiaxed microstructure exhibited a mean value of 43.6° which was close to that of the reference material (43.4°). The standard deviation of 1.0°, however, was three times higher than that of the reference material and indicative of the degree of inhomogeneity caused by large grains

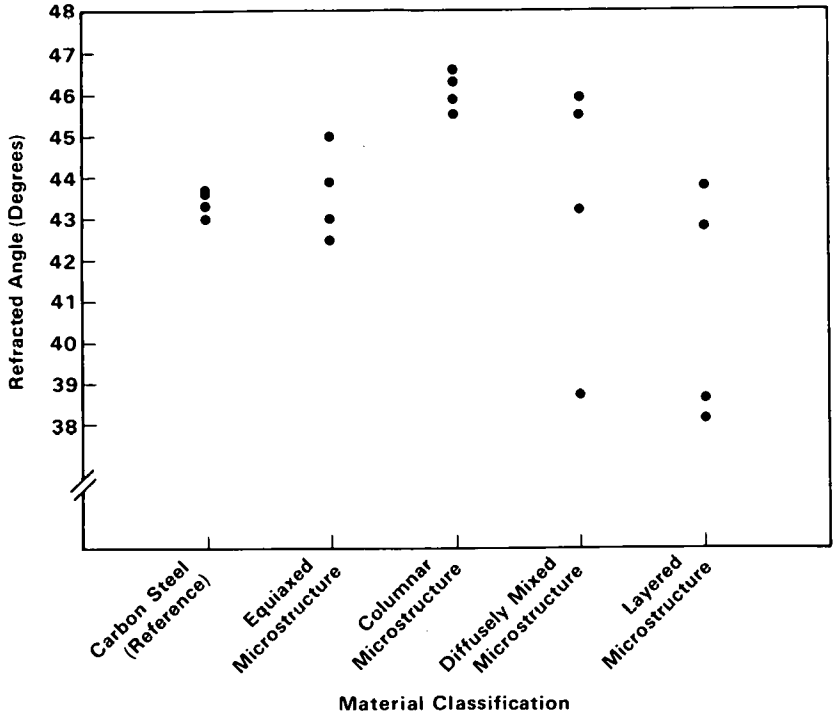

FIGURE 6.7. Effective Refracted Angles for 1-MHz, 45°, Longitudinal Waves

relative to a 1-MHz wave (6-mm wave length). (The 0.3° standard deviation from the reference material was believed to solely relate to set-up variations.)

The values from the columnar microstructure had a 46.1° mean which indicated that the maximum energy flow was redirected as predicted by anisotropic wave behavior. The standard deviation of 0.4° was effectively equal to that of the reference and indicated that the material was essentially as homogeneous as the reference material.

For the mixed-microstructures, data taken from the diffusely-mixed-microstructure had a 43.3° mean and a 2.9° standard deviation. This variation was 10 times higher than that of the reference material. Data from the layered-microstructure had a 40.8° mean and a 2.5° standard deviation which was 8 times higher than that of the reference material.

The significance of the refracted-angle results was the increased standard deviation of the equiaxed sample and the extremely large standard deviations of both materials having a mixed microstructure.

Another parameter selected to quantify field distortion was the field-position variation normalized to field width. When inspecting a selected material volume, sufficient field overlap was designed into the scan procedure to ensure that the detection sensitivity remained high for a defect anywhere within the material volume of interest. Obviously, if a small field width

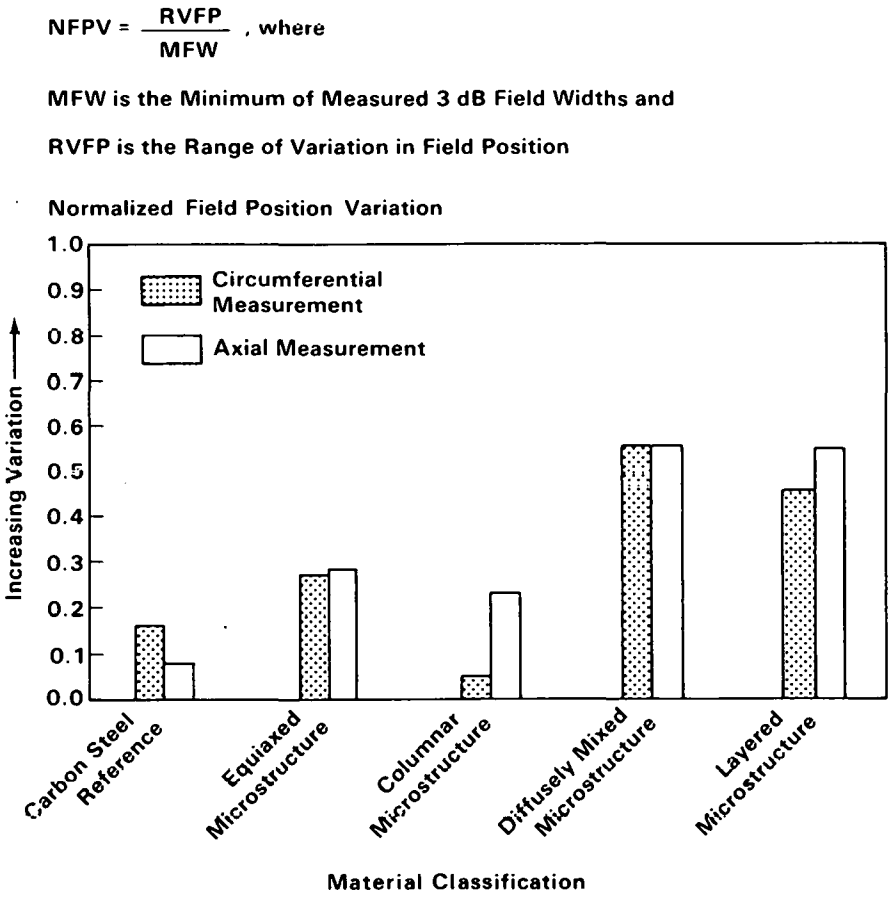

FIGURE 6.8. Positional Variation of Longitudinal-Wave Fields

existed, then the allowable field displacement error would be small. Likewise, if a large field width existed, then the field-displacement error may be larger. Therefore, the field-position variation was normalized to field width and was calculated by measuring the difference between the extreme field positions unique to a microstructure and dividing by the smallest of the four -3 dB field widths. Values were obtained along both the circumferential and axial axes and plotted (Figure 6.8). As previously stated, the variations associated with the reference samples were assumed to be indicative of set-up variation and were 16% and 8% for the circumferential and axial values, respectively.

For CCSS material, increased variation was expected for the equiaxed material and ranged between 27% and 28% for values pertaining to measurement along both pipe axes. A low circumferential value of 5% was obtained for the columnar samples; however, the axial value was 23%. This latter value might seem high since the standard deviation of the refracted angle was small; however, the axial, -3 dB, field width of the columnar scans also was reduced and produced a higher normalized value. The two mixed microstructural forms

had values ranging from 45% to 55%. This could be important since the scan patterns on a pipe use circumferential increments as high as 50%. If two successive measurements were made and the field misdirection was outward from the two positions, then a material volume thought to have been inspected by past procedures might have been skipped.

Ultrasonic field mapping was useful in evaluating the distortion resulting from a UT field propagating through a section of CCSS pipe. Through-transmission measurements employing a longitudinal-wave-microprobe receiver and a 1-MHz, 45°, longitudinal-wave transmitter with a 38-mm diameter crystal were used. Distortion was initially evaluated by examining 20 field maps to determine if the ultrasonic field maintained spatial coherency. Distortion was also examined by measuring parameters from the field maps and including the effective refracted angle and the variation of field-position normalized by field width. To quantify the distortional variation of a microstructure, four field maps were acquired from unique material volumes of each microstructural classification.

Spatial coherency of the transmitted ultrasonic field was rated high for the pure microstructural forms of CCSS and moderate for the mixed microstructural forms of CCSS. Further analysis indicated that the refracted angle varied between 38° and 47° for CCSS. The largest standard deviation of refracted angle occurred for the mixed microstructural forms (2.9°), which also had the largest normalized positional variation (55%). These measurements indicate the increased difficulty of assuring a 50% field overlap when inspecting CCSS.

Due to the difference in field distortion, the worst-case material classification (mixed equiaxed-columnar microstructure) should be assumed for an inspection. An alternative is to continuously determine the microstructure as a scan is performed and to interrupt the data acquisition process and implement an appropriate technique customized to the detected microstructure when the probe passes to a different microstructure. This latter choice assumes an effective microstructural classifier and that an effective inspection technique exists for each of the possible microstructures.

Concerning field mapping in solids, the technique of applying a longitudinal-wave microprobe to a 45° facet for improved reception of 45° longitudinal waves was beneficial. Prior techniques (applying the microprobe normal to the far surface) biased image features toward smaller refracted angles because of receiver directivity. Application of the microprobe to the facet produced a ±1 dB change in receiving sensitivity over a broad angular range centered about 45°.

6.3.3 Future Work

Weld-overlay work will be limited to either completing the drafted RIL or restructuring the information into a NUREG report.

CCSS work will focus on collecting all the pertinent information accumulated by PNL concerning CCSS. This will include the CCSSRRT, selective frequency filtering of ultrasonic signals for CCSS microstructures, ultrasonic

field distortion, and ultrasonic attenuation. CCSS work will also continue to document microstructures, conduct ultrasonic attenuation measurements from the relevant microstructures, and acquire ultrasonic field maps from complex material microstructures.

Far-side inspection and dissimilar metal weld evaluations will include sample acquisition and metallography, and the ultrasonic field maps to document field distortion.

A study on reducing microstructural background noise of ultrasonic signals is planned.

6.4 SURFACE ROUGHNESS CONDITIONS

6.4.1 Introduction

The objective for this work was to establish specifications such that an effective and reliable ultrasonic inspection is not prevented by the condition of the inspection surface. Past efforts included an attempt to quantify the effect produced by inspection surface irregularities. The approach was redefined to cooperate with EPRI in establishing a mathematical model to be used as an engineering tool for deriving guidelines for surface specifications.

6.4.2 Status of Work Performed

Activities for this reporting period included formulation of a coordination plan between EPRI, NRC, the Center for NDE (CNDE) at Ames Laboratory, and PNL; a visit by CNDE personnel at PNL; an exchange of data between CNDE and PNL; and development of better experimental procedures by PNL for obtaining quantitative data for comparing to the model predictions. The following paragraphs describe a comparison between the CNDE and PNL data, and PNL development of a novel shear-wave microprobe for shear-wave reception.

6.4.2.1 Comparison of CNDE Ultrasonic Model and PNL Experimental Data

Both EPRI, through the CNDE at Ames Laboratory, and the Research Branch of the NRC, through PNL, have developed capabilities that are uniquely suited for establishing a validated model. Since CNDE has extensive experience in the computational modeling of ultrasonic wave propagation fields in solid materials, EPRI and the NRC have established a three-year time frame in which the two organizations, through the referenced institutes, will cooperate in attempting to determine and validate an ultrasonic computer model. To facilitate the cooperation between CNDE and PNL, a coordination plan was formulated which assigned individual and joint responsibilities to both CNDE and PNL.

Although the coordination plan was neither finalized nor approved formally until July 1988, work proceeded as if it was in effect. Mr. B. P. Newberry of CNDE visited PNL in October 1987 to overview the model capabilities, tour the PNL experimental facilities for ultrasonic field measurements, and discuss the interaction between CNDE and PNL. Dr. M. S. Good of PNL met with Dr. R. B.

Thompson of CNDE while attending the 8th Annual EPRI NDE Information Meeting to establish the ultrasonic setup parameters (Table 6.1) that would be used by PNL to experimentally map the field and by CNDE to predict UT fields using the mathematical model. The first data exchange was completed in February 1988, and it involved an immersion scan with isotropic materials.

TABLE 6.1. Ultrasonic Setup Parameters

Ultrasonic Technique:	Immersion
Transducer Characteristics:	38-mm (1.5-in.) diameter, 1 MHz
Transducer Excitation:	1.0 MHz continuous wave
Incident Angles:	18.9° in water to produce 45° vertically polarized shear waves in the sample
	10.2° in water to produce 45° longitudinal waves in the sample
Sample Characteristics:	13.3-cm (5.25-in.) thick carbon steel block (flat and coplanar surfaces)
Couplant:	Water (room temperature)
Stand-off Distance:	24.5 cm (9.6 in.) (1.0 near-field in water)
Measured Quantity:	Ultrasonic amplitude map on sample side opposite transducer

Analysis of the exchanged data initiated the first step toward model validation, which was to examine model performance in its present form. At the time of data acquisition, the model was able to make predictions for immersion techniques where a fluid such as water was used as the couplant. Future CNDE work will entail model refinement and adaptation for contact techniques (i.e., a solid wedge will be used to generate a specified refracted angle in the component being inspected).

The acquired ultrasonic field maps are shown in Figures 6.9 through 6.13. Model predictions of the L-wave and SV-wave fields are illustrated, respectively, in Figures 6.9 and 6.10. The remaining field maps are experimental data of the L-wave (Figure 6.11) and that of the SV-wave (Figures 6.12 and 6.13). Two figures are provided for the SV-wave experimental data since two different microprobes were used for SV-wave reception.

Subjectively, the model predictions of the ultrasonic field appear very similar to the two experimental maps where an L-wave microprobe was used for signal reception. However, a more objective means of comparison is sought to quantify the comparison for model validation. One proposed method is to normalize the data and perform a point-by-point comparison by either a

difference or dB calculation. (This was not accomplished since absolute values were not obtained on a point-by-point basis.) An alternative means of comparing data is to define measurable parameters from the image features and compare the resultant measurements.

Six parameters were defined as follows: -3, -6, and -14 dB field widths along both the short and long field axes[a] (subscripts S and L). Measurements were made of these parameters from the respective field maps (see Table 6.2).

TABLE 6.2. Measured Ultrasonic Field Parameters

Wave Mode	Field Width	CNDE Data (cm)	PNL Data L-Wave Microprobe (cm)	PNL Data S-Wave Microprobe (cm)	Percent of PNL Field Width Relative to CNDE Field Width L-Wave Microprobe	Percent of PNL Field Width Relative to CNDE Field Width S-Wave Microprobe
L	-3 dB_S	3.91	3.60	--	92	--
	-3 dB_L	6.48	5.37	--	83	--
	-6 dB_S	5.54	5.21	--	94	--
	-6 dB_L	9.30	7.36	--	79	--
	-14 dB_S	6.68	7.80	--	117	--
	-14 dB_L	11.45	11.57	--	101	--
SV	-3 dB_S	2.74	2.83	2.19	103	80
	-3 dB_L	3.91	4.38	2.01	112	51
	-6 dB_S	3.50	3.80	3.22	109	92
	-6 dB_L	5.71	5.58	3.02	98	53
	-14 dB_S	4.76	5.82	5.41	122	114
	-14 dB_L	6.87	7.96	7.35	116	107

Expected discrepancies in the data (see Table 6.3) were formed by examining where either the model or experimental measurements deviated from the phenomena being evaluated (i.e., ultrasonic amplitude). The model was known to not include material attenuation, while the experimental data did not compensate for receiver directivity. (Figure 6.14 illustrates receiver directivity. Superimposed on the graphs are arcs corresponding to the included angle of rays for signal reception for either the microprobe applied normal to the unaltered surface, or to the microprobe oriented normal to the impingent wave front.)

(a) The long axis is analogous to the major axis of an ellipse and is contained within the sample plane opposite the transducer. The short axis is analogous to the minor axis of an ellipse and is also contained within the sample plane opposite the transducer. Therefore, the refracted angle varies along the long axis and is related to linear translation along the axis by an arctangent function.

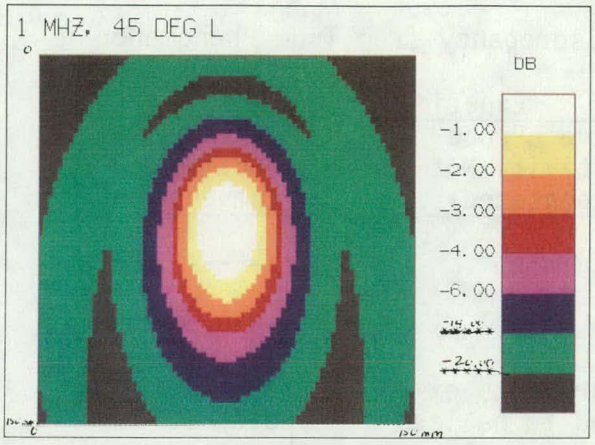

FIGURE 6.9.

45° L-Wave Beam Map - Theory

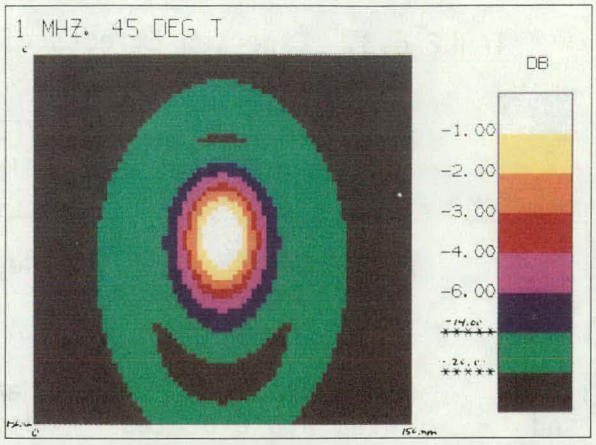

FIGURE 6.10.

45° SV-Wave Beam Map - Theory

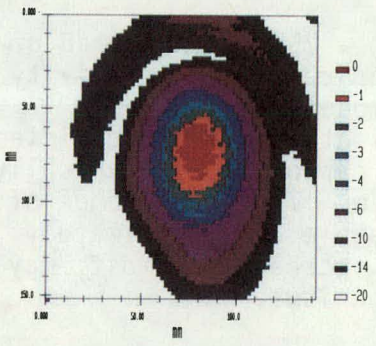

FIGURE 6.11.

Ultrasonic Field Map of a 45° L Wave in Steel (Receiver: L-Wave Microprobe)

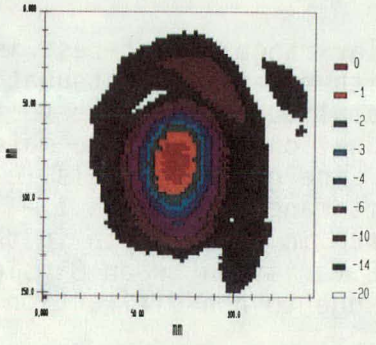

FIGURE 6.12.

Ultrasonic Field Map of a 45° SV Wave in Steel (Receiver: L-Wave Microprobe)

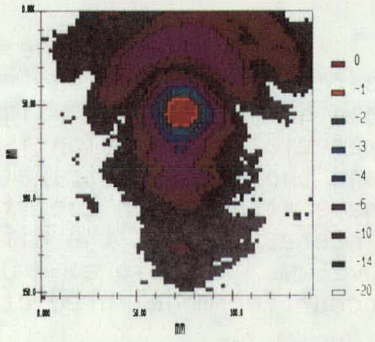

FIGURE 6.13.

Ultrasonic Field Map of a 45° SV Wave in Steel (Receiver: S-Wave Microprobe Rotated for SV-Wave Reception)

TABLE 6.3. Expected Effects of Discrepancy from True Phenomenon

Parameter	Model Prediction (No Material Attenuation)	Experimental Data (L-Wave μProbe Directivity Not Compensated)	Experimental Data (S-Wave μProbe Directivity Not Compensated)
-3, -6, and -14 dB_S	Negligible	Negligible	---
-3, -6, and -14 dB_L	Model field map measurements expected to be greater than true value with error increasing with dB drop.	Measurements expected to be less than true value with error increasing with dB drop.	Measurements expected to be less than true value with error increasing with dB drop. (Relative to L-wave μprobe, error is less for refracted angles < 45° and is greater for refracted angles > 45°).

Assuming that the angular range of interest is 45° ± 25°, then the dB or percentage variation from either material attenuation or receiver directivity can be calculated. Signal amplitude error due to the model not including material attenuation is a function of both the material attenuation coefficient and the distance traveled. Fine grained metals (e.g., carbon steel) typically have attenuation coefficients ranging between 1 - 3 dB/m. The ± 25° range of interest limits the difference in path length in the sample to approximately 0.25 m. Therefore, a 0.8 dB variation or an 8% signal increase, at most, may occur for model predictions due to non-diffraction mechanisms.

Signal reduction due to receiver directivity may be measured as shown in Figure 6.14. For the L-wave microprobe at normal incidence to the sample surface opposite the transducer and receiving a 45° ± 25° L-wave, a -4.5 dB variation (i.e., a 41% signal reduction) may occur. For the L-wave microprobe at normal incidence to the sample's surface opposite the transducer and receiving a 45° ± 25° SV-wave, a -9.2 dB variation (i.e., a 65% signal reduction) may occur. For the S-wave microprobe at normal incidence to the sample's surface opposite the transducer and receiving a 45° ± 25° SV-wave, a -10.2 dB variation (i.e., a 69% signal reduction) may occur.

Due to these discrepancies, the field width from the experimentally measured field maps are expected to always be less than either the true value or those obtained from the model prediction; that is, if the model is accurate. (A corollary to this is that the expected trends should be valid when comparing experimentally acquired data to the model predictions.) The long axis field widths are expected to be the most affected especially for large dB drops. Large dB drops result in a wider aperture and cause microprobe directivity to further restrict the measured field parameters.

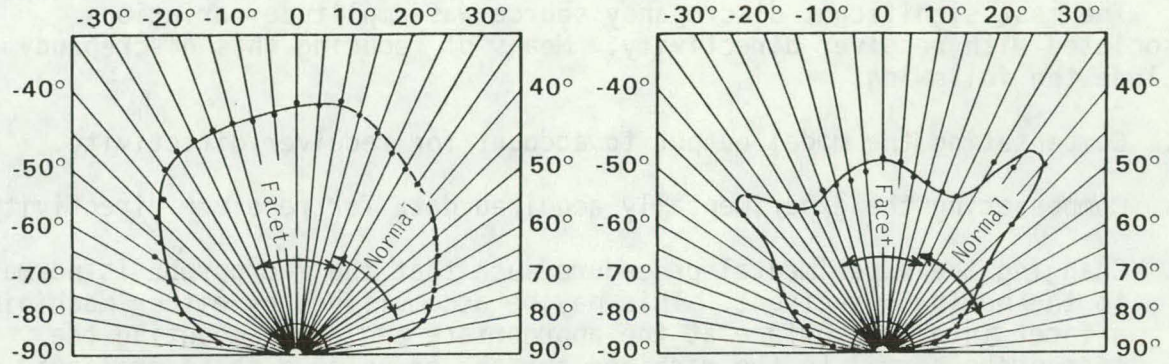

a) Longitudinal Wave Microprobe: 4MHz, L-Wave Directive Pattern

c) Shear-Wave Microprobe: 2MHz, SV-Wave Directive Pattern

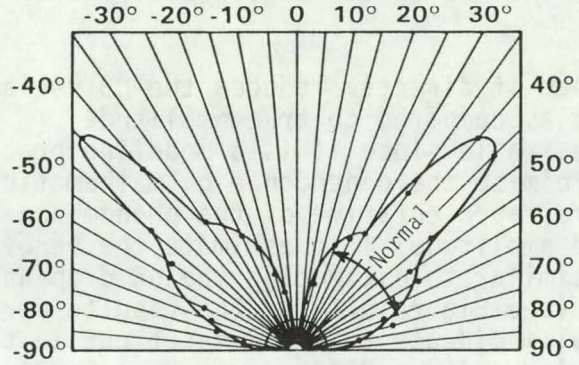

b) Longitudinal Wave Microprobe: 2MHz, SV-Wave Directive Pattern

FIGURE 6.14. Microprobe Receiver Directivity Patterns

The expected trend was supported by the L-wave field maps for the -3 and -6 dB field widths; however, the -14 dB field widths of the L-wave field map and the SV-wave field widths behaved in a manner opposite to the expected trend. For the L-wave field map, the experimentally measured -3 dBS and -6 dBS were 92% and 94% of the respective model values, while the long axis field widths were 83% and 79% of the model values. For the L-wave field map, the experimentally measured -14 dBS was 117% of the model value, while the long axis field width was 101% of the model value. For the SV-wave field map, the experimentally measured field widths were generally greater than those made from the model predictions.

The CNDE model predictions and the PNL experimental measurements differed since the model was predicting a phenomenon different than that which was directly measured. The main difficulty as discussed above was the variation in reception efficiency due to receiver directivity. However, even with this difference, expected trends were formulated and compared to the data. The expected trends were confirmed for the principal amplitude portion of the L-wave field (i.e., levels $\geq$ -6 dB). However, the data conflicted with the expected trends for the lower amplitude portions of the L-wave field (i.e., levels $\leq$ -14 dB) and the shear-wave field data.

The most significant discrepancy source was amplitude variations associated with receiver directivity. Means of reducing this discrepancy include the following:

1. Compensating the model output to account for receiver directivity.

2. Compensating the experimentally acquired data for receiver directivity.

3. Changing the experimental procedure such that the microprobe is normal to the nominal wavefront. This may be accomplished by either machining a facet into the surface at the appropriate angle and mounting the microprobe normal to the machined surface or using a solid or liquid material to refract the wave front and mount the microprobe such that the microprobe is normal to the nominal refracted angle (see Figures 6.14a and 6.14c).

Method 3 is the most desirable since it directly reduces the dB variation associated with the experimental values as compared to true amplitude measurements. Method 1 is the least desirable since it is a modeling process in itself. It is only reasonable to minimize the dependence on mathematics and to emphasize measurements which are more representative of the phenomenon being evaluated (i.e., ultrasonic field amplitude). To estimate the benefit of implementing Method 3, an analysis similar to estimating the dB drop and percent signal reduction was performed (see Figure 6.14). The results were that for the L-wave microprobe at normal incidence to a 45° facet cut in the side opposite the transducer and receiving a 45° ± 25° L-wave, a -1.0 dB variation or a 11% signal reduction may occur. For the S-wave microprobe at normal incidence to a 45° facet cut in the side opposite the transducer and receiving a 45° ± 25° SV-wave, a -2.0 dB variation or a 21% signal reduction may occur.

Conclusions and a recommendation for future work are as follows:

1. Conclusion: The model predictions of the ultrasonic field appeared to be very similar to experimental maps of the same immersion setup.

2. Recommendation: The experimental measurements should be repeated with the microprobe normal to the wavefront and the measurements compared to the model.

3. Conclusion: The model was accurate for the high amplitude portions of the L-wave field (i.e., levels $\geq$ 6 dB).

4. Conclusion: The model may be in error for low amplitude portions of the L-wave field (i.e., levels $\leq$ -14 dB).

5. Conclusion: The model may be in error for the SV-wave field.

In view of Item 2, PNL began refining ultrasonic microprobes and data acquisition techniques so that the experimental data would be an accurate representation of the predictions. This effort resulted in longitudinal-wave

microprobe refinements (See Figure 6.5) and development of the shear-wave microprobe (Good and Green 1988b) discussed below.

6.4.2.2 Development of a Novel Shear-Wave Microprobe

A very small aperture ultrasonic probe for detecting shear waves was desired for ultrasonic shear-wave field mapping (Good and Green 1988a, Good and Van Fleet 1987a and 1987b). Several designs of such a probe were developed and evaluated. During the course of probe development, a very interesting phenomenon was observed and used to build an improved shear-wave microprobe that is unique in design and capability. Design evolution, advantages, and applications of this new probe are described below.

The probes described in this report (Figure 6.15) use a metal cone with a sharp tip. The cone tip makes intimate contact with the solid specimen thereby coupling sound within the specimen to the cone. The tip contact area is small (typically 0.3-mm diameter) and may be considered a point contact for most ultrasonic applications. A piezoelectric element is used to convert acoustic energy in the cone into an electrical signal.

a) Shear-Wave Piezoelectric Bonded to Flat Cone

b) Longitudinal-Wave Microprobe Centered on Rounded Cone

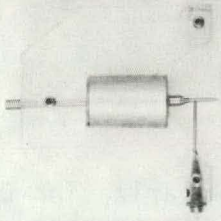

c) Longitudinal-Wave Microprobe Attached to Side of Extended Cone

FIGURE 6.15. Shear-Wave Microprobe Design Utilizing Steel Cones

The progression of shear-wave microprobe designs began with right circular cones with a flat top for bulk-shear-wave reception by a shear-wave crystal (Figure 6.15a). This design was improved by rounding the cone head to produce an area of concentrated mode-converted surface waves (Figure 6.15b). The most recent design utilized an extended cone with both a micro-piezoelectric

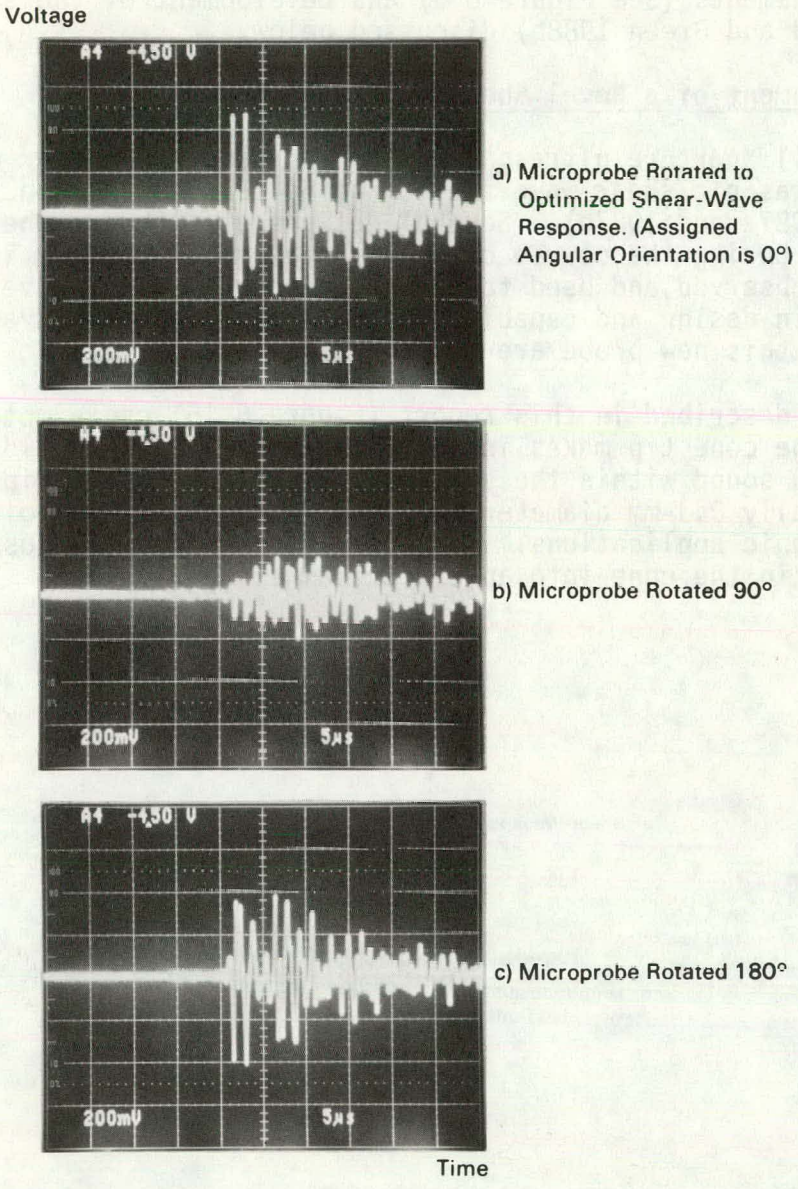

FIGURE 6.16. Shear-Wave Polarization Displayed by RF Signals from a Flat-Cone Microprobe

crystal for surface-wave reception and a cylinder of surface-wave damping material (Figure 6.15c).

The flat-top-cone design consisted of a 3-mm diameter shear-wave piezoelectric crystal bonded to the cone-top and encapsulated with polyurethane. This device was able to receive a 0° shear wave transmitted by pulsed excitation of a shear-wave piezoelectric crystal bonded to a 5-cm thick glass cube. However, the signal response, as shown in Figure 6.16, contained many spurious signal-reverberations from the cone. To further investigate

the source of extraneous signals, several cone designs were made and evaluated using the existing shear-wave microprobe as a diagnostic instrument by sliding the microprobe cone tip against the periphery of the cone being evaluated.

A strong signal was observed from two opposite sides on the top-surface of the flat cones. Each signal then propagated from the corner toward the center of the cone-top. A hypothesis was that the bulk shear wave impinged upon the corner and resulted in either a diffracted shear wave or a mode converted surface wave. To minimize this effect, the next generation of probes consisted of spherical cone heads (Figure 6.17).

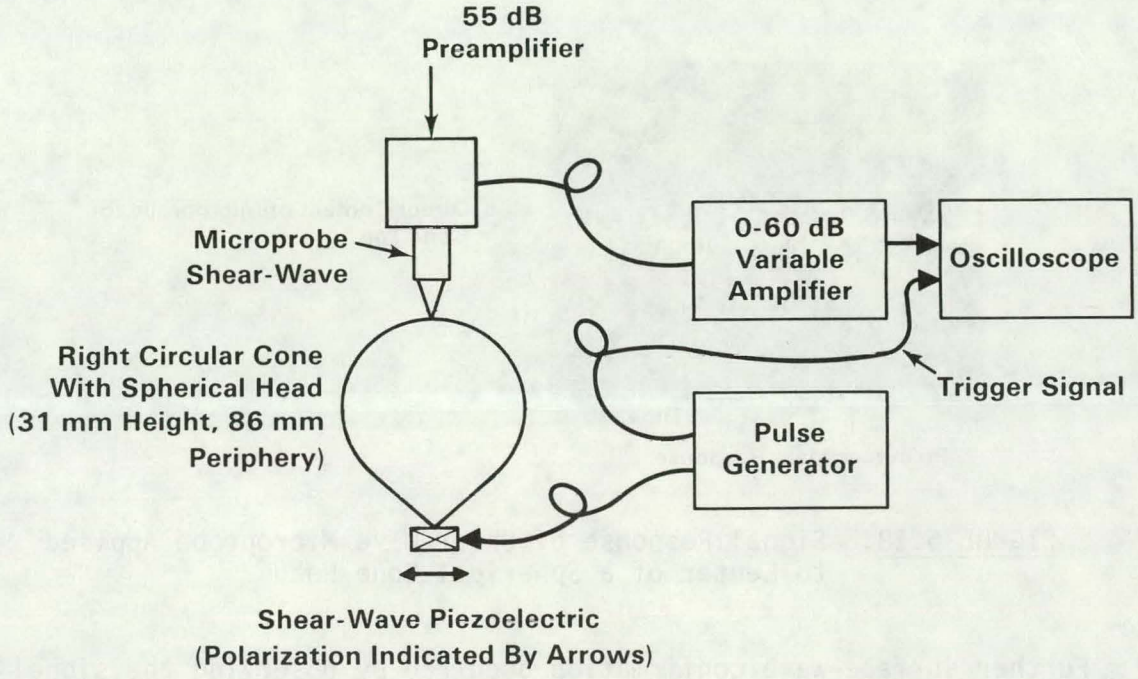

FIGURE 6.17. Block Diagram of Instrumentation for Investigating Wave-Propagation Mechanisms in Cones

The signal response from a microprobe placed at the center of a cone with a spherical head indicated that the signal consisted of both a shear-wave precursor and a large surface-wave response (Figure 6.18). The arrival time of the precursor corresponded to a bulk shear wave traveling from the cone tip to the cone-head center. The arrival time of the main signal response corresponded to a surface wave traveling along the cone periphery. Although signals were previously noted traveling up and down the cone sides, they were thought to be from divergence of the bulk shear wave and its interaction with the sides of the cone.

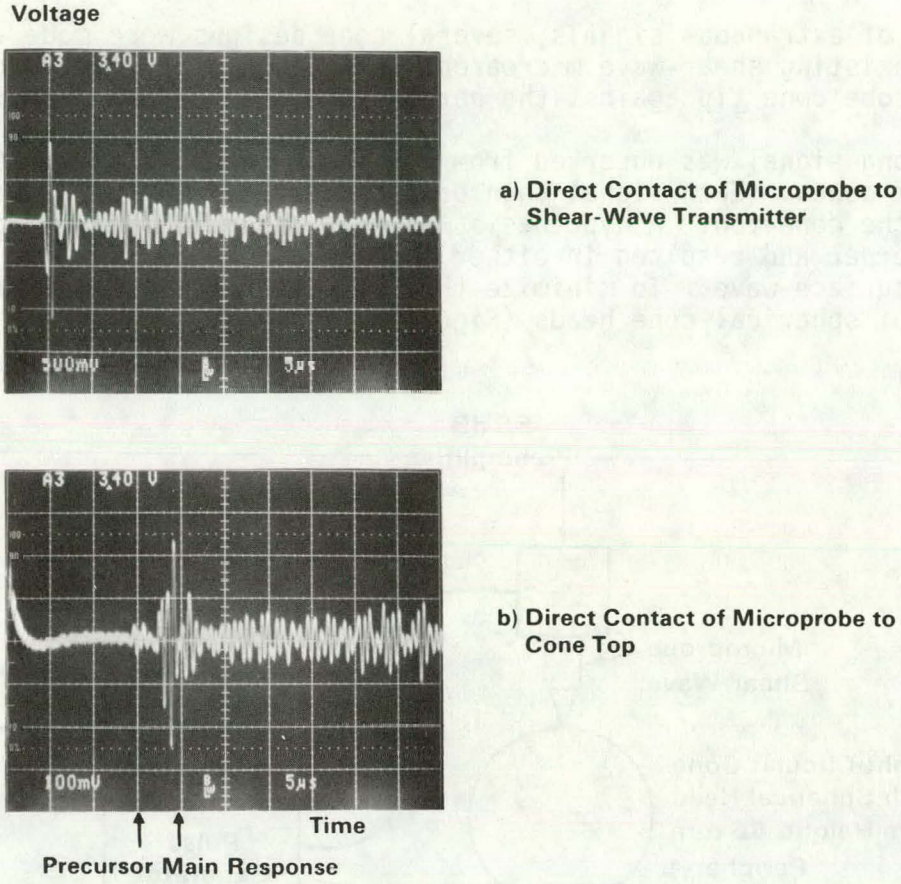

FIGURE 6.18. Signal Response of Shear-Wave Microprobe Applied to Center of a Spherical Cone Head

Further surface-wave confirmation occurred by observing the signal response from an asymmetrical point on the cone (Figure 6.19). Signal reception was accomplished by a longitudinal-wave microprobe applied to the cone surface to detect the surface normal component of the surface wave. The small-diameter crystal also enabled reception of high frequency signals since the crystal was contained entirely within either a compressive or rarefactive zone (10 MHz for a 0.3-mm microprobe aperture). Arrival times between signals 1 and 5 and signals 2 and 6 were predicted to equal 54.2 μs and measured 57.8 μs and 57.6 μs, respectively. Another supportive point was the match between the surface-wave pattern based on the arrival times of signals 1 and 2 and that of the remaining signal train.

A rounded-cone-top design (Figure 6.15b) was made which guided the surface waves to the cone-top center in order to form an area of concentrated surface waves. A longitudinal-wave micro-crystal was bonded at the focal region, unfortunately, sensitivity was lower than expected. Misplacement of the microcrystal from the cone center was examined by removing the steel shield around the cone top, shearing off the crystal, and monitoring signal reception by means of a longitudinal-wave microprobe coupled to the cone with petrolatum.

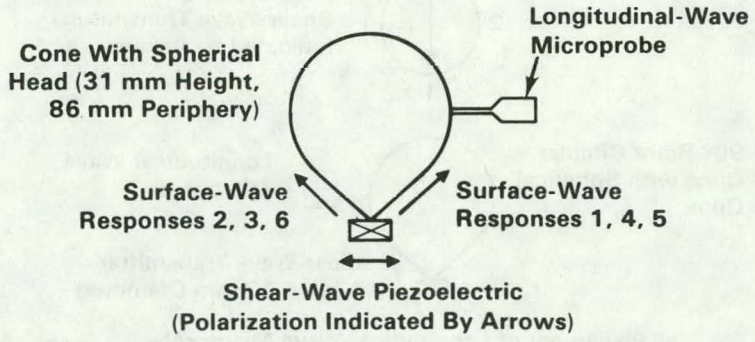

a) Placement of Longitudinal-Wave Microprobe on Cone

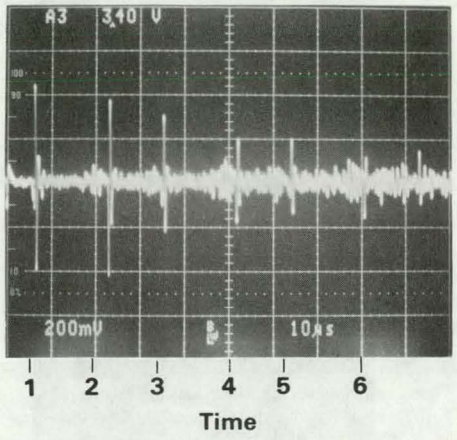

Signal No.	Arrival Time (μS)
1	6.4
2	22.8
3	35.8
4	51.8
5	64.2
6	80.4

b) Microprobe response

FIGURE 6.19. Surface-Wave Response from a Longitudinal-Wave Microprobe Applied to Side of Cone with Spherical Head

Sensitivity decreased as the crystal was centered. A hypothesis that was formulated and confirmed was that the two surface waves were phase reversals of each other (Figure 6.20). Thus, off-axis placement of the microprobe selectively caused high and low sensitivity to various frequencies because of interference. Another approach to provide greater fidelity was reception of only one surface wave.

An extended cone (Figure 6.15c) was designed in which the cone-vertex angle was made small in order to restrict the energy redistribution around the cone to increase sensitivity. The longitudinal-wave microprobe was placed close to the tip to minimize sound loss; and the extraneous, surface-wave reverberations were damped by inserting the extended cone into a cylinder of putty. To evaluate signal reception, a reference signal was provided by bonding a shear-wave transducer to a 51-mm thick glass cube. The received signal from the extended-cone, shear-wave microprobe, as shown in Figure 6.21b,

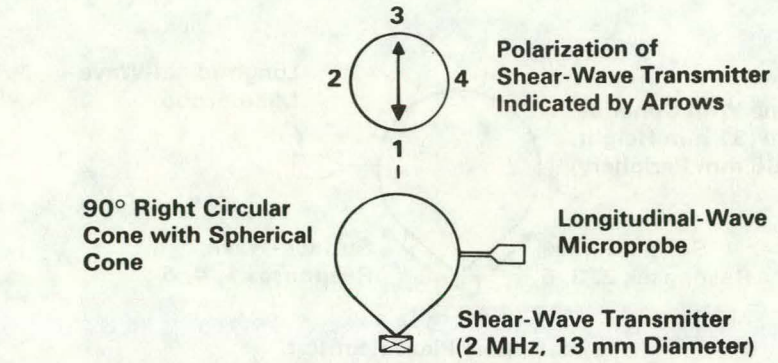

a) Placement of Longitudinal-Wave Microprobe

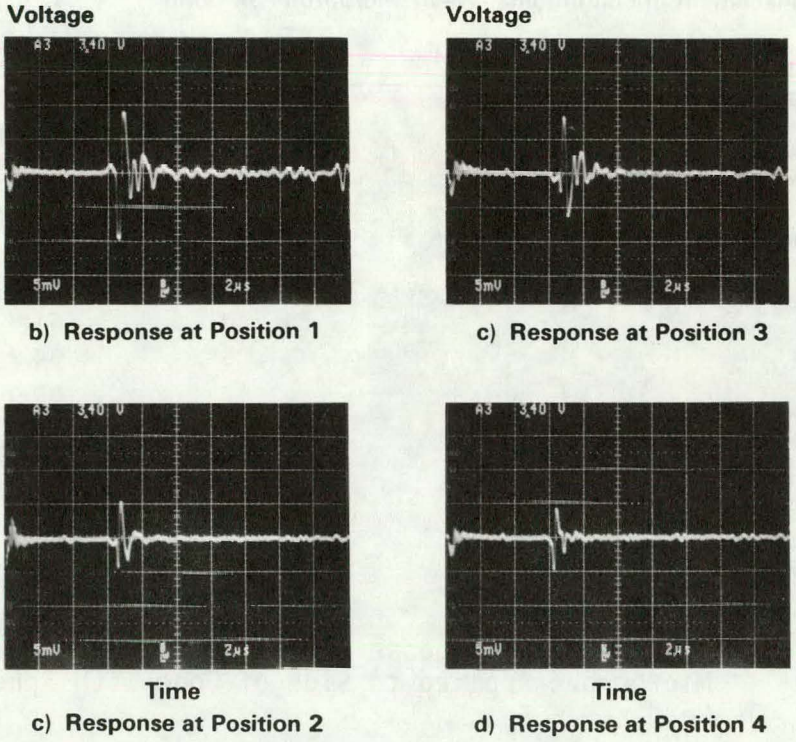

b) Response at Position 1

c) Response at Position 3

c) Response at Position 2

d) Response at Position 4

FIGURE 6.20. Examination of Surface-Wave Phase from Shear-Wave Excitation of Cone Tip

displayed limited signal ringing and was much improved over the initial flat-top-cone design. An hypothesis was that the latter portion of the main-signal response might be from the surface wave on the far side and other wave modes coupled between the two cone-sides. If true, application of the longitudinal-wave microprobe to the tip region of a cone used in the previous designs would weaken the interaction by increasing the distance between the cone sides, thus increasing signal clarity. As observed in Figure 6.21c, the main signal response was improved, which indicates that a possible means of improving the present design is to use an extended cone having a larger vertex angle. Another possibility is to use a smoother transition in cone cross-sectional diameter as a function of displacement along the cone axis.

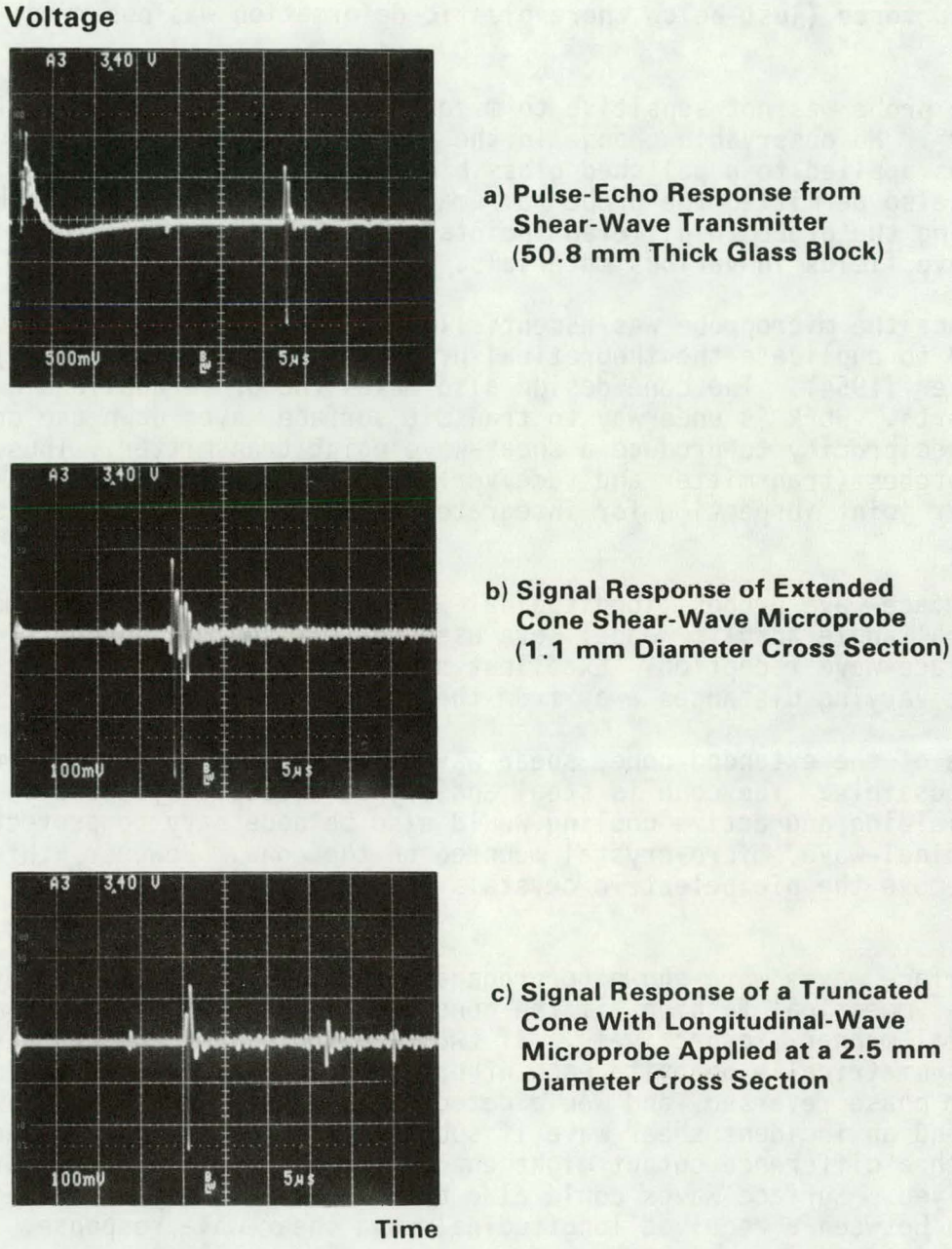

FIGURE 6.21. Response of Extended-Cone Microprobe to an Incident Shear Wave

These probes were very durable since the cone tip was hardened steel and the longitudinal-wave microprobe was rigidly held in place against the cone-side. The microprobe could be quickly moved away from the applied surface, and reapplied to another location using a small force normal to the surface. No problems were noted with frequent application of the microprobe except that the cone tip occasionally left a small depression in the material. Futhermore,

a small normal force was preferred since sensitivity enhancement due to increased force (just below where plastic deformation was observed) was marginal.

The probe was not sensitive to misalignments away from the surface normal up to 10°. No observable change in the time-domain signal was noted when the probe was applied to a polished glass block and angled at 10°. The polished surface also permitted the probe to remain in contact with the block while traversing the probe to different points. This may be useful for mapping shear-wave fields in various materials.

Since the microprobe was essentially a point receiver, directivity was expected to duplicate the theoretical predictions of Roderick (1950) and Pursey and Miller (1954). The cone design also makes the probe applicable for use on small parts. Work is underway to transmit surface waves down the cone-sides, and by reciprocity to produce a shear-wave point transmitter. Thus, a paired set of probes (transmitter and receiver) might be used for applications such as solder joint inspection for integrated circuits as well as ultrasonic welding.

Surface-wave probes (longitudinal-wave piezoelectric crystal mounted on a critical angle acrylic wedge) were used to test the microprobe's capability for surface-wave reception. Excellent sensitivity was observed for surface waves at varying distances away from the surface-wave transmitter.

Use of the extended-cone, shear-wave microprobe for high temperature work may be possible. The cone is steel and may be effectively cooled. Special heat shielding and active cooling would also be necessary to protect the longitudinal-wave, micro-crystal mounted on the cone. However, this design would remove the piezoelectric crystals from direct contact with an inspection piece.

Surface waves were shown to propagate up the cone sides in a symmetrical or anti-symmetrical fashion, if the cone tip was displaced in a normal or tangential manner, respectively. If two longitudinal-micro-crystals were placed symmetrically opposite each other, the received signals would be in phase or phase reversed, and would detect an incident longitudinal wave if summed and an incident shear wave if subtracted. Furthermore, an added crystal pair with a difference output might enable both shear-wave polarizations to be received. Surface waves could also be discriminated by examining the phase relation between a received longitudinal- and shear-wave response. Thus, a single point receiver might be capable of receiving all three wave-modes simultaneously while also being able to uniquely discriminate each mode.

It is concluded that a novel shear-wave microprobe was developed which utilizes mode conversion to surface waves. The advantages of this probe included: durability, consistency of signal reception with probe misalignment up to 10°, couplantless inspection, true point receiver, suitability for use on small parts, good sensitivity to surface waves, possible application to high temperature work, and possible simultaneous reception and discrimination of longitudinal, shear, and surface waves.

6.4.3 Future Work

A three-year effort was planned of which one year has now been completed. During the next year, this subtask will continue to involve collection of experimental data for both development and evaluation of the CNDE model. Upon model validation, PNL will acquire the mathematical model and use the model during the third year as an engineering tool to derive guidelines for surface specifications.

6.5 CHARACTERIZATION OF FIELD PIPE

6.5.1 Introduction

The objective of this subtask is to provide pipe weld specimens that can be used to help determine the effectiveness and reliability of ultrasonic inservice inspection (UT/ISI) that is performed on BWR piping. This goal will be accomplished by supporting PNL laboratory studies and providing specimens that will be used in other work such as PISC III.

6.5.2 Status of Work Performed

Weld specimens were acquired from Monticello and Vermont Yankee BWR nuclear power plants. These welds were removed from the pipe remnants in FY 1986. Due to high amounts of alpha contamination on the Monticello specimens, it was decided to decontaminate only the 11 Vermont Yankee specimens and wait until FY87 to have the 28 Monticello weld specimens decontaminated. A complete characterization was performed by PNL personnel on the 11 Vermont Yankee weld specimens; this included ultrasonic and penetrant examinations. The 28 Monticello weld specimens were decontaminated by an off-site contractor in FY87. Upon completion of the decontamination, PNL personnel performed weld profile measurements and penetrant examinations on all Monticello weld specimens. These results were recorded on data sheets in summary form. Some of these weld specimens were then manually UT and SAFT scanned to help select a specimen matrix for the PISC-III exercise. These data were thoroughly analyzed and a test matrix was selected for PISC-III.

6.5.3 Future Work

All work proposed under this subtask has been completed. The future plans for the remaining Monticello and Vermont Yankee weld specimens have not been finalized. This decision will be made at the end of 1988. Shipment of the four weld specimens (RREJ-4 & 5, RRAJ-5, N2B-4, and B128-2) that are scheduled to be used in the PISC-III exercise in Europe have been deferred until an Ispra decision is received regarding shipment of the five safe-end weld specimens. If the Europeans elect to have the safe-end specimens shipped, then the four weld specimens will be placed in a strong, tight container and will be included in the same C-van. If they decide not to have the five safe-end specimens shipped at that time, an overseas container will need to be purchased and the other weld specimens will be packaged and shipped. If the safe-ends are not shipped to Europe, then they will be made available to other U.S. research laboratories for use on materials and welding characterization

projects. If these specimens are not utilized within some period of time, then they will be packaged and sent to a disposal site for burial.

6.6 PISC-III ACTIVITIES

6.6.1 Introduction

The objective of this work is to contribute to the international Programme for the Inspection of Steel Components III (PISC III) to facilitate current studies on the reliability, capability, and parametric analysis of NDE techniques, procedures, and applications. This includes full-scale vessel testing; piping inspections; and human reliability, real components, nozzles and dissimilar metal welds, and modeling studies on ultrasonic interactions. This data will be used in quantifying the inspection reliability of ultrasonic procedures and the sources and extent of errors impacting the reliability.

The primary areas in which PNL participated include Action No. 1 on Real Contaminated Structures Tests (RCS), Action No. 2 on Full-Scale Vessel Tests (FSV), Action No. 3 on Nozzles and Dissimilar Metals Welds (NDM), Action No. 4 on Round-Robin Tests on Austenitic Steels (AST), Action No. 6 on Ultrasonic Testing Modeling (MOD), and Action No. 7 on Human Reliability Exercises (REL). These actions are being followed to ensure that conditions, materials, and practices in the U.S. are being included in the work so that the results are transferable to the U.S.

6.6.2 Status of Work Performed

The RCS work is being followed and efforts have been expended to provide some safe-ends removed from the Monticello plant for this Action. These safe-ends became available when the recirculation system was replaced. These safe-ends are extremely hot, and most of them have contact readings on their storage cylinders in excess of 1R at the hottest place. Five safe-ends are being considered of which two have weld overlays and three were not overlaid. One of the weld overlays had reported a through-wall crack during the weld overlay process. Problems have been encountered because the safe-ends have high alpha contamination, and the hot cells at Ispra are set up for shielding and were not designed to handle high alpha contamination. This activity is still on hold until the alpha contamination issue can be resolved.

Participation in the NDW has been in the form of aiding the coordination of the samples that will be coming to the U.S. in 1989. This involves contacting the inspection groups and ensuring arrangements and schedules will be met during the slotted inspection time.

Since PNL staff are major contributors to design, implementation, and analysis of studies in the AST, work has taken place in trying to gain further participation by U.S. teams for the round-robin tests and the parametric studies. Results by the two implantation methods of defects into CCSS should be available for assessment next reporting period, and a Japanese-contributed specimen should be shipped to PNL for introduction of thermal fatigue cracks in the near future.

Participation has occurred in the PISC-III Managing Board meetings to follow and advise on issues as they develop.

6.6.3 Future Work

These activities will be followed with appropriate input as needed and directing information to the NRC or Code committees as it becomes available and is pertinent to their needs.

7.0 REFERENCES

Doctor, S. R., J. D. Deffenbaugh, M. S. Good, E. R. Green, P. G. Heasler, F. A. Simonen, J. C. Spanner, and T. T. Taylor. 1988. Nondestructive Examination (NDE) Reliability for Inservice Inspection of Light Water Reactors. NUREG/CR-4469, PNL-5711, Vol. 7. Pacific Northwest Laboratory, Richland, Washington.

Doctor, S. R., J. D. Deffenbaugh, M. S. Good, E. R. Green, P. G. Heasler, F. A. Simonen, J. C. Spanner, and T. T. Taylor. 1989. Nondestructive Examination (NDE) Reliability for Inservice Inspection of Light Water Reactors. NUREG/CR-4469, PNL-5711, Vol. 8. Pacific Northwest Laboratory, Richland, Washington.

Good, M. S. and E. R. Green. 1988a. "Mapping of 1-MHz, 45° Longitudinal Fields in Centrifugally Cast Stainless Steels, submitted for publication in Review of Progress in Quantitative Nondestructive Evaluation, edited by D. O. Thompson and D. E. Chimenti (Plenum Press, New York, 1989), Vol. 8.

Good, M. S. and E. R. Green. 1988b. "A Shear-Wave Microprobe Utilizing Surface-Wave Mode Conversion," submitted for publication in Review of Progress in Quantitative Nondestructive Evaluation, edited by D. O. Thompson and D. E. Chimenti (Plenum Press, New York, 1989), Vol. 8.

Good, M. S. and L. G. Van Fleet. 1987a. "Ultrasonic Beam Profiles in Coarse Grained Materials," in 8th International Conference on NDE in the Nuclear Industry, edited by D. Stahl (American Society for Metals International, Metals Park, Ohio, 1987) pp. 657-666.

Good, M. S. and L. G. Van Fleet. 1987b. "Mapping of Ultrasonic Fields in Solids," in Review of Progress in Quantitative Nondestructive Evaluation, edited by D. O. Thompson and D. E. Chimenti (Plenum Press, New York, 1988), Vol. 7A, pp. 637-646.

Green, E. R. and G. A. Mart. 1988. "Modeling Frequency Domain Effects for Ultrasonic Flaw Detection," in Proceedings of the 1988 Review of Progress in Quantitative NDE, Plenum Press, New York.

Miller, G. F. and H. Pursey, The Field and Radiation Impedance of Mechanical Radiators on the Free Surface of a Semi-Infinite Isotropic Solid, Royal Society, A, vol. 223, pp. 521-541, 1954.

Roderick, R. L., The Radiation Pattern from a Rotationally Symmetric Stress Source on a Semi-Infinite Solid, Metals Research, Brown University, 1950.

Sugnet, W. R., G. J. Boyd, and S. R. Lewis. 1984. Oconee PRA: A Probabilistic Risk Assessment of Oconee, Unit 3. NSCA-60, Electric Power Research Institute, Palo Alto, California.

Wright, R. E., J. A. Stevenson, and W. F. Zuroff. Pipe Break Frequency Estimation for Nuclear Power Plants. NUREG/CR-4407, Idaho National Engineering Laboratory, Idaho Fall, Idaho 1987.

NRC FORM 335 (2-89) NRCM 1102, 3201, 3202

U.S. NUCLEAR REGULATORY COMMISSION

BIBLIOGRAPHIC DATA SHEET

(See instructions on the reverse)

1. REPORT NUMBER (Assigned by NRC. Add Vol., Supp., Rev., and Addendum Numbers, if any.)

NUREG/CR-4469
PNL-5711
Vol. 9

2. TITLE AND SUBTITLE

Nondestructive Examination (NDE) Reliability for Inservice Inspection of Light Water Reactors

Semi-Annual Report: April - September 1988

3. DATE REPORT PUBLISHED

MONTH: November YEAR: 1989

4. FIN OR GRANT NUMBER

FIN B2289

5. AUTHOR(S)

SR Doctor, JD Deffenbaugh, MS Good, ER Green, PG Heasler, FA Simonen, JC Spanner, TT Taylor

6. TYPE OF REPORT

Technical

7. PERIOD COVERED *(Inclusive Dates)*

April-September 1988

8. PERFORMING ORGANIZATION – NAME AND ADDRESS *(If NRC, provide Division, Office or Region, U.S. Nuclear Regulatory Commission, and mailing address; if contractor, provide name and mailing address.)*

Pacific Northwest Laboratory
PO Box 999
Richland, WA 99352

9. SPONSORING ORGANIZATION – NAME AND ADDRESS *(If NRC, type "Same as above"; if contractor, provide NRC Division, Office or Region, U.S. Nuclear Regulatory Commission, and mailing address.)*

Division of Engineering
Office of Nuclear Regulatory Research
U.S. Nuclear Regulatory Commission
Washington, DC 20555

10. SUPPLEMENTARY NOTES

11. ABSTRACT *(200 words or less)*

Evaluation and Improvement of NDE Reliability for Inservice Inspection of Light Water Reactors (NDE Reliability) Program at the Pacific Northwest Laboratory was established by the Nuclear Regulatory Commission to determine the reliability of current inservice inspection (ISI) techniques and to develop recommendations that will ensure a suitably high inspection reliability. The objectives of this program include determining the reliability of ISI performed on the primary systems of commercial light-water reactors (LWRs); using probabilistic fracture mechanics analysis to determine the impact of NDE unreliability on system safety; and evaluating reliability improvements that can be achieved with improved and advanced technology. A final objective is to formulate recommended revisions to ASME Code and Regulatory requirements, based on material properties, service conditions, and NDE uncertainties. The program scope is limited to ISI of the primary systems including the piping, vessel, and other inspected components. This is a progress report covering the programmatic work from April 1988 through September 1988.

12. KEY WORDS/DESCRIPTORS *(List words or phrases that will assist researchers in locating the report.)*

nondestructive evaluation, nondestructive testing, cast stainless steel, weld overlay, fracture mechanics, PISC II, PISC III, ultrasonic testing, ultrasonic equipment characterization, ASME Code, performance demonstration

13. AVAILABILITY STATEMENT

Unlimited

14. SECURITY CLASSIFICATION

(This Page) Unclassified

(This Report) Unclassified

15. NUMBER OF PAGES

16. PRICE

☆ U.S. GOVERNMENT PRINTING OFFICE: 1990-253-460

NUREG-CR/4469
PNL-5711
Vol. 9
R5

DISTRIBUTION

No. of Copies

OFFSITE

2 J. Muscara
NRC/RES
Mail Stop NL-007

C. Z. Serpan
NRC/RES
Mail Stop NL-007

R. A. Hermann
NRC/RES
Mail Stop 9H-15

M. R. Hum
NRC/NRR
Mail Stop 9H-15

C. Y. Cheng
NRC/NRR
Mail Stop 9H-15

J. P. Durr
NRC/Region I

S. B. Ebneter
NRC/Region I

A. R. Herdt
NRC/Region II

J. J. Blake
NRC/Region II

K. Ward
NRC/Region III

D. Danielson
NRC/Region III

No. of Copies

D. S. Kupperman
Materials Science Center
Argonne National Laboratory
9700 S. Cass Avenue
Building 212
Argonne, IL 60439

FOREIGN

W. E. Gardner
Risley Nuclear Labs
UKAEA
Risley Warrington
Chesire
United Kingdom

M. J. Whittle
NDT Application Centre
CEGB Scientific Services
Timpson Road
Manchester M23 9LL
United Kingdom

ONSITE

50 Pacific Northwest Laboratory

M. C. Bampton
S. H. Bush
L. A. Charlot
J. D. Deffenbaugh
J. Divine
S. R. Doctor (28)
M. S. Good
E. R. Green
P. G. Heasler
P. H. Hutton
D. K. Lemon/G. J. Posakony
F. A. Simonen
J. C. Spanner
G. M. Stokes
T. T. Taylor
T. V. Vo
Technical Report Files (5)
Publishing Coordination (2)

UNITED STATES
NUCLEAR REGULATORY COMMISSION
WASHINGTON, D.C. 20555